

# **Hydraulic Properties for Unsaturated Water Flow in Aggregated Volcanic Ash Soils**

**Rudiyanto**

A thesis submitted in fulfillment of the requirements  
for the degree of Doctor of Philosophy

**Department of Sustainable Resource Sciences  
Graduate School of Bioresources  
Mie University  
December 2013**



*With water we have made all living things*

-The Quran, Al-Anbiyaa: 30

I dedicate this thesis to all soil physicists, in the past, present and future, for their wonderful ideas, persistent attempts and contribution



# ACKNOWLEDGMENTS

Despite only my name is written in the cover of this a PhD thesis, this thesis is a result from the idea, inspiration, assistance, and guidance of many people especially my main supervisor, Prof. Dr. Nobuo Toride. Therefore, first of all, I would like to express my sincere gratitude to him who gave me the opportunity to do a PhD at Mie University, Japan. He introduced me to soil physics especially about dual porosity hydraulic properties, the evaporation method, hysteretic model as well as volcanic ash soils, Andisols. His scientific insight helped me to understand this study, to decide which direction should be taken, and to accomplish this study. His surprising knowledge, perfect guidance, great inspiration, brilliant ideas, thinking outside the box, and research philosophy such as focus on the objective and improvements, attention to the position of paper in the scientific stream, concern to the readers and conciseness in writing and audiences in presentation always impressed me. I also would like to thank for his financial support for me. I am really honored to be his PhD student.

I would like to thank to Prof. Dr. Atsushi Hashimoto and Prof. Dr. Hiroshi Ehara as the committee member for their constructive comments at preliminary evaluation. I am indebted to Dr. Kunio Watanabe as also the committee member for providing an important device: a dew point potentiometer, WP4 for my experiment and his valuable comments on the evaporation method paper. Dr. Masaru Sakai as the committee member is also owed my deep gratitude for verifying the derivation of the hysteretic model, helpful discussion, useful comments and suggestion and providing the setup of the evaporation experiment especially Basic source codes for data acquisition using the CR1000 data logger.

A great appreciation is given Prof. Dr. Jirka Šimůnek for finalization and responses on the reviewer comments for the hysteretic model paper. A special acknowledgement is given to Prof. Dr. 'Rien' van Genuchten for finalization and improving the quality of the evaporation method paper in short periods.

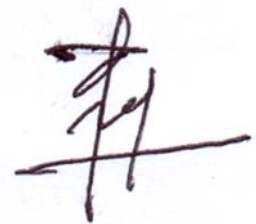
I would like to expresses sincere gratitude to the Ministry of Education, Culture, Sports, Science and Technology (MEXT) of the Government of Japan for the awards of

scholarship during this study. Many thanks are also extended to Prof. Dr. Budi Indra Setiawan for his generous support, kindness and visiting to Mie on 28 July 2013.

Further, I am thankful to Dr. Dimitar Antonov, and Chen Daiwin for their helpful hand, assistance and nice friendship. Many thanks are also given to all members of Environmental Soil Physics and Hydrology laboratory: Takafumi Hoshino who gave me his data for an evaporation method, Masato Oishi; from his miscible displacement data set, i.e., tensiometer and TDR reading pairs, I obtained an idea to develop a hysteretic model of hydraulic properties for dual porosity soils, Tomomi Wake, who introduced an experiment setup for the evaporation method, Tetsuya Kito, Shoko Oda, Kotake Ken, Tohru Nishida, Yudai Hisayuki etc. for their kind help and delightful friendship.

I am likewise grateful to my parents who always pray for me. I believe their prayer made me keep patience doing the relentless efforts and made everything possible. I owe you so much that I cannot return in any ways. My deepest thanks are also due to my beloved wife, Maulidiani, and my lovely daughter, 'Mizuki' Nur Amina who deserve a big hug for sharing all ups and downs while I am studying aboard with a great patience, understanding and care.

Finally, I thank everyone -might not have mentioned in this acknowledgements- who helped me during my study.

A handwritten signature in dark ink, consisting of stylized, overlapping strokes that form a unique, cursive-like representation of the name Rudiyanto.

Rudiyanto  
Mie University

# SUMMARY

Numerical analysis of soil water flow is frequently used to assess water management in agriculture. Hydraulic properties (i.e., water retention,  $\theta(h)$  and unsaturated hydraulic conductivity,  $K(h)$  or  $K(\theta)$ ) are required for that analysis. Among soil physical properties, the unsaturated hydraulic conductivity is the most difficult to measure. This thesis mainly describes determination of a wide range of unsaturated hydraulic conductivity of Andisols based on the evaporation method. Subsequently, a hysteretic model for hydraulic properties of Andisols was proposed. Furthermore, roles of aggregate structure of Andisols were also numerically evaluated for water management in the root zone layer.

**Chapter 2** reviews the uniqueness of Andisols because of a well-developed and stable aggregate structure made up of noncrystalline minerals (e.g., allophane, imogolite, ferrihydrite). Several hydraulic functions for aggregated soils were also presented. This chapter also provides the procedure of the inverse method mainly focusing on the evaporation method for determining hydraulic properties. A hysteretic model based on Kool and Parker (1987) derived from the scaling methods was also reviewed.

In **Chapter 3**, parameters of the bimodal van Genuchten (VG) hydraulic functions for two aggregated Andisols were inversely determined using the evaporation method. Initial estimates of the water retention parameters were determined from separate retention measurements, which facilitated rapid convergence of the parameter optimization process regardless of the number of optimized parameters. When the bimodal water retention parameters were fixed according to the independently measured retention data from near saturation to very low pressure heads down to  $-10^5$  cm, it was possible to estimate the unsaturated conductivity,  $K(h)$ , by optimizing only two conductivity parameters ( $K_s$ ,  $\ell$ ). Since the flat region of the bimodal retention curve at intermediate pressures is difficult to measure precisely, however, we still recommend optimizing all bimodal VG parameters to yield the best overall results. Including water retention data at very low pressure heads in the dry range extended the applicable range of the model predictions, at least down to pressure heads of approximately  $-10^4$  cm. This confirms that collecting water retention data over a wide range of pressure heads will

give very useful prior information to the parameter estimation process for not only Andisols but also other soils.

**Chapter 4** proposes a hysteretic model of hydraulic properties for dual porosity soils based on the bimodal van Genuchten (VG) model and the Kool and Parker (K&P) hysteresis model. Hysteresis is considered only in the first pore domain, affecting mainly higher water contents, while a nonhysteretic behaviour is assumed in the second pore domain, affecting mainly lower water contents. The main drying and wetting curves are described with the same set of parameters, except for the  $\alpha_1$  parameter, which is different for the drying curve,  $\alpha_1^d$ , and for the wetting curve,  $\alpha_1^w$ . The scanning hysteresis loops in the first subregion are also described using the K&P model. The hysteretic water retention model agrees reasonably well with drying and wetting retention curves and scanning loops observed for Andisols. Although the corresponding unsaturated hydraulic conductivity, evaluated using the Mualem pore-size distribution model, as a function of the water content,  $K(\theta)$ , is nonhysteretic for higher water contents, unrealistic hysteresis occurs in  $K(\theta)$  for lower water contents. In order to obtain an ‘almost’ nonhysteretic  $K(\theta)$  function for the entire range of water contents, an additional constraint on the value of the  $\alpha_1$  parameter for  $K(\theta)$  is imposed, and a single value  $\alpha_1^k$  is used for both drying and wetting curves.

**Chapter 5** reports roles of aggregate structure for Andisols in the root zone layer through numerical water flow evaluation. Similar to sandy loam soil, Kumamoto Andisol exhibits large infiltration and drainage rate from root zone because of large  $K_s$  which is resulted in from interaggregate pores. Kumamoto Andisol shows greater water and air storage, the potential and actual plant available water (PAW) than those in sandy loam and clay soils. For water storage and the potential and actual PAW, Kumamoto Andisol is similar to clay soil; however, for air storage, Kumamoto Andisol has similarity to sandy loam soil. Intraaggregate pores are responsible on water storage and the potential and actual PAW. Contrary, interaggregate pores are responsible on soil aeration. Aggregated structure that developed in Kumamoto Andisol accounts combination of sandy loam and clay soils properties.



# **TABLE OF CONTENTS**

## **ACKNOWLEDGEMENTS**

## **SUMMARY**

## **TABLE OF CONTENTS**

### **1 GENERAL INTRODUCTION**

#### **1.1 PROBLEM DEFINITION**

#### **1.2 OBJECTIVES**

#### **1.3 OUTLINE OF THESIS**

### **2 LITERATURE REVIEW**

#### **2.1 UNIQUENESS OF PHYSICAL PROPERTIES OF ANDISOLS**

#### **2.2 UNSATURATED WATER FLOW**

#### **2.3 DUAL POROSITY HYDRAULIC FUNCTIONS**

#### **2.4 WATER RETENTION CURVE MEASUREMENT**

#### **2.5 ESTIMATION OF SOIL UNSATURATED HYDRAULIC CONDUCTIVITY BASED ON THE EVAPORATION METHOD**

##### **2.5.1 Inverse method for unsaturated hydraulic conductivity**

##### **2.5.2 Estimation of the bimodal VG using inverse method**

##### **2.5.3 Soil evaporation experiment**

#### **2.6 HYSTERETIC MODEL OF HYDRAULIC PROPERTIES**

##### **2.6.1 Hysteretic model for water retention**

##### **2.6.2 Unsaturated hydraulic conductivity**

#### **2.7 CONCLUSIONS**

#### **2.8 REFERENCES**

### **3 ESTIMATING THE UNSATURATED HYDRAULIC CONDUCTIVITY OF ANDISOLS USING THE EVAPORATION METHOD**

#### **3.1 INTRODUCTION**

#### **3.2 MATERIALS AND METHODS**

##### **3.2.1 Evaporation experiment**

##### **3.2.2 Bimodal van Genuchten model**

##### **3.2.3 Parameter optimization**

### 3.3 RESULTS AND DISCUSSION

#### 3.3.1 Parameter estimation

#### 3.3.2 Water retention data at low pressure head

#### 3.3.3 Pressure head measurement range

### 3.4 CONCLUSIONS

### 3.5 REFERENCES

## **4 A HYSTERETIC MODEL OF HYDRAULIC PROPERTIES FOR DUAL POROSITY SOILS**

### 4.1 INTRODUCTION

### 4.2 MATERIALS AND METHODS

#### 4.2.1 Observed hysteretic water retention

#### 4.2.2 Hysteretic model

### 4.3 RESULTS AND DISCUSSION

#### 4.3.1 Main wetting and drying branches

#### 4.3.2 Scanning retention curves

#### 4.3.3 Unsaturated hydraulic conductivity

### 4.4 CONCLUSIONS

### 4.5 REFERENCES

## **5 ROLES OF AGGREGATE STRUCTURE OF ANDISOLS IN WATER FLOW IN THE ROOT ZONE**

### 5.1 INTRODUCTION

### 5.2 THEORETICAL CONSIDERATION

#### 5.2.1 Governing equation of water flow

#### 5.2.2 Soil hydraulic functions

### 5.3 MATERIALS AND METHODS

#### 5.3.1 Materials

#### 5.3.2 Numerical analysis of water flow

### 5.4 RESULTS AND DISCUSSION

#### 5.4.1 Soil water infiltration and surface runoff

#### 5.4.2 Redistribution of water in soil

#### 5.4.3 Drainage from the root zone

5.4.4 Water and air storage and the potential and actual plant available water (PAW)

5.4.5 Roles of inter and intra aggregate pores

5.5 CONCLUSIONS

5.6 REFERENCES

## **6 CONCLUDING REMARKS AND PERSPECTIVES**

6.1 CONCLUSIONS

6.2 FUTURE PERSPECTIVES

6.3 REFERENCES

## **LIST OF SYMBOLS AND ABBREVIATIONS**



## CHAPTER 1

# GENERAL INTRODUCTION

### 1.1 PROBLEM DEFINITION

Andisols in US soil taxonomy (Soil Survey Staff, 1999) or Andosols in the World Reference Base for Soil Resources (WRB Classification) (FAO, et al., 1988) or “Kurobokudo (黒ボク土)” in Japanese (The Third Division of Soils, 1973) meaning the black-fluffy soils are commonly used to refer to volcanic ash soils. Henceforth, Andisols are used to refer the volcanic ash soils for simplification. Andisols cover more than 124 million ha or approximately 0.84 % of the earth’s surface (Takahashi and Shoji, 2002). Despite the areas of Andisols are relatively small extent of the world surface, Andisols are very important resources owing to huge populations living in these regions (Shoji et al., 1993).

Figure 1.1 shows distribution of Andisols in the world. Major locations of Andisols are found around the Pacific ring: on the west coast of South America, in Central America, the Rocky Mountains, Alaska, Japan, the Philippine Archipelago, Indonesia, Papua New Guinea and New Zealand. Andisols are also prominent on many islands in the Pacific: Fiji, Vanuatu, New Hebrides, New Caledonia, Samoa and Hawaii. In Africa, Andisols can be found along the Rift Valley, in Kenya, Rwanda and Ethiopia and on Madagascar. In Europe, Andisols were obtained in Italy, France, Germany and Iceland (FAO, et al., 1988; Soil Survey Staff, 1997 and Takahashi and Shoji, 2002).

In Japan, Andisols are widely distributed about 6.8 million hectares or 18% of the territory, especially at Hokkaido, Tohoku, Kanto and Kyushu districts as shown Fig. 1.2 (Takahashi and Shoji, 2002). The area of Andisols are used for cultivation about 1.35 million hectares of Andisols, comprising 24% of total area of agriculture in Japan.

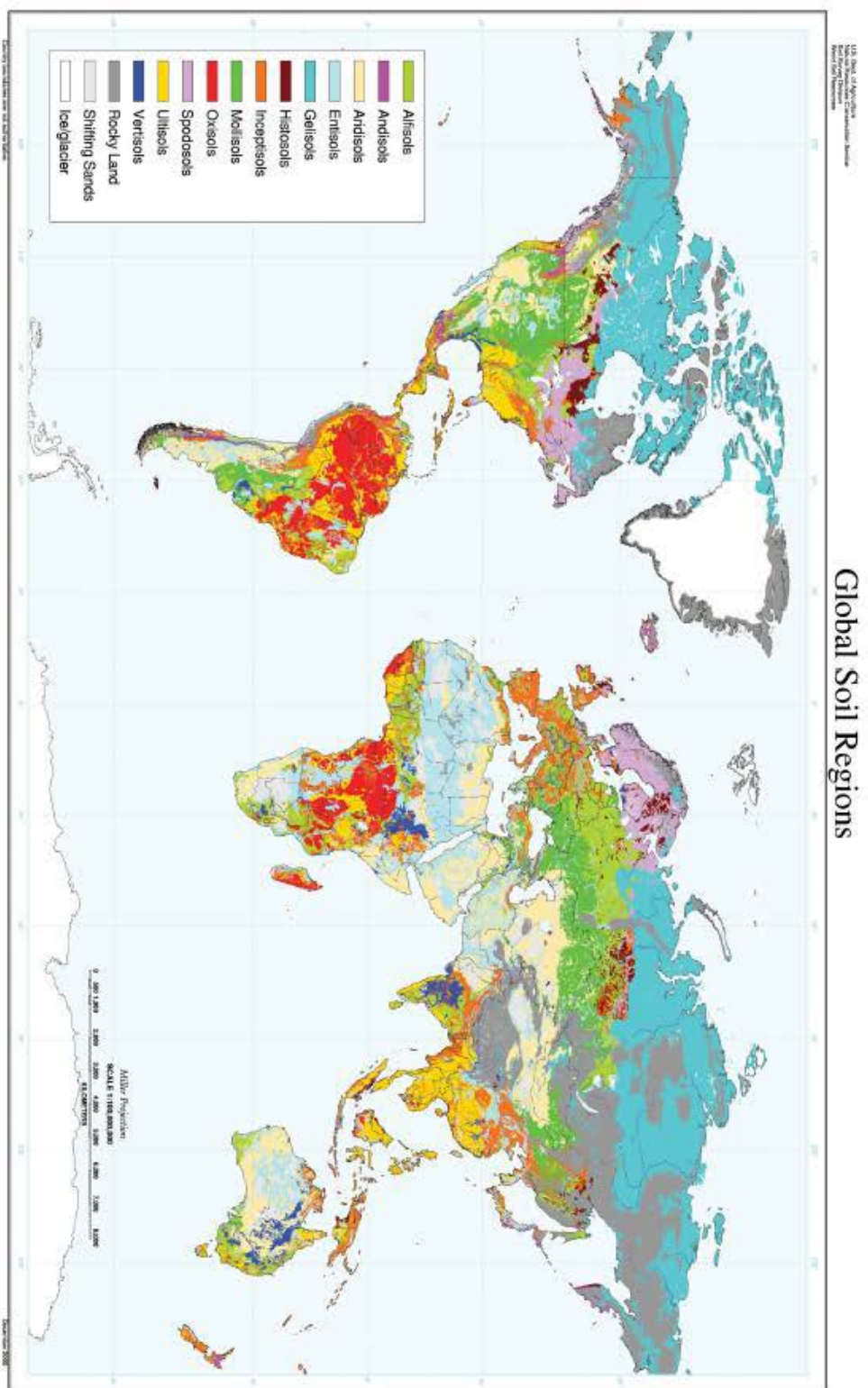


Fig. 1.1. Worldwide distribution of volcanic ash soils (Andisols) (World Soil Resources Staff, 1997).

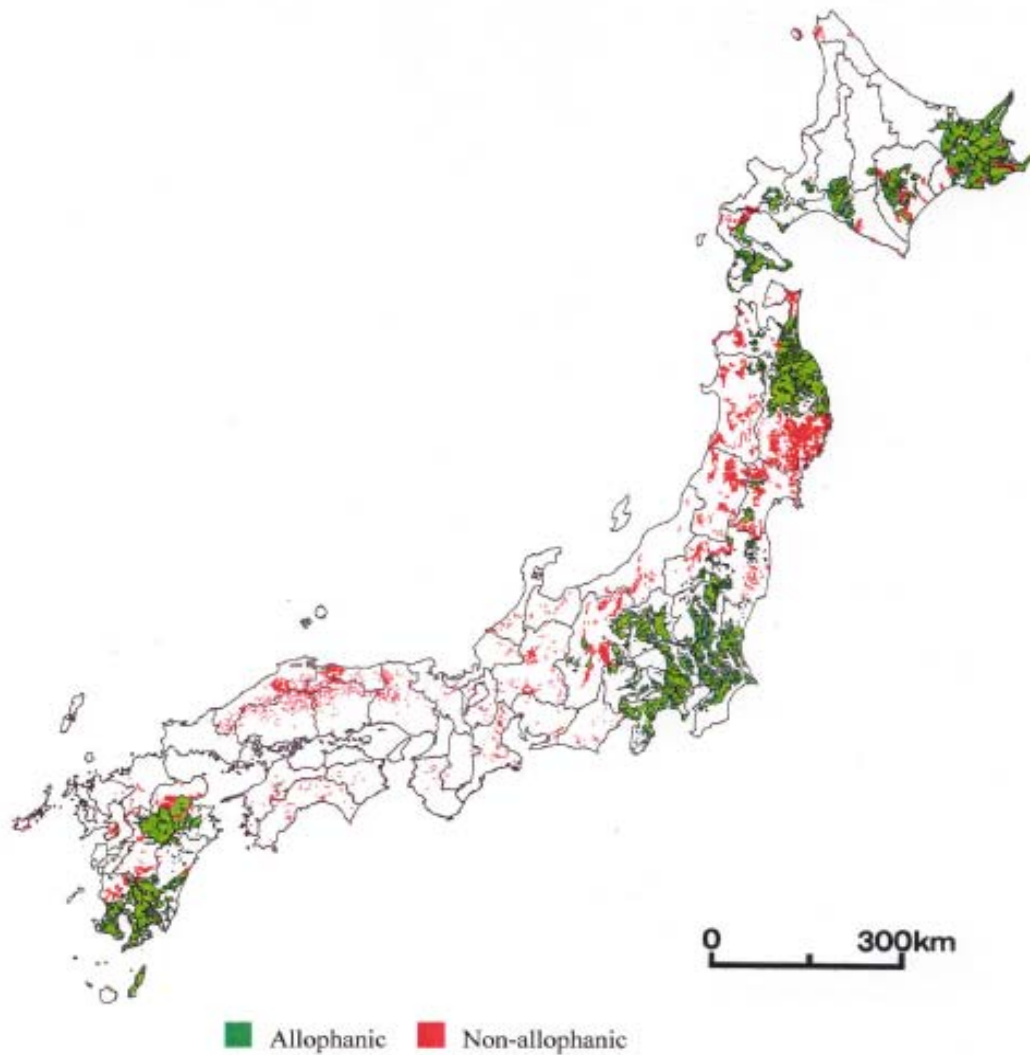


Fig. 1.2. Distribution of allophanic and nonallophanic volcanic ash soils in Japan (Takahashi and Shoji, 2002).

Andisols play an important role for resources of agriculture, particularly upland crop production. From a physical point of view, Andisols are known as the most productive soil in the earth owing to high water retention, high drainage rate and high plant water and nutrient availability (Shoji et al., 1993). Those valuable properties are as a result of the strong natural aggregation of particles in Andisols (Nanzyo et al., 1993; Shoji et al., 1993; Shoji and Takahashi, 2002; Nanzyo, 2002; and Dahlgren et al., 2004).

The aggregated structure of Andisols is developed well and made by noncrystalline materials (e.g., allophane, imogolite) for allophanic Andisols and Aluminum-humus complexes for nonallophanic Andisols (Mizota and van Reeuwijk, 1989). Figure 1.2 shows distribution allophanic Andisols that occupy 69.9% of land area of total Andisols in Japan and nonallophanic Andisols (30.1%) (Takahashi and Shoji, 2002; Saigusa and Matsuyama, 1989). As the aggregated soils, Andisols often characterized as dual porosity soil where interaggregate pores and intraaggregate pores are created surrounding the aggregates and within the aggregates, respectively (Miyamoto et al., 2003; Hamamoto et al., 2009b; Chamindu Deepagoda et al., 2012). This aggregation will strongly influence the water flow, solute transport and many processes in Andisols.

Knowledge of soil hydraulic properties is required to analyze water flow and solute transport in the unsaturated zone. The Richards equation, as the standard model to describe water flow in the vadose zone, relies on soil hydraulic properties defined as the constitutive relationships between the volumetric water content,  $\theta$ , the pressure head,  $h$ , and the soil hydraulic conductivity,  $K$ , i.e., the soil water retention,  $\theta(h)$  and the unsaturated hydraulic conductivity,  $K(h)$  or  $K(\theta)$  functions (Durner and Flühler, 2005; and Šimůnek, 2005).

Many investigations on  $\theta(h)$  of Andisols showed unique shape (Miyamoto et al., 2003; Hamamoto et al., 2009a; Hamamoto et al., 2009b; Kato et al., 2011; and Chamindu Deepagoda et al., 2012). They obtained that  $\theta(h)$  of Andisols exhibits stepwise or two subcurves with high water content in a wide range of pressure head (Fig. 1.3a). Based on pore size distribution which consists of two peaks (Fig. 1.3b), Miyamoto et al. (2003) characterized that the first peak at larger pore size represents the existence of interaggregate pores, while the second peak at smaller pore size represents the existence of intraaggregate pores. Figure 1.4 shows schematic diagram representing



water distribution in aggregate soil depending on saturation degree (Miyamoto et al., 2003).

Miyamoto et al. (2003) showed that larger aggregate size of Andisols leads to steeper slope in the first subcurve and smaller air entry region of  $\theta(h)$  (Fig. 1.3a) which is similar to  $\theta(h)$  of sandy soils. Because of capillary hysteresis in interaggregate pores, a hysteretic  $\theta(h)$  might exist at the first subcurve which also similar in sandy soils. To date, quite limited study was carried out to investigate hysteretic water retention of Andisols.

Although the second subcurve of hydraulic properties of Andisols cover in lower pressure head, high water content still remains in this region (Fig. 1.3a). Thus the measurement of hydraulic properties of Andisols until low pressure head is still necessary. However, measurements of  $K(h)$  of Andisols were conducted only limited in high pressure head (Ritter et al., 2004; Fontes et al., 2004). Moreover, because the estimation of  $K(h)$  especially at low pressure head is known the most difficult among soil physical properties, only few effort was conducted to estimate a wide range of  $K(h)$ .

One of the most popular methods for estimating  $K(h)$  is parameter estimation based on the evaporation method (Šimůnek et al., 1998, Hopmans et al., 2002). This method is suitable for intermediate range of pressure heads,  $h >$  about -700 cm. To extend the estimate range of  $K(h)$ , Sakai and Toride (2007) included the water retention data from saturation down to low pressure head in the objective function. This technique might be able to yield reliable estimates for  $K(h)$  until low pressure head and or beyond the measurement range of tensiometers in the evaporation experiment.

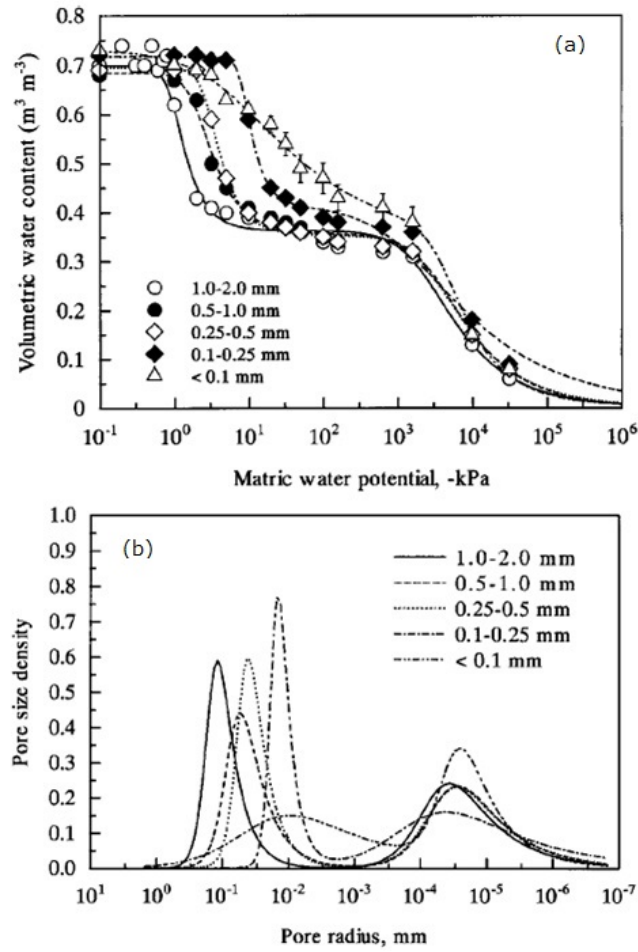


Fig. 1.3. (a) Water retention and (b) pore size density,  $d\theta(h)/d \log_{10} h$  for Andisols with different aggregate size (Miyamoto et al., 2003).

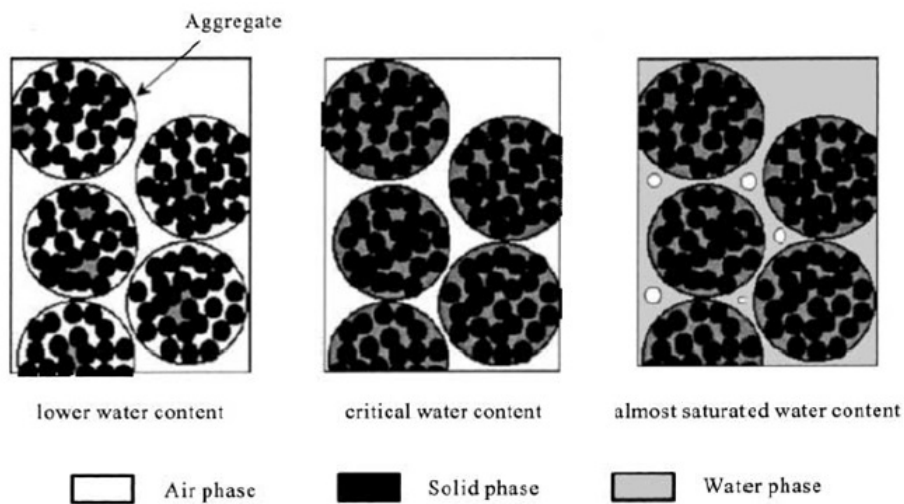


Fig. 1.4. Schematic diagram representing water distribution in aggregate soil depending on saturation degree (Miyamoto et al., 2003).

## 1.2 AIMS OF THE THESIS

- (1) To estimate a wide range of the unsaturated hydraulic conductivity of Andisols based on the evaporation method.
- (2) To observe hysteretic water retention of Andisols and propose a hysteretic model of hydraulic properties for Andisols.
- (3) To numerically evaluate roles of aggregate structure of Andisols in water flow in the root zone layer.

## 1.3 THESIS OUTLINE

Figure 1.5 shows the structure of this thesis and how to read. **Chapter 2** reviews the unique physical properties of Andisols, hydraulic functions for aggregated soils, experimental design and parameter estimation for estimating hydraulic properties especially based on the evaporation method. How to derive the hysteretic model based on Kool and Parker (1987) for the main loop as well as scanning loops was also depicted.

**Chapter 3** describes the determination of a wide range of hydraulic properties of Andisols was conducted inversely using the evaporation method. Different optimized parameter sets and range of pressure head measurements were compared. Moreover, inclusion of a wide range of water retention in the objective function was addressed to extend the applicability of the estimated hydraulic properties until low pressure head was discussed and the results were validated.

**Chapter 4** presents measurement of hysteretic water retention and development of hysteretic water retention model for Andisols. Moreover, the used of hysteretic water retention parameters for predicting non hysteretic unsaturated hydraulic conductivity in term of water content was also discussed.

In **Chapter 5**, the estimated hydraulic properties in **Chapter 3** was used for evaluating the roles of interaggregate and intraaggregate pores of Andisols in the root zone layer based on numerical evaluation of water flow. Infiltration followed by redistribution were conducted and compared in Andisol, sandy loam and clay soils.

Finally **Chapter 6** summarizes the conclusion and the future perspective of the results from this thesis.

## 1 General Introduction

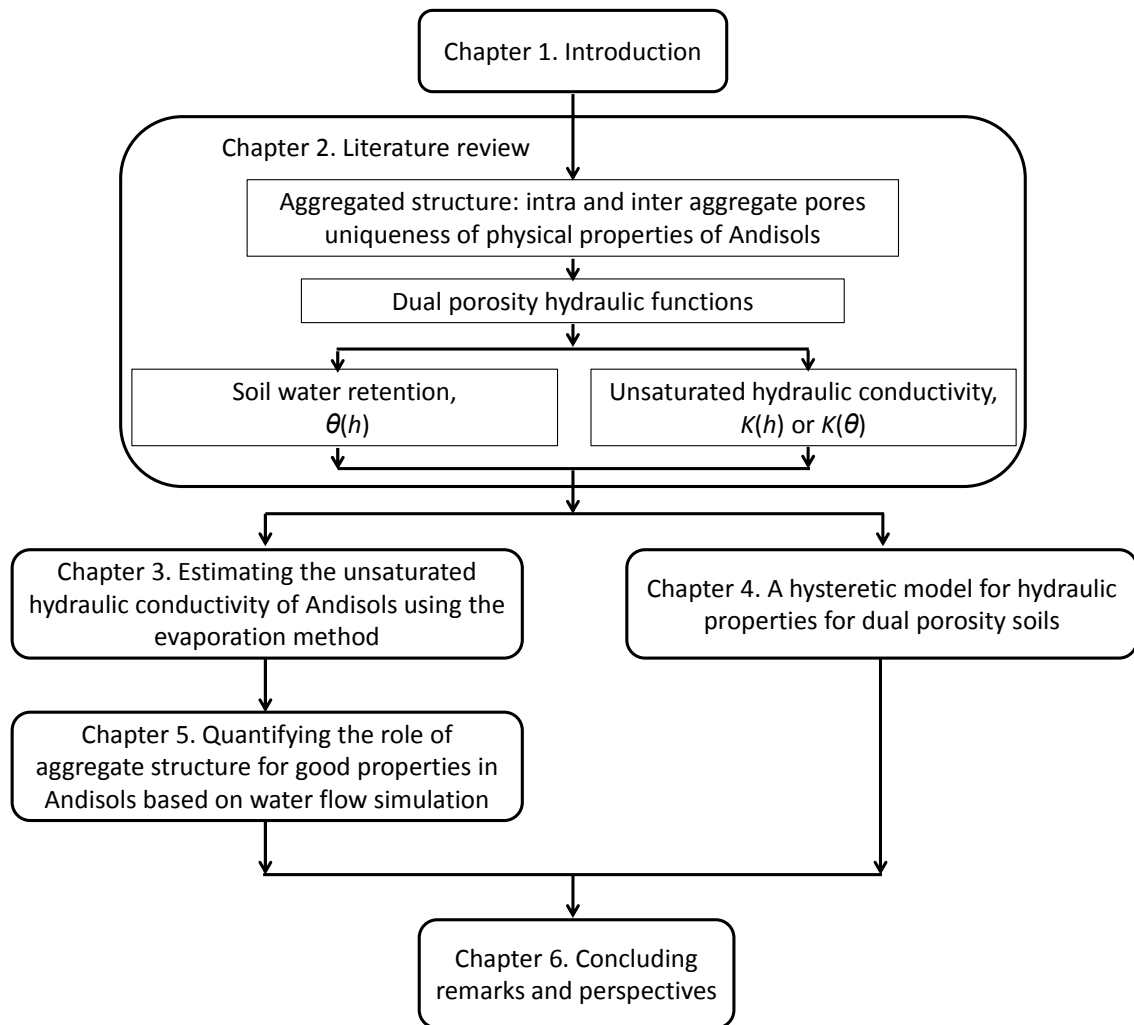


Fig. 1.5. The schematic of thesis outline.

## 1.4 REFERENCES

- Chamindu Deepagoda, T.K.K., P. Moldrup, M.P. Jensen, S.B. Jones, L.W. de Jonge, P. Schjønning, K. Scow, J.W. Hopmans, D.E. Rolston, K. Kawamoto, and T. Komatsu. 2012. Diffusion Aspects of Designing Porous Growth Media for Earth and Space. *Soil Sci. Soc. Am. J.* 76: 1564-1578. doi: 10.2136/sssaj2011.0438
- Dahlgren, R.A., M. Saigusa, and F.C. Ugolini. 2004. The nature, properties and management of volcanic soils. *Adv. Agron.* 82:113-182. doi:10.1016/S0065-2113(03)82003-5
- Durner, W. 1994. Hydraulic conductivity estimation for soils with heterogeneous pore structure. *Water Resour. Res.* 30:211-223. doi:10.1029/93WR02676
- Durner, W., and H. Flühler. 2005. Soil hydraulic properties. *Encyclopedia of Hydrological Sciences*, John Wiley & Sons, Ltd. doi:10.1002/0470848944
- FAO. 1988. *Soil Map of the World. Revised Legend.* Reprinted with corrections. World Soil Resources Report 60. FAO, Rome.
- Fontes, J.C., M.C. Gonçalves, and P.S. Pereira. 2004. Andosols of Terceira, Azores: measurement and significance of soil hydraulic properties. *Catena.* 56:145–154. Special issue (Volcanic soil resources: occurrence, development and properties, Arnalds O, Stahr K, eds). doi:10.1016/j.catena.2003.10.008
- Hopmans, J.W., J. Šimůnek, N. Romano, and W. Durner. 2002. Simultaneous determination of water transmission and retention properties: Inverse methods. p. 963–1008. *In* J.H. Dane and G.C. Topp (ed.) *Methods of soil analysis. Part 4.* SSSA Book Ser. 5. SSSA, Madison, WI.
- Hamamoto, S., K. Seki, and T. Miyazaki. 2009a. Effect of aggregate structure on VOC gas adsorption onto volcanic ash soil. *J Hazard Mater.* 166:207-212. doi:10.1016/j.jhazmat.2008.11.008
- Hamamoto, S., M.S.A.Perera, A.C.Resurreccion, K.Kawamoto, S.Hasegawa, T.Komatsu, and P.Moldrup. 2009b. The solute diffusion coefficient in variably compacted, unsaturated volcanic ash soils. *Vadose Zone J.* 8:942-952. doi:10.2136/vzj2008.0184
- Kato, C., T. Nishimura, H. Imoto, and T. Miyazaki. 2011. Predicting soil moisture and temperature of andisols under a monsoon climate in Japan. *Vadose Zone J.* 10:541-551. doi:10.2136/vzj2010.0054

- Miyamoto, T., T. Annaka, and J. Chikusi. 2003. Soil aggregate structure effects on dielectric permittivity of an andisol measured by time domain reflectometry. *Vadose Zone J.* 2:90-97. doi:10.2136/vzj2003.9000
- Mizota, C., and L. P. van Reeuwijk. 1989. Clay mineralogy and chemistry of soils formed in volcanic material in diverse climatic region. Soil Monograph 2. ISRIC. Wageningen. 185 p.
- Nanzoyo, M., S. Shoji, and R. Dahlgren. 1993. Physical characteristics of volcanic ash soils. In: Shoji, S., M. Nanzoyo, R.A. Dahlgren. Volcanic ash soils: Genesis, properties, and utilization. Elsevier Amsterdam, the Netherlands. p:89-207. doi:10.1016/S0166-2481(08)70268-X
- Nanzoyo, M. 2002. Unique properties of volcanic ash soils. *Glob. Environ. Res.* 6: 99-112.
- Ritter, A., R. C.M. Muñoz-Carpena, M. Regalado, Vanclooster and S. Lambot. 2004. Analysis of alternative measurement strategies for the inverse optimization of the hydraulic properties of a volcanic soil. *J. Hydrol.* 295:124-139. doi:10.1016/j.jhydrol.2004.03.005
- Saigusa, M., and N. Matsuyama. 1998. Distribution of allophanic Andisols and Non-allophanic Andisols in Japan. *Tohoku J. Agr. Res.* 48:75-83
- Šimůnek, J. 2005. Chapter 78: Models of Water Flow and Solute Transport in the Unsaturated Zone, In: M. G. Anderson and J. J. McDonnell (Editors), *Encyclopedia of Hydrological Sciences*, John Wiley & Sons, Ltd., Chichester, England, 1171-1180.
- Shoji, S., M. Nanzoyo, and R. Dahlgren. 1993. Productivity and utilization of volcanic ash soils. In: Shoji, S., M. Nanzoyo, R.A. Dahlgren. Volcanic ash soils: Genesis, properties, and utilization. Elsevier Amsterdam, the Netherlands. p:209-251. doi:10.1016/S0166-2481(08)70269-1
- Shoji, S., and T. Takahashi. 2002. Environmental and agricultural significance of volcanic ash soils. *Glob. Environ. Res.* 6:113-135.
- Soil Survey Staff. 1997. National Soil Survey Handbook. Title 430-VI. U.S. Government Printing Office, 732 N. Capitol Street, NW, Washington, DC 20401.
- Soil Survey Staff. 1999. Soil Taxonomy 2<sup>nd</sup> edition. Agricultural Handbook 436; Natural Resources Conservation Service, USDA, Washington DC, USA, pp. 869.

## 1 General Introduction

Takahashi, T., and S. Shoji. 2002. Distribution and classification of volcanic ash soils.  
Glob. Environ. Res. 6:83-97.

The Third Division of Soils. 1973. Criteria for making soil series and a list of soil series.  
The first approximation. Nat. Inst. Agr. Res., Japan (in Japanese).

## 1 General Introduction



## CHAPTER 2

# LITERATURE REVIEW

### 2.1 UNIQUE PHYSICAL PROPERTIES OF ANDISOLS

Andisols show many unique properties from other mineral soils. One of the uniqueness of Andisols can be seen from physical properties (Nanzyo et al., 1993). The bulk density of Andisols is extremely low ranging from 0.4 to 0.8 g cm<sup>-3</sup> while the general values for mineral soils ranges from 1.2 to 1.8 g cm<sup>-3</sup>. Hence the total porosity of Andisols generally ranges between 0.6 and 0.85 cm<sup>3</sup> cm<sup>-3</sup> which is higher than those in other mineral soils (0.3 to 0.6 cm<sup>3</sup> cm<sup>-3</sup>). In allophanic Andisols, the low bulk density is due to high porosity caused by well-developed high aggregate structures (Fig. 2.1) made of noncrystalline minerals (e.g., allophane, imogolite, ferrihydrite), while for non-allophanic Andisols, accumulation of a large amount of humus lead to highly porous aggregation. The bulk density of Andisols decreases with increasing concentrations of active Al and Fe for allophanic Andisols and humus content for non-allophanic Andisols (Dahlgren et al., 2002; and Nanzyo, 2002). Low bulk density of Andisols provides easy tillage and less energy for root growth (Nanzyo et al., 1993; and Shoji et al., 1993).

Because of well-developed highly aggregated structures made up of noncrystalline minerals, Andisols can retain a lot of amount of water in wide range of pressure head (Nanzyo et al., 1993; Shoji et al., 1993; Nanzyo, 2002) and are often characterized as dual porosity soils (Miyamoto et al., 2003). Water retention of Andisols is consisted of two subcurves which indicate that interaggregate and intraaggregate pores are existed. Allophane greatly contributes to the retention at low pressure because its fine particle-size and hollow spherical structure can accommodate water molecules in both intra- and inter-spherical pores (Nanzyo et al., 1993). These characteristics lead to large plant available water (PAW) (Shoji et al., 1993) which is defined as the difference between 33 kPa water content (or the field capacity) and 1500 kPa water content (or the permanent wilting point). Low bulk density of Andisol yields excellent water storage for root growth which can produce high yields of upland crops.

## 2 Literature review

Blonquist et al. (2006) conceptualized dual porosity system resulted by aggregate structure in dual porosity soils. They outlined five important physical conditions, or stages, of the porous medium as shown in Fig. 2.2: (1) The soil is completely dry. (2) The intra-aggregate pores are partially saturated but the inter-aggregate pores are air filled. (3) At the critical water content,  $\theta_{hc}$  where intraaggregate pores are water saturated and all interaggregate pores are air filled. (4) The intraaggregate pores are water saturated and the interaggregate pores fill with water under gravity, creating a layered system that has water-saturated interaggregate pores at the base and air filled inter-aggregate pores at the top. (5) Both intra and interaggregate pores are water saturated and there is no air in the soil.

High pores structure in Andisols that developed by noncrystalline minerals also yielded increasing both saturated and unsaturated hydraulic conductivity (Nanzyo et al., 1993). Motomura (1979) in Shoji et al. (1993) reported that the saturated hydraulic conductivity of Andisols in wetland rice varies from  $10^{-3}$  to  $10^{-4}$  cm s<sup>-1</sup> and is 10-100 times greater than Gray lowland soils or other paddy soils. For the unsaturated hydraulic conductivity, Hasegawa, (1986); Iwata (1966); and Iwata et al. (1988) in Shoji et al. (1993) showed that Andisols also have higher hydraulic conductivity than other mineral soils such as clayey alluvial soils and red/yellow soils, respectively. High conductivity leads to large drainage rate and good aeration (Shoji et al., 1993) and it will provide favorable condition for optimum growth of upland crop. Conversely, it gives negative impact on paddy field because of percolation of irrigation water and leaching of plant nutrient (Nanzyo et al., 1993).

Soil texture of Andisols which content high allophonic is difficult to analysis because of difficulties in dispersing allophonic soil during particle distribution analysis. Noncrystalline Al and Fe content in Andisols inhibit dispersion of mineral particles (Nanzyo et al., 1993; Fontes et al., 2004). Soil texture may not show a valid meaning for Andisols (Warkentin and Maeda, 1974), for instance: the saturated hydraulic conductivity of Andisols which contain high clay shows higher than  $10^{-4}$  m s<sup>-1</sup>, whereas the hydraulic conductivity of general soils which also contain high clay is lower than  $10^{-6}$  m s<sup>-1</sup> (Iwata et al., 1995).



Fig. 2.1. Andisol from Mie, Japan (Leij et al., 2012).

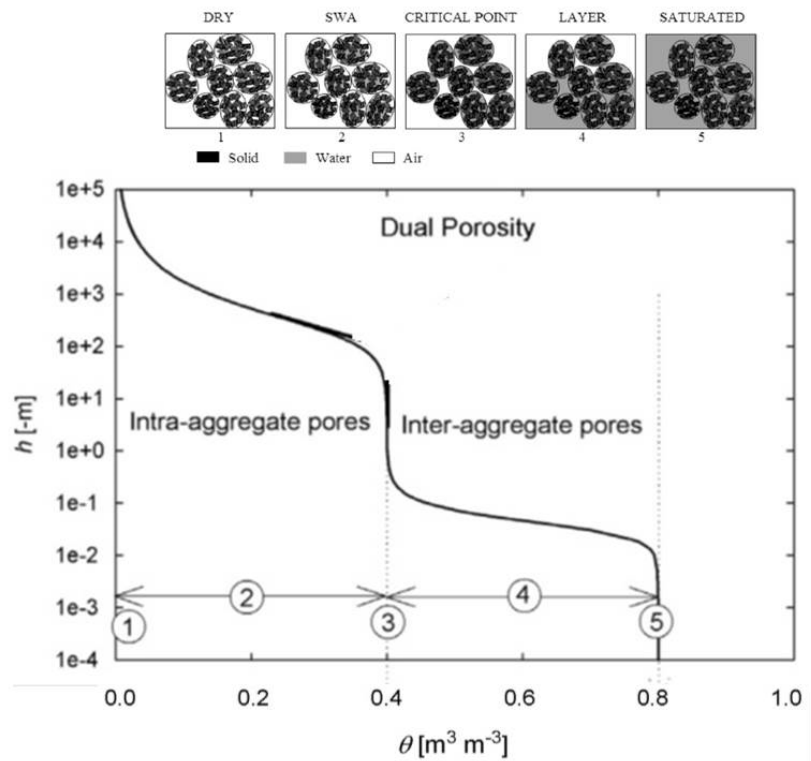


Fig. 2.2. Schematic describing aggregate structure and illustrating the five described physical conditions (stages) of soil water retention (Blonquist et al., 2006).

## 2 Literature review

In environmental issue, the high water storage and high hydraulic conductivity of Andisols also are important to reduce flood during rainy season (Shoji and Takahashi, 2002). High rainfall will be infiltrated rapidly and then some of water stored in its pore and some of water drained quickly. Because of rapid infiltration reduced runoff, stable aggregate and strong resistance of dispersion, Andisols also have a strong resistance on soil erosion (Shoji and Takahashi, 2002). Therefore, almost physical properties of Andisols are excellent for crop production as well as environment protection (Dahlgren, et al., 2004). Those properties strongly contribute to maintaining high productivity of Andisols (Shoji et al., 1993).

### 2.2 UNSATURATED WATER FLOW

When soil is partially saturated, an air phase is existing, and then pressure head in unsaturated soil is negative because of traction to solid surfaces and the surface tension of the air. Consequently the water flow channels are significantly different from those in saturated soil (Jury and Horton, 2004). In head units, the Buckingham-Darcy flux law may be expressed for vertical water flow in unsaturated soils as (Jury and Horton, 2004):

$$J_w = -K(h) \frac{\partial H}{\partial z} = -K(h) \frac{\partial (h+z)}{\partial z} = -K(h) \frac{\partial h}{\partial z} - K(h) \quad [2.1]$$

where  $H = h + z$  is the hydraulic head in unsaturated soil [L],  $K(h)$  is the unsaturated hydraulic conductivity [ $L T^{-1}$ ] and the water flux,  $J_w$  [ $L T^{-1}$ ] is the water flow per unit cross-sectional area per unit time. The first term in the right side,  $-K(h) \partial h / \partial z$  is the capillary flux, that is water flux due to the capillarity, while the second one,  $-K(h)$  is the gravity flux, that is water flux due to the gravity.

Generally, wetting or drying of the soil will occur as water flows, and the matric potential and water content will be functions of time as well as of space. To describe that transient water flow, the water conservation equation, also called the mass balance or continuity equation is used and given by.

$$\frac{\partial J_w}{\partial z} + \frac{\partial \theta}{\partial t} + r_w = 0 \quad [2.2]$$

where  $\theta$  is the volumetric water content [ $L^3 L^{-3}$ ] and  $r_w$  is the sink term (i.e., water uptake of plant roots).

Inserting the Buckingham-Darcy flux law, Eq. [2.1] into the continuity equation Eq. [2.2], and assuming vertical water flow and no plant roots ( $r_w = 0$ ) results in the Richard equation:

$$\frac{\partial \theta}{\partial t} = \frac{\partial}{\partial z} \left[ K(h) \left( \frac{\partial h}{\partial z} + 1 \right) \right] \quad [2.3]$$

where  $\theta$  is the volumetric water content [ $L^3 L^{-3}$ ],  $h$  is the soil water pressure head [ $L$ ],  $K(h)$  is the hydraulic conductivity [ $L T^{-1}$ ],  $t$  is time [ $T$ ];  $z$  is the vertical coordinate [ $L$ ]. Eq. [2.3] may not be solved in the form it is in, because it contains two unknown  $\theta$  and  $h$  in only one equation. Eq. [2.3] can be solved since two boundary conditions and initial condition are specified and  $\theta(h)$  and  $K(h)$  are known.

### 2.3 DUAL POROSITY HYDRAULIC FUNCTIONS

Water retention of aggregated soil such as Andisols exhibits stepwise shape which indicated existing dual porosity system namely inter and intra aggregate pores. The first and second subcurves represent contributions of cumulative water in interaggregate and intraaggregate pores, respectively. The unimodal VG model (van Genuchten, 1980) were reported could not describe soil water retention of aggregated soil properly (Durner, 1994). To overcome limitation of the unimodal VG model, some dual porosity retention functions were proposed which aggregated soils are viewed as consisting of two pore systems, each with its own retention function and interacted instantaneously (i.e., instantaneous equilibrium). Two pore systems are assumed can be described by a linear superposition of each pore size system (Durner, 1992, 1994; Ross and Smettem, 1993; Seki, 2007, Romano et al., 2011).

Durner (1992, 1994) proposed dual porosity retention function, which was built by a linear superposition of two the van Genuchten type (van Genuchten, 1980):

$$S = \frac{\theta(h) - \theta_r}{\theta_s - \theta_r} = w_1 S_1 + w_2 S_2 \quad [2.4]$$

and  $S_i$  is given by

$$S_i = \left[ 1 + (\alpha_i |h|)^{n_i} \right]^{-m_i} \quad [2.5]$$

## 2 Literature review

where  $i$  represent pore system- $i$  ( $= 1$  or  $2$ ),  $w_i$  is the weighing factor subject to  $0 < w_i < 1$  and  $\sum w_i = 1$ . Parameter shapes are  $\alpha_i$ ,  $n_i$  and  $m_i = 1 - 1/n_i$  subject to the conditions  $\alpha_i > 0$  and  $n_i > 1$ . If  $w_i = 0$ , Eq. (1) is equal to be the unimodal VG model. In addition,  $S$  is the effective saturation,  $h$  and  $\theta$  is the pressure head [L] and the volumetric water content [ $L^3 L^{-3}$ ], respectively;  $\theta_s$  and  $\theta_r$  are the saturated and the residual volumetric water content, respectively.

For the unsaturated hydraulic conductivity, the analytical expression of the closed-form between dual porosity retention function (Durner, 1992, 1994) and the Mualem model (1976) is given by (Priesack and Durner, 2006):

$$K(S) = K_s (w_1 S_1 + w_2 S_2)^\ell \frac{\left( w_1 \alpha_1 \left[ 1 - \left( 1 - S_1^{1/m_1} \right)^{m_1} \right] + w_2 \alpha_2 \left[ 1 - \left( 1 - S_2^{1/m_2} \right)^{m_2} \right] \right)^2}{(w_1 \alpha_1 + w_2 \alpha_2)^2} \quad [2.6]$$

where  $K_s$  and  $\ell$  are the saturated hydraulic conductivity [ $L T^{-1}$ ] and the pore connectivity and tortuosity factor [-], respectively. Figure 2.3 shows an example of the bimodal VG (Priesack and Durner, 2006) to describe soil water retention and unsaturated hydraulic conductivity of an aggregated loam soil from Smettem and Kirkby (1990). It can be seen that the characteristic of the unsaturated hydraulic conductivity, Eq. [2.3] is also a superposition of conductivities of two the van Genuchten model that is the same with its soil water retention.

The hydraulic characteristics defined by Eqs. [2.4 – 2.6] contain 9 unknown parameters:  $\theta_r$ ,  $\theta_s$ ,  $\alpha_1$ ,  $n_1$ ,  $\alpha_2$ ,  $n_2$ ,  $w_2$ , (7 retention parameters)  $\ell$ , and  $K_s$  (2 conductivity parameters). Of these,  $\theta_r$ ,  $\theta_s$ , and  $K_s$  have a physical meaning, whereas  $\alpha_1$ ,  $n_1$ ,  $\alpha_2$ ,  $n_2$ ,  $w_2$ , and  $\ell$  are essentially empirical parameters determining the shape of the retention and hydraulic conductivity functions. Afterwards, the bimodal VG model is used to refer the bimodal hydraulic functions in Eqs. [2.4 – 2.6]. Other forms of the bimodal functions can be found in (Ross and Smettem, 1993; Seki, 2007, Romano et al., 2011).

Although the bimodal VG model is widely used for describing water retention of Andisols and showed excellent results for an entire range of pressure heads as reported in many studies (Miyamoto et al., 2003; Hamamoto et al., 2009; Kato et al., 2011; and Chamindu Deepagoda et al., 2012), the application of the bimodal VG model for unsaturated hydraulic conductivity of Andisols is still limited.

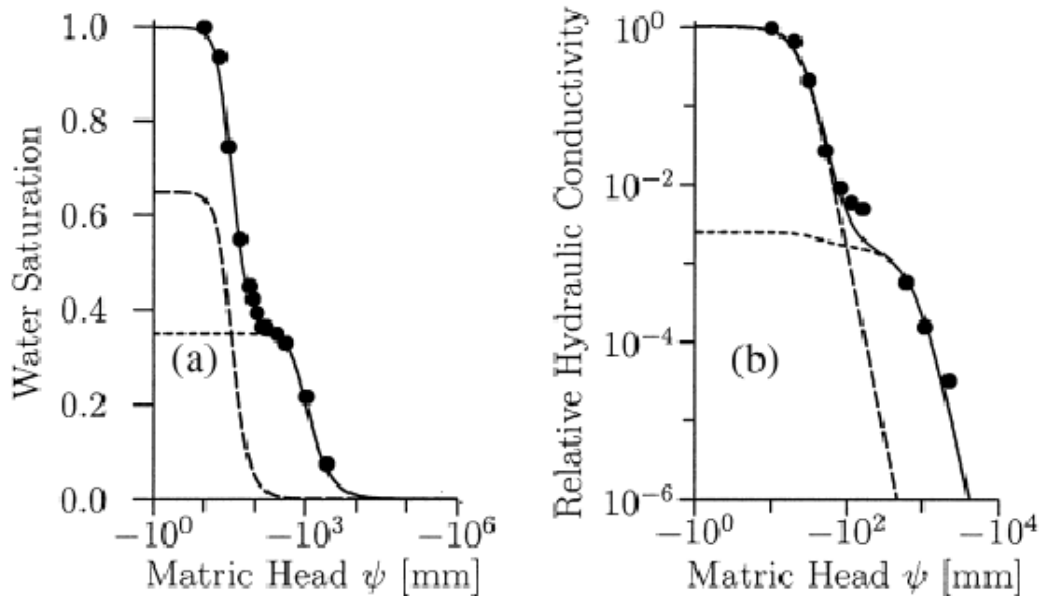


Fig. 2.3. Illustrations of the bimodal VG model for soil water retention and unsaturated hydraulic conductivity. Solid lines represent the total retention and conductivity curve, while the dash lines refer to the subcurves (Priesack and Durner, 2006).

## 2.4 WATER RETENTION CURVE MEASUREMENT

Water retention curve shows the relationship between water content and pressure head. Water content can be measured directly using the gravimetric method by placing the sample in a convection oven at  $105^\circ\text{C}$  for 24 h (Jury and Horton, 2004). For pressure heads from water saturated soil to very dry soil, several methods can be used depend on range of pressure heads.

A hanging water column is for range about  $-200 \text{ cm} < h < 0$ . Since contact between the samples and the porous ceramic is good and water content of the samples is still high, equilibrium will be reached rapidly (i.e., 24 hours) (Jury and Horton, 2004). Then, a pressure plate is generally for range about  $-15000 \text{ cm} < h < \text{about } -200 \text{ cm}$ . Since, this porous plate has a very high flow resistance due to a fine-pored porous plate; it might take time to equilibrate. Thus, the time of equilibrium is difficult to estimate (Jury and Horton, 2004). The loss of hydraulic contact between the samples and the plate is major source of error in the pressure plate method (Cresswell et al., 2008; Bittelli and Flury, 2009). For  $h < -15000 \text{ cm}$ , equilibration over saturated salt solutions

can be used (Jury and Horton, 2004). However, lack of equilibrium will result in errors in water potential measurements (Scanlon et al., 2002; Jury and Horton, 2004).

Recently, the Dew Point Potentiometer (WP4) (Decagon Devices, Inc., Pullman, WA) was widely used for  $-3 \times 10^6 \text{ cm} < h < -1 \times 10^4 \text{ cm}$ . The WP4 measures the vapor pressure,  $p$  of the air using a chilled mirror, and computes the saturation vapor pressure,  $p_o$ , of the sample from its temperature. Subsequently, the sample water potential ( $\psi$ , Pa) is calculated using (Scanlon et al., 2002):

$$\psi = \frac{RT}{M} \ln \frac{p}{p_o} \quad [2.7]$$

where  $p$  is the vapor pressure of the air,  $p_o$  is the saturation vapor pressure at sample temperature,  $R$  is the gas constant ( $8.314 \text{ J mol}^{-1} \text{ K}^{-1}$ ),  $T$  is the Kelvin temperature of the sample, and  $M$  is the molecular mass of water ( $1.8 \times 10^{-5} \text{ m}^3 \text{ mol}^{-1}$ ). The ratio between  $p$  and  $p_o$  is the equilibrium relative humidity, that is, the relative humidity of the air space in equilibrium with soil under isothermal conditions in a sealed container.

The WP4 measures water potential in very short time (i.e., 5 to 10 minutes). The accuracy is 1% from  $-3 \times 10^3 \text{ cm}$  to  $-3 \times 10^6 \text{ cm}$ . Therefore, the WP4 is known as a very robust instrument that is fast, accurate and easy laboratory measurements of water potential (Scanlon et al., 2002). Maček et al. (2013) could extend range of the WP4 to the higher pressure heads up to approximately  $-3 \times 10^3 \text{ cm}$  with considerable care.

## **2.5 ESTIMATION OF UNSATURATED HYDRAULIC CONDUCTIVITY BASED ON THE PARAMETER ESTIMATION**

### **2.5.1 Inverse method for unsaturated hydraulic conductivity**

The parameters of soil hydraulic functions can be determined by either fitting the observed soil hydraulic data from the direct method or fitting the processes of water flow such as cumulative flux, pressure head change or water content change through the inverse method. Generally, measurement of soil hydraulic data using the direct method is more difficult than measurement of processes in transient flow experiment of the inverse method where it can be conducted much more flexibility in experimental boundary condition (Hopmans et al., 2002). The transient water flow experiments that commonly used in the inverse method are the multistep and the evaporation method for



high pressure and intermediate range of pressure head, respectively (Hopmans et al., 2002; Schelle et al., 2010). Moreover, the inverse method can estimate simultaneously water retention and hydraulic conductivity (Hopmans et al., 2002). Therefore, the inverse method becomes more popular than the direct method.

Basically, four components are required in the inverse method in order to estimate soil hydraulic functions (Hopmans et al., 2002; Minasny and Field, 2005): (1) the governing equation to simulate water flow, (2) parameters of hydraulic functions to describe  $\theta(h)$  and  $K(h)$  curves, (3) the objective function to account deviation between output of water flow model and the measured the processes of water flow (e.g., pressure head, water content or cumulative flow as a function of time); and (4) the optimization procedure to optimize parameters of hydraulic functions by minimization of the objective function. Figure 2.4 shows the schematic of the measurement, modeling and optimization for the inverse method.

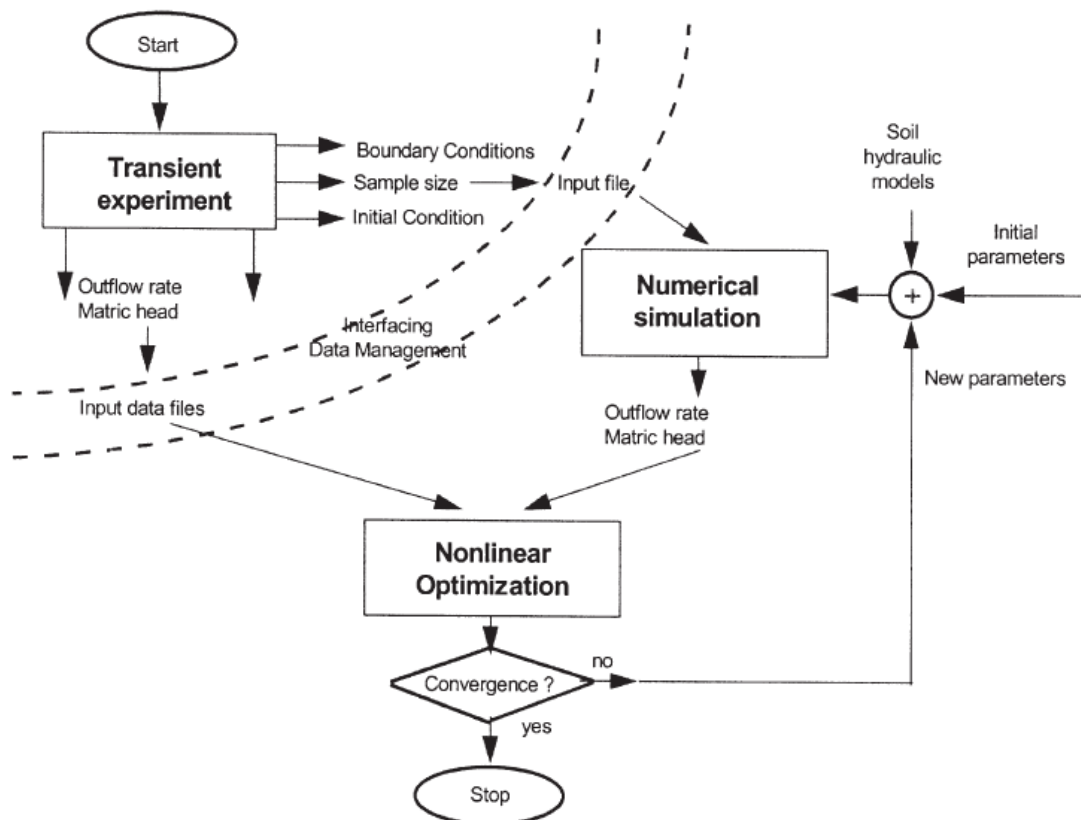


Figure 2.4. Flow chart of the inverse method illustrating the integration of measurement, modeling, and optimization (Hopmans et. al, 2002).

## 2 Literature review

Hopmans et al. (2002) pointed out that the success of the inverse method depends on suitability and quality of three factors: (1) the experimental design, that is, the choice of boundary condition, the location and time resolution of the measurement sensor and the degree of accuracy of the experimental data; (2) the suitability of the transient flow model and hydraulic functions; and (3) the robustness of the optimization algorithm. If any of these three components is unsatisfactory, the inverse method may diverge.

One dimensional vertical variably saturated water flow in soil is usually described using the Richard equation, Eq. [2.3]. The Richard equation had been frequently used in the inverse modeling and showed successfully (Šimůnek et al., 1998; Zurmühl and Durner, 1998; Romano and Santini, 1999; Minasny and Field, 2005). Hydrus 1D as a software of the inverse method implements the Richard equation as governing equation of water flow (Šimůnek et al., 2008).

To solve the Richard equation, soil hydraulic functions are required. A proper soil hydraulic function is very important in the inverse method. Unsuitable soil hydraulic functions will lead to inaccurate parameters or even divergence. Most hydraulic functions assume that the predictive  $K(h)$  is coupled water retentions with the Mualem model (Hopmans et al, 2002). They also pointed out that number and correlation of hydraulic parameters will affect on selection of optimized parameters as well as success of the inverse method.

The objective function that describes discrepancy between the observed and fitted the processes flow is minimized by the optimization procedure. Šimůnek and Hopmans (2002) discussed more detail several formulations for the objective function. The weighted least square problem commonly is used for formulation of the objective function (Šimůnek and Hopmans, 2002; Hopmans et al, 2002) given by:

$$\phi(\beta, y) = \sum_{j=1}^{j=m_y} v_j \sum_{i=1}^{i=n_j} w_{i,j} [y_j^*(z, t_i) - y_j(z, t_i, \beta)]^2 \quad [2.8]$$

where the right-hand side represents the residuals between the measured ( $y_j^*$ ) and model predicted ( $y_j$ ) space–time variables using the soil hydraulic parameters of the optimized parameter vector,  $\beta$ . The first summation describes sums the residual for all measurement of type of flow parameter  $m_y$ , whereas the variable  $n_j$  in the second summation denotes the number of measurements for a certain measurement type  $j$ . The

weight  $v_j$  is used for normalization of the type of flow parameter. It is usually set to be a variance those type flow parameter. Another weigh  $w_{ij}$  is used for the individual measured data.

Generally, not only flow processes of pressure head measurements but also water volume should be included in the objective function. Only one value of the water volume is needed in the objective function in order to position the retention curve along the  $\theta$  axis. Without this information, neither  $\theta_s$  or  $\theta_r$  can be estimated because of their mutual correlation (Šimůnek et al., 1998). Hydrus 1D provides almost all types of the water flow processes can be included in the objective function (e.g., pressure head and water content as a function of time, cumulative flux, independent measurement data of soil hydraulic properties, etc.) (Šimůnek et al., 2008).

The optimization procedure is used to optimize the hydraulic parameters by minimizing the objective function. Several methods were proposed as the optimize procedure and work iteratively (Šimůnek and Hopmans, 2002). The Marquardt–Levenberg method (Marquardt, 1963) is known a very effective method, which has become a standard in nonlinear least square fitting among soil scientists and hydrologists (van Genuchten, 1981; Kool et al., 1985, 1987). This method gives a confidence interval of the parameter solution. However, this method requires good starting estimation to obtain a convergence (Minasny and Field, 2005). Hydrus 1D implemented this method as the optimization procedure (Šimůnek et al., 2008).

The general problem about  $\theta_r$  in the inverse method was reported. Šimůnek et al. (1998) obtained that the optimized  $\theta_r$  is high uncertainty due to intermediate range of pressure head measurements in the inverse method. van Dam et al. (1994) recommended that  $\theta_r$  should not optimized, since the maximum pressure that applied in outflow experiment is about -1000 cm, because  $\theta_r$  refers to lower pressure head. van Dam et al. (1994), Šimůnek et al. (1998) and Schelle et al. (2010) recommended to include water content at low pressure head or directly residual water content in the objective function.

Extrapolation beyond the range of measurement from tensiometer reading does not guarantee accurate estimates because of a high level uncertainty (Šimůnek et al., 1998; Minasny and Field, 2005). Inclusion of independently measured information

beyond the measurement range, i.e., water contents at some high suction, or directly the residual water content, could greatly decrease this uncertainty.

Detail review on the inverse method for estimating soil hydraulic properties can be found in (Kool et al., 1987). Recently, Hopmans et al. (2002) also discussed more detail on guidance for not only how to perform the inverse method but also some transient water flow experiments.

### 2.5.2 Estimation of the bimodal VG model using the inverse method

Although the bimodal VG model was introduced in 1994, the first investigation of estimation of the bimodal VG parameters using the inverse method was performed in 1998 by Zurmühl and Durner. They conducted the multistep method as transient water flow experiment and analyzed whether  $\theta(h)$  and  $K(h)$  parameters of the bimodal VG model can be identified by the inverse method or not, because the bimodal VG model has large number of parameters. They concluded that the parameters can be identified if the bimodality of the pore system is well developed due to uncorrelated parameters. It means that the increased number of parameters does not impose problems in the inverse method. Moreover, from the experimental data, they also showed it is possible to determine the bimodal VG model parameters from the multistep outflow experiment, inversely.

Subsequently, Spohrer et al. (2006) determined  $\theta(h)$  and  $K(h)$  for the bimodal VG parameters for a tropical Acrisol using the inverse method of the transient flow experiment (TFE) from four layer soils in the field. They involved five variables, (1) water content change ( $\theta$  vs  $t$ ), (2) pressure head change ( $h$  vs  $t$ ), (3) soil water retention ( $h$  vs  $\theta$ ), (4)  $K(h)$  at  $h=-2\text{cm}$  and (5)  $\theta$  at  $pF=4.2$  from the pedotransfer function in the objective function. The initial values of estimation for  $\theta(h)$  were from fitted measured  $\theta(h)$ . The initial estimation for  $K_s$  and  $\ell$  were obtained from matching  $K$  at  $h = -2\text{cm}$  and trial error values, respectively. As a result, they succeed to estimate 25 parameters of the bimodal VG simultaneously. They obtained that the bimodal VG model can describe well the measured  $\theta(h)$ . The optimized  $K(h)$  matched well with  $K(h)$  from the instantaneous profile method. A good simulation result of TFE was also achieved. The optimized  $K_s$  of the bimodal VG model showed realistic result.

Schwärzel and Punzel (2007) used the bimodal VG model in the inverse method of the hood infiltrometer. They showed that the bimodal VG model could improve the agreement of observed and fitted water content change compared with the unimodal VG model. It indicated the bimodal VG model can describe hydraulic function near saturated, properly.

Recently, Schelle et al. (2010) estimated the bimodal VG parameters for sandy soil using the multistep outflow. They obtained the bimodal VG model was able to describe contribution of not only capillary flow but also film flow on the unsaturated hydraulic conductivity of sand soil. Kato et al. (2011) presented the estimation of the bimodal VG parameters for Andisol based on the evaporation method and then they used the estimation for prediction of the dynamic water flow as well as temperature transport in the field. They obtained that modification of the estimation of  $\theta_s$  and a weighing factor,  $w_2$  were needed to improve the prediction of soil moisture and temperature in Andisols.

Most applications of the bimodal VG were concerned with improved descriptions of the unsaturated conductivity function near saturation in attempts to account for the effects of macropores (Zurmühl and Durner, 1998; Iden and Durner, 2007; Durner and Iden, 2011). Very few studies have applied the bimodal VG model to the unsaturated hydraulic conductivity function of aggregated soils. Moreover, optimization of the large number of parameters in the bimodal VG model still becomes a major challenge.

### 2.5.3 Soil evaporation experiment

One of the most popular of the transient water flow experiments for the inverse method in the laboratory is soil water evaporation experiment. The evaporation method can estimate hydraulic functions for intermediate range of pressure head (Hopmans et al., 2002). Generally, the evaporation method can produce soil hydraulic functions for  $h > -700$  cm which is the range of tensiometer reading. Recently, Schindler et al. (2010) could extend the measurement range till about -4000 cm of pressure head using interpolation from air entry value (AEV) of tensiometers porous ceramic caps.

Associated with the design of the evaporation experiment, Šimůnek et al. (1998) evaluated the number of tensiometers in the evaporation method. They found that one tensiometer is adequate to guarantee precise estimation of the soil hydraulic function

within measurement range. According to their sensitivity analysis, the tensiometer at closer to the soil surface exhibits a higher sensitivity to the inverse method than deeper locations. The sensitivity increases with progress of time. They also concluded that two stages of the evaporation rate did not show any benefits compared with a single rate, expect for accelerating the experiment.

Romano and Santini (1999) performed sensitivity analysis from the numerical evaporation experiments to evaluate experimental design of the evaporation method. They showed: (1) The height of soil sample does not affect the sensitivities of pressure head to the different parameters of the soil hydraulics functions; (2) The more identifiable the soil hydraulic parameters can be achieved by steeper hydraulic gradient which can be taken at greater times. Furthermore, they used the response surface to analyze the effect of the evaporation rate. They suggested that the higher evaporation rate may lead to divergent result in the inverse method for fine-textured soil. Conversely, for coarse textured soil, the higher evaporation rate produces better convergence in the inverse method.

A smooth function is important to reduce the weighing errors on the calculation of evaporation rate and to allow extending the weighing interval. To obtain a smooth function of the evaporation rate for except of sandy soils, Schindler and Muller (2006) used a linear function on fitting water loss by evaporation. For sand soils, they suggested using a quadratic function. Subsequently, Schindler et al. (2010) applied a quadratic function for all soils.

## **2.6 HYSTERETIC HYDRAULIC PROPERTIES**

### **2.6.1 Hysteretic model for soil water retention**

Soil water retention can be obtained from two ways: (1) desorption where saturated soil is gradually dried by decreasing pressure head and (2) sorption where dry soil sample is gradually wetted by increasing pressure head (Radcliffe and Šimůnek, 2010). Soil water retentions from these ways are not unique where water content of desorption (drying) is higher than sorption (wetting) at the same pressure head. This dependence of the equilibrium content and state of soil water upon the direction processes which is called hysteresis (Hilel, 2002). Figure 2.5 presents a typical hysteresis for single porosity of soil water retention curve. All soil water retention data

are enclosed within a main hysteresis loop, consisting of the main drying curve (MDC) and the main wetting curve (MWC).

Hysteresis occurs because of several factors such as (Hopmans and Dane, 1986; Hilel, 2002; Jury and Horton, 2004): (1) the geometric non uniformity of individual pores which produces the ink-bottle effect, (2) entrapped air which has a different volume during wetting and drying process, (3) the difference contact angle between an advancing and a receding liquid front over a solid surface or the rain drop effect. The schematic of the ink-bottle effect and the rain drop effect are shown in Fig. 2.6.

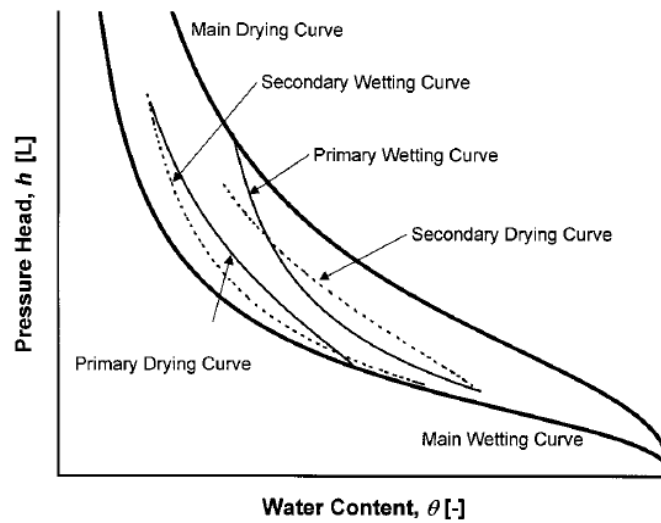


Fig. 2.5. Hypothetical hysteresis for water retention curve of single porosity soil: main, primary, and secondary wetting and drying curves departing from the main wetting and the main drying curves (Šimůnek et al., 1999).

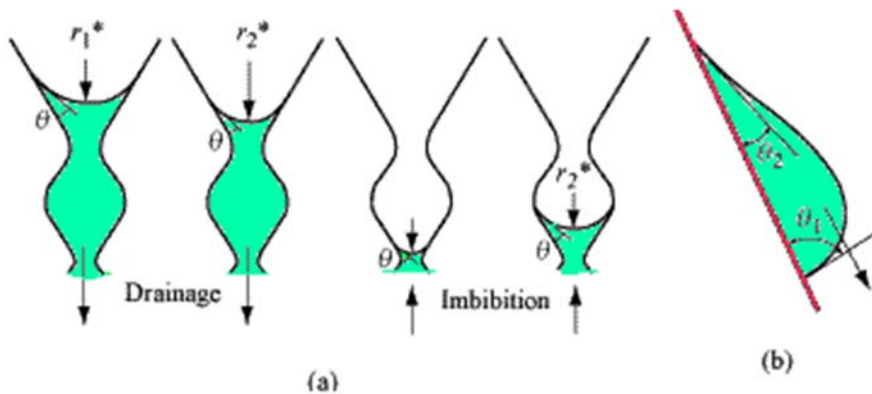


Fig. 2.6. (a) Ink bottle and (b) raindrop effects

([http://www.interpore.org/reference\\_material/mgfc-course/mgfcunsdis.html](http://www.interpore.org/reference_material/mgfc-course/mgfcunsdis.html))

The neglect of hysteresis will lead to highly inaccuracy in soil water flow with composite process where wetting and drying process occur simultaneously (Lenhard et al., 1991; Hillel, 2002) especially on the mass balance. Therefore, considerable efforts to develop hysteretic models that can be included in water flow modeling have been conducted. The historical development of hysteretic models can be found in (Pham et al. 2005).

The various hysteretic models to describe soil water retention can be grouped into two categories: physical model based on the domain theory of capillary hysteresis and an empirical model that produces the scanning loops according to the scale from known main drying and wetting curve. Kool and Parker (1987) showed that the dependent domain models (physical models) are probably most accurate; however, these models may not be easy to apply in the numerical code. Conversely, the empirical models are more simple and easier to implement in the numerical code (Kosugi et al., 2002). Thus, some programs of water flow incorporate the empirical model. For instance, Hydrus 1D, 2D/3D apply the empirical model of hysteresis from Kool and Parker (1987) that was modified from Scott et al. (1983) to account the air entrapment.

The main hysteresis loops of Kool and Parker (1987) is assumed that main draying and wetting retention curves can be described by the unimodal VG model (van Genuchten, 1980):

$$S(h) = \frac{\theta(h) - \theta_r}{\theta_s - \theta_r} = \left[ 1 + |\alpha h|^n \right]^{-m} \quad [2.9]$$

where,  $S$  is the effective saturation;  $\theta(h)$  the volumetric water content [ $L^3 L^{-3}$ ];  $h$  is pressure head [ $L$ ];  $\theta_s$  and  $\theta_r$  are the saturated and residual water content, respectively;  $\alpha$  [ $L^{-1}$ ] and  $n$  are the curve shape parameters, and  $m=1-1/n$ . We denote the main draying curve,  $\theta(h)$  by  $\theta^d(h)$  and the main wetting curve by  $\theta^w(h)$ . Parameters sets are  $(\theta_s^d, \theta_r^d, \alpha^d, n^d)$  and  $(\theta_s^w, \theta_r^w, \alpha^w, n^w)$  for the main drying and wetting curves, respectively. To simplify, we assume  $\theta_r^d = \theta_r^w = \theta_r$  and  $\theta_s^d = \theta_s^w = \theta_s$  which mean the main hysteresis loop is closed at both residual and saturation water content. Furthermore,  $n^d = n^w = n$ . Therefore the parameter sets differ only for  $\alpha^w > \alpha^d$  and then the number of parameters reduces from eight to five. Figure 2.7 displays the main hysteresis loop based on the Kool and Parker model.



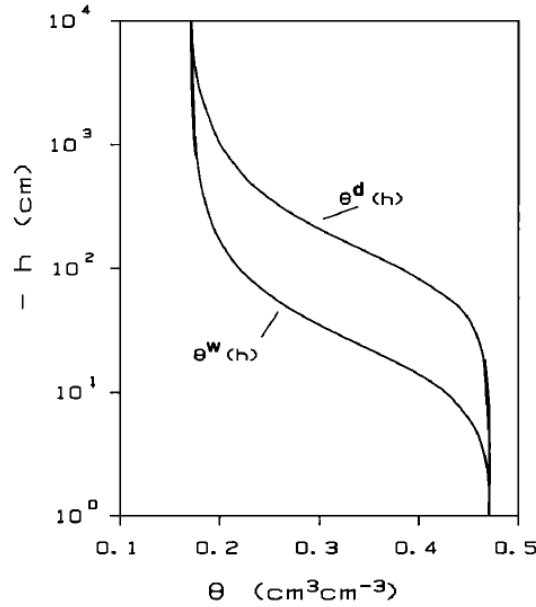


Fig. 2.7. Main hysteresis loop based on the Kool and Parker model with  $n^d = n^w = n$ ,  $\alpha^w > \alpha^d$ ,  $\theta_r^d = \theta_r^w = \theta_r$  and  $\theta_s^d = \theta_s^w = \theta_s$  (Kool and Parker, 1987)

The prediction of scanning curves in the  $\theta(h)$  is calculated using an empirical scaling model (Scott et al., 1983; Kool and Parker, 1987). Figure 2.8 shows the scheme how to obtain the scanning curves based on the scaling method. Drying scanning curves (DSC) are scaled from the main drying curve (MDC), whereas wetting scanning curves (WSC) are scaled from the main wetting curve (MWC).

A drying scanning curve beginning at a reversal point  $(\theta_\Delta, h_\Delta)$  is scaled from the MDC (see Fig. 2.8a). Assuming that the DSC under the consideration merges with the MDC at the residual water content,  $\theta_r$ , thus  $\theta_r^d = \theta_r$ . The DSC differs from the MDC only for the saturated water content. If the DSC passes through the reversal point  $(\theta_\Delta, h_\Delta)$ , then the fictitious saturated water content,  $\theta_s^*$  that replaces  $\theta_s$  in the MDC is calculated by (Kool and Parker, 1987 and Kosugi et al., 2002):

$$\frac{\theta^d(h_\Delta) - \theta_r^d}{\theta_s^d - \theta_r^d} = S^d(h_\Delta) = \frac{\theta_\Delta - \theta_r}{\theta_s^* - \theta_r} \quad [2.10]$$

Eq. [2.18] can be rearranged as:

$$\theta_s^* = \frac{\theta_\Delta - \theta_r [1 - S^d(h_\Delta)]}{S^d(h_\Delta)} \quad [2.11]$$

## 2 Literature review

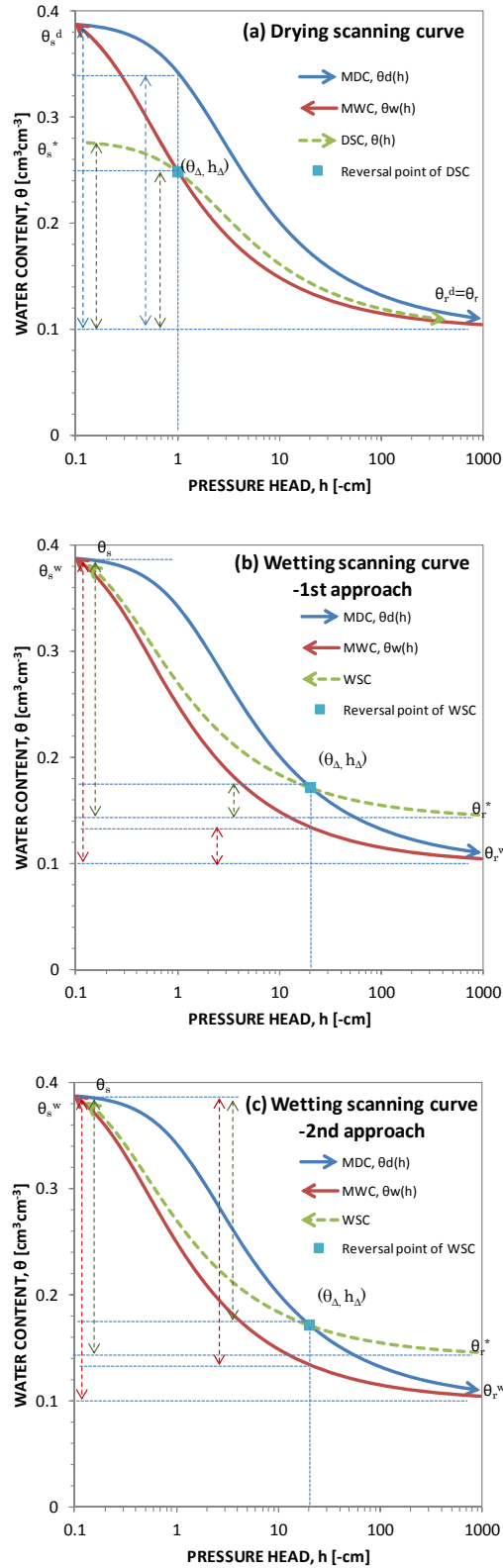


Fig. 2.8. Prediction of (a) the drying and (b and c) the wetting scanning curves based on the scaling method of the Kool and Parker model. Adaption from Kroes et al. (2009)

## 2 Literature review

The relationship between  $\theta$  and  $h$  for the DSC that passes through the reversal point  $(\theta_\Delta, h_\Delta)$  is given by

$$\frac{\theta(h) - \theta_r}{\theta_s^* - \theta_r} = S^d(h) \quad [2.12]$$

Note that Eq. [2.12] is the same with the MDC if the reversal point  $(\theta_\Delta, h_\Delta)$  is equal to  $(\theta_s, 0)$ .  $S^d(h)$  is calculated using Eq. [2.9].

Similarly, a wetting scanning curve (WSC) is scaled from the MWC (see Fig. 2.8b). The WSC beginning at a reversal point  $(\theta_\Delta, h_\Delta)$  differs from the MWC only at the residual water content,  $\theta_r$  and closes at  $\theta_s$ . The WSC passes through the reversal point  $(\theta_\Delta, h_\Delta)$ , the fictitious residual water content,  $\theta_r^*$  that replaces  $\theta_r$  in the MWC is calculated by (Kool and Parker, 1987 and Kosugi et al., 2002):

$$\frac{\theta^w(h_\Delta) - \theta_r^w}{\theta_s^w - \theta_r^w} = S^w(h_\Delta) = \frac{\theta_\Delta - \theta_r^*}{\theta_s - \theta_r^*} \quad [2.13]$$

Rearrange:

$$\theta_r^* = \frac{\theta_\Delta - \theta_s S^w(h_\Delta)}{1 - S^w(h_\Delta)} \quad [2.14]$$

The relationship between  $\theta$  and  $h$  for the WSC is given by

$$\frac{\theta(h) - \theta_r^*}{\theta_s - \theta_r^*} = S^w(h) \quad [2.15]$$

Note that Eq. [2.15] is the same with the MWC if the reversal point  $(\theta_\Delta, h_\Delta)$  is equal to  $(\theta_r, -\infty)$ .  $S^w(h)$  is calculated using Eq. [2.9].

Šimůnek et al. (2008) used different approaches to derive the DSC and WSC of (Kool and Parker, 1987). Scaling equation for the drying scanning curve is given by:

$$\theta(h) = \theta_r^* + \alpha_\theta [\theta^d(h) - \theta_r^d] \quad [2.16]$$

where  $\theta^d(h)$  is the main drying curve and  $\theta(h)$  is the drying scanning curve. Scaling factor,  $\alpha_\theta$  is unknown and should be determined. By assuming

$$\theta_r^* = \theta_r^d \quad [2.17]$$

Substituting the reversal point,  $(\theta_\Delta, h_\Delta)$  into Eq. [2.16]:

$$\theta_\Delta = \theta_r^d + \alpha_\theta [\theta^d(h_\Delta) - \theta_r^d] \quad [2.18]$$

We obtain

## 2 Literature review

$$\alpha_{\theta} = \frac{\theta_{\Delta} - \theta_r^d}{\theta^d(h_{\Delta}) - \theta_r^d} \quad [2.19]$$

If we substitute Eq. [2.19] into Eq. [2.16] yield:

$$\frac{\theta^d(h_{\Delta}) - \theta_r^d}{\theta^d(h) - \theta_r^d} = \frac{\theta_{\Delta} - \theta_r^*}{\theta(h) - \theta_r^*} \quad [2.20]$$

At  $h = 0$  (saturation),  $\theta^d(h) = \theta_s^d$  and  $\theta(h) = \theta_s^*$ . If  $\theta_r^* = \theta_r^d$ , Eq. [2.20] will be identical with Eq. [2.10].

Scaling equation for the wetting scanning curve (Šimůnek et al., 2008) is following:

$$\theta(h) = \theta_r^* + \alpha_{\theta} [\theta^w(h) - \theta_r^w] \quad [2.21]$$

where  $\theta^w(h)$  is the main wetting curve and  $\theta(h)$  is the wetting scanning curve. The  $\theta_r^*$  and  $\alpha_{\theta}$  are unknown and should be determined. A reversal point at  $(\theta_{\Delta}, h_{\Delta})$  is substituted into Eq. [2.21]:

$$\theta_{\Delta} = \theta_r^* + \alpha_{\theta} [\theta^w(h_{\Delta}) - \theta_r^w] \quad [2.22]$$

and the saturation point at  $(\theta_s, h = 0)$  for wetting scanning curve and the saturation point at  $(\theta_s^w, h = 0)$  for the main wetting curve, substituting these points to Eq. [2.22] results in:

$$\theta_s = \theta_r^* + \alpha_{\theta} [\theta_s^w - \theta_r^w] \quad [2.23]$$

To obtain  $\alpha_{\theta}$ ,  $\theta_r^*$  is eliminated by subtracting Eq. [2.23] from Eq. [2.22], we obtain

$$\alpha_{\theta} = \frac{\theta_{\Delta} - \theta_s}{\theta^w(h_{\Delta}) - \theta_s^w} \quad [2.24]$$

After  $\alpha_{\theta}$  is known,  $\theta_r^*$  can be calculated from Eq. [2.24]:

$$\theta_r^* = \theta_s - \alpha_{\theta} [\theta_s^w - \theta_r^w] \quad [2.25]$$

If there is no air entrapment  $\theta_s = \theta_s^w$ . If air entrapment affect, the main loop will be not closed at saturation:  $\theta_s^w < \theta_s < \theta_s^d$ , Kool and Parker (1987) approximated  $\theta_s$  based on C. S. Land formulation (Aziz and Settari, 1979):

$$\theta_s = \theta_s^d - \frac{\theta_s^d - \theta_{\Delta}}{1 + R(\theta_s^d - \theta_{\Delta})} \quad [2.26]$$

with

## 2 Literature review

$$R = \frac{1}{\theta_s^d - \theta_s^w} - \frac{1}{\theta_s^d - \theta_r^d} \quad [2.27]$$

Substituting Eq. [2.24] into Eq. [2.21] lead to:

$$\frac{\theta_s^w - \theta^w(h_\Delta)}{\theta_s^w - \theta_r^w} = \frac{\theta_s - \theta_\Delta}{\theta_s - \theta_r^*} \quad [2.28]$$

Eq. [2.28] will be equal to the scaling scheme in the Fig. 2.7c. If we added  $(\theta_s^w - \theta_r^w)/(\theta_s^w - \theta_r^w)$  at the left side and  $(\theta_s - \theta_r^*)/(\theta_s - \theta_r^*)$  at the right side, it will be equal to Eq. [2.13]. It showed that there are two approaches of the scaling method to derive the DSC and the WSC which give identical results. For the DSC, Eq. [2.12] is identical with Eq. [2.16]. Eq. [2.15] is equal to Eq. [2.21] for the MWC.

The scanning curve based on the scaling method of Kool and Parker (1987) does not yield closed scanning loops, leading as a result to an artifact of a pumping effect, when pressure head undergoes cyclic changes of increase and decrease (Huang et al., 2005; Werner and Lockington, 2006; and Mualem and Beriozkin, 2009) as shown in Fig. 2.9. To avoid the artifact of a pumping effect, Parker & Lenhard (1987) and Huang et al. (2005) forced closure of the scanning loops. The main drawback of the above scaling models is that the calculated drying scans are parallel to the main drying curve in the range of the air entry capillary pressure, displaying as a result significant discrepancies from the experimental data (Mualem and Beriozkin, 2009).

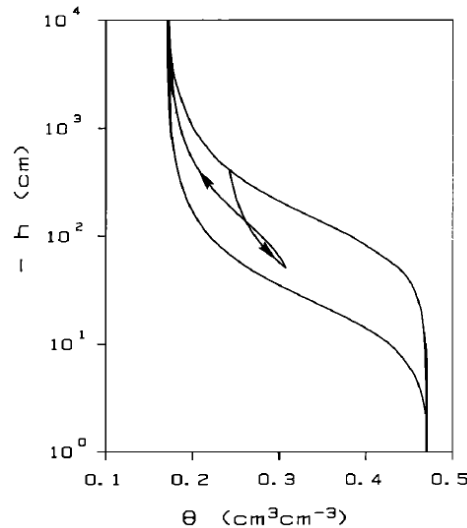


Fig. 2.9. Illustration of pumping effect on the scanning curve resulted in by the Kool and Parker model where the secondary drying unclosed with the reversal point of primary wetting curve (Kool and Parker, 1987).

### 2.6.2 Unsaturated hydraulic conductivity

If measurement results of water retention exhibit hysteresis, conversely, the relationship of experimental data for the unsaturated hydraulic conductivity and water content,  $K(\theta)$  show non hysteretic (Plagge et al., 2005; Mualem, 1986). The unsaturated hydraulic conductivity is generally predicted from soil water retention using the Mualem model. The closed form of the van Genuchten model and Mualem model which widely used is able to produced non hysteretic  $K(\theta)$  with condition:  $\theta_s^d = \theta_s^w$ ,  $\theta_r^d = \theta_r^w$ ,  $n^d = n^w$ , but  $\alpha^d$  and  $\alpha^w$  may different (van Genuchten, 1980 and Kool and Parker, 1987). Figure 2.10 presents the illustration of hysteretic  $K(h)$  and non-hysteretic  $K(\theta)$  from those constraints. Both  $K(h)$  from drying and wetting closed at  $K_s$ . As pressure head decrease, both  $K(h)$  also decrease where  $K(h)$  of drying is higher than  $K(h)$  for same pressure head. Conversely,  $K(\theta)$  is identical for drying and wetting for same water content.

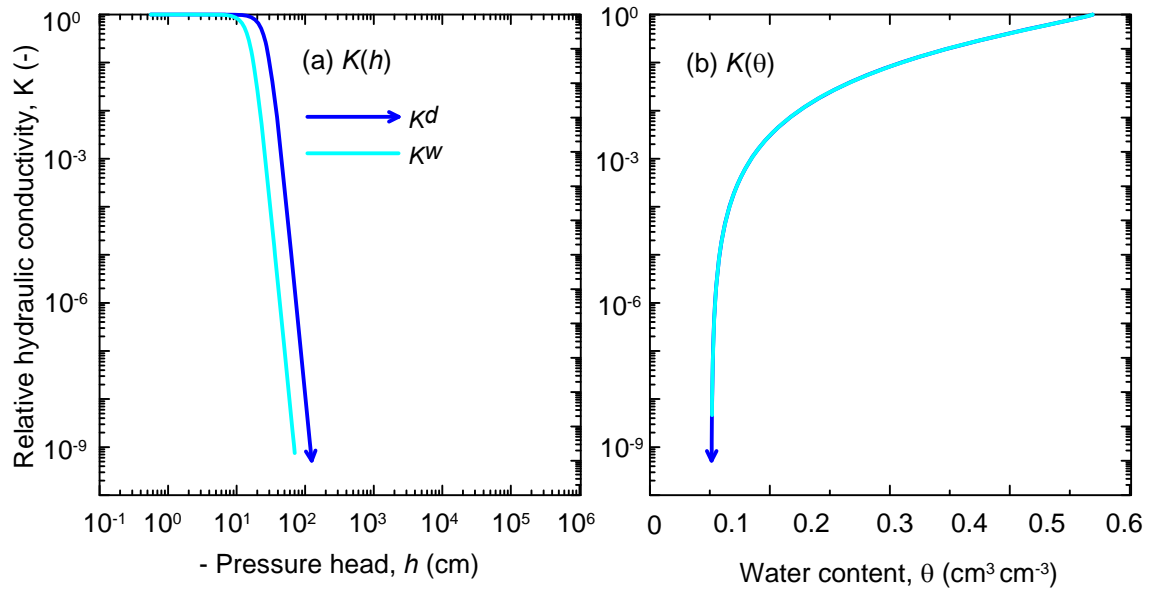


Fig. 2.10. Illustration for calculation of unsaturated hydraulic conductivity from the main drying and wetting curves of the Kool and Parker model based on the van Genuchten – Mualem model with  $\theta_s^d = \theta_s^w$ ,  $\theta_r^d = \theta_r^w$ ,  $n^d = n^w$ , and  $\alpha^d < \alpha^w$ . (a) Hysteretic  $K(h)$  and (b) Non hysteretic  $K(\theta)$ .

## 2.7 CONCLUSIONS

Owing to a well-developed and stable aggregated structure made up of noncrystalline minerals (e.g., allophane, imogolite, ferrihydrite), Andisols exhibit unique physical properties such as low bulk density, high porosity, and stepwise water retention curve reflecting interaggregate and intraaggregate pores. The developed aggregate structure leads to Andisols have valuable properties for agriculture and environment.

The bimodal VG model is used for describing water retention of Andisols in many studies; on the other hand its application for unsaturated hydraulic conductivity is still limited. Determination of the large number of parameters in the bimodal VG model is a major challenge. The evaporation method is widely used for determining unsaturated hydraulic conductivity from near saturation until intermediate range of pressure head, (i.e.,  $0 > h > -700$  cm). To extend the applicability of the estimate of hydraulic properties, water retention ranges from near saturation until low of pressure heads can be included in the objective function together with the observed pressure head from tensiometer reading in the evaporation experiment. To provide water retention data at low pressure heads, which difficult to measure in the past, the WP4 probably can be used because of quickness and accurateness.

Kool and Parker hysteretic model is straightforward and might be able to involve hysteretic hydraulic properties in the bimodal VG model for dual porosity soils, albeit this model resulted in unclosed scanning curves.

## 2.8 REFERENCES

- Ahrenholz, B., J. Tölke, P. Lehmann, A. Peters, A. Kaestner, M. Krafczyk, and W. Durner. 2008. Prediction of capillary hysteresis in porous material using lattice Boltzmann methods and comparison to experimental data and a morphological pore network model. *Adv. Water Resour.* 31:1151–1173. doi:10.1016/j.advwatres.2008.03.009
- Aziz, K., and A. Settari. 1979. *Petroleum Reservoir Simulation*. pp. 395-401, Applied Science, Barking, United Kingdom.
- Bittelli, M., and M. Flury. 2009. Errors in water retention curves determined with pressure plates and their effect on soil hydraulic functions. *Soil Sci. Soc. Am. J.* 73:1453-1460. doi:10.2136/sssaj2008.0082
- Blonquist, J. M., Jr., S.B. Jones, I. Lebron, and D.A. Robinson. 2006. Microstructural and phase configurational effects determining water content: Dielectric relationships of aggregated porous media, *Water Resour. Res.* 42:W05424. doi:10.1029/2005WR004418
- Chamindu Deepagoda, T.K.K., P. Moldrup, M.P. Jensen, S.B. Jones, L.W. de Jonge, P. Schjønning, K. Scow, J.W. Hopmans, D.E. Rolston, K. Kawamoto, and T. Komatsu. 2012. Diffusion Aspects of Designing Porous Growth Media for Earth and Space. *Soil Sci. Soc. Am. J.* 76: 1564-1578. doi: 10.2136/sssaj2011.0438
- Cresswell, H.P., T.W. Green, and N.J. McKenzie. 2008. The adequacy of pressure plate apparatus for determining soil water retention. *Soil Sci. Soc. Am. J.* 72:41–49. doi:10.2136/sssaj2006.0182
- Dahlgren, R.A., Saigusa, M., and Ugolini, F.C. 2004. The nature, properties and management of soils. *Adv. Agron.* 82:113–182. doi:10.1016/S0065-2113(03)82003-5
- Durner, W. 1994. Hydraulic conductivity estimation for soils with heterogeneous pore structure. *Water Resour. Res.* 30:211-223. doi:10.1029/93WR02676
- Durner, W., B. Schultze, and T. Zurmühl. 1997. State-of-the-Art in Inverse Modeling of Inflow/Outflow Experiments. In M. Th. van Genuchten, F. J. Leij, and L. Wu (ed.) *Proc. Int. Workshop on Characterization and Measurement of the Hydraulic Properties of Unsaturated Porous Media*, October 22-24, 1997, University of California, Riverside, CA.



- Figueras, J., and M.M. Gribb. 2009. Design of a user-friendly automated multistep outflow test system. *Vadose Zone J.* 8:523-529. doi:10.2136/vzj2008.0016
- Finsterle, S., Sonnenborg, T.O., Faybishenko, B. 1998. Inverse modeling of a multistep outflow experiment for determining hysteretic hydraulic properties. Paper LBNL-41749. Lawrence Berkeley National Laboratory, Berkeley, CA.
- Fontes, J.C., M.C. Gonçalves, and P.S. Pereira. 2004. Andosols of Terceira, Azores: measurement and significance of soil hydraulic properties. *Catena*. 56:145–154. Special issue (Volcanic soil resources: occurrence, development and properties, Arnalds O, Stahr K, eds). doi:10.1016/j.catena.2003.10.008
- Hamamoto, S., M.S.A.Perera, A.C.Resurreccion, K.Kawamoto, S.Hasegawa, T.Komatsu, and P.Moldrup. 2009. The solute diffusion coefficient in variably compacted, unsaturated volcanic ash soils. *Vadose Zone J.* 8:942-952. doi:10.2136/vzj2008.0184
- Hasegawa, S. 1986. Soil water movement in upland fields converted from paddy fields. *Soil Physical Conditions and Plant Growth, Japan*, 53: 13-19 (in Japanese).
- Hopmans, J.W., J. Šimůnek, N. Romano, and W. Durner. 2002. Simultaneous determination of water transmission and retention properties: Inverse methods. p. 963–1008. *In* J.H. Dane and G.C. Topp (ed.) *Methods of soil analysis. Part 4. SSSA Book Ser. 5. SSSA, Madison, WI.*
- Huang, H.C., Y.C. Tan, C.W. Liu, and C.H. Chen. 2005. A novel hysteresis model in unsaturated soil. *Hydrol. Process.* 19:1653–1665. doi:10.1002/hyp.5594
- Iwata, S., T. Tabuchi, and B.P.Warketin. 1995. *Soil-water interactions: mechanisms and applications*. 2nd ed. Marcel Dekker, New York.
- Iwata, S., 1966. The characteristics of water movement in soils during drainage with special reference to field moisture capacity. *Bull. Natl. Inst. Agric. Sci.*, B17: 149-176 (in Japanese, with English abstract).
- Jury, W. and R. Horton. 2004. *Soil Physics*. 6th Edition. John Wiley & Sons. New York. p. 390.
- Karunarathna A.K., T. Chhoden, K. Kawamoto, T. Komatsu, P. Moldrup, and L.W. de Jonge 2010. Estimating hysteretic soil-water retention curves in hydrophobic soil by a mini tensiometer-TDR coil probe, 19th World Congress of Soil Science, 1-6 August, Brisbane, Australia.

## 2 Literature review

- Kato, C., T. Nishimura, H. Imoto, and T. Miyazaki. 2011. Predicting soil moisture and temperature of andisols under a monsoon climate in Japan. *Vadose Zone J.* 10:541-551. doi:10.2136/vzj2010.0054
- Konyai, S., V. Sriboonlue, and V. Trelo-ges, 2009. The effect of air entry values on hysteresis of water retention curve in saline soil. *Am. J. Enviro. Sci.* 5:341-345. doi:10.3844/ajessp.2009.341.345
- Kool, J.B., and Parker, J.C. 1987. Development and evaluation of closed-form expressions for hysteretic properties. *Water Resour. Res.* 23:105–114. doi:10.1029/WR023i001p00105
- Kool, J.B., J.C. Parker, and M.Th. van Genuchten. 1987. Parameter estimation for unsaturated flow and transport models—A review. *J. Hydrol.* 91:255–293. doi:10.1016/0022-1694(87)90207-1
- Kosugi, K. 1996. Lognormal distribution model for unsaturated soil hydraulic properties. *Water Resour. Res.* 32:2697–2703. doi:10.1029/96WR01776
- Kosugi, K., J.W. Hopmans, and J.H. Dane. 2002. Parametric models. p. 739–757. In J.H. Dane and G.C. Topp (ed.) *Methods of soil analysis. Part 4. SSSA Book Series.* 5. SSSA, Madison WI.
- Kroes, J.G., J.C. Van Dam, P. Groenendijk, R.F.A. Hendriks, and C.M.J. Jacobs. 2009. SWAP version 3.2. Theory description and user manual. Alterra, Wageningen.
- Kutílek, M., 2004. Soil hydraulic properties as related to soil structure. *Soil Tillage Res.* 75:175–184. doi:10.1016/j.still.2004.07.006
- Kutílek M, L. Jendele, M.Krejca. 2009. Comparison of empirical, semi-empirical and physically based models of soil hydraulic functions derived for bi-modal soils. *J. Contam. Hydrol.* 104:84-89. doi:10.1016/j.jconhyd.2008.10.007
- Lehmann, F., Stauffer, F., Hinz, C., Dury, O., and Flühler, H. 1998, Effect of Hysteresis on Water Flow in Sand Column with a Fluctuating Capillary Fringe. *J. Contam. Hydrol.* 33:81–100. doi:10.1016/S0169-7722(98)00066-7
- Leij, F.J., N. Toride, M.S. Field, and A. Sciortino. 2012. Solute transport in dual-permeability porous media, *Water Resour. Res.* 48:W04523. doi:10.1029/2011WR011502

- Lenhard, R.J., J.C. Parker, and J.J. Kaluarachchi. 1991. Comparing Simulated and Experimental Hysteretic Two-Phase Transient Fluid Flow Phenomena. *Water Resour. Res.* 27:2113–2124. doi:10.1029/91WR01272
- Maček, M., J. Smolar, and A. Petkovšek. 2013. Extension of measurement range of dew-point potentiometer and evaporation method. *Proc. 18th Int. Conf. on Soil Mechanics and Geotechnical Engineering*, pp. 1137-1142, Paris.
- Minasny B., and D.J. Field. 2005. Estimating soil hydraulic properties and their uncertainty: The use of stochastic simulation in the inverse method of the evaporation method. *Geoderma*. 126:277-290. doi:10.1016/j.geoderma.2004.09.015
- Miyamoto, T., T. Annaka, and J. Chikusi. 2003. Soil aggregate structure effects on dielectric permittivity of an andisol measured by time domain reflectometry. *Vadose Zone J.* 2:90-97. doi:10.2136/vzj2003.9000
- Motomura, S., 1979. Physical properties of soil groups distributed in the lowland. In: *Soil Physical Conditions and Plant Growth*. Youkendo, Tokyo, pp. 60-71 (in Japanese).
- Mualem, Y. 1976. A new model for predicting the hydraulic conductivity of unsaturated porous media. *Water Resour. Res.* 12:513–522. doi:10.1029/WR012i003p00513
- Mualem, Y. 1984. Modified dependent domain theory of hysteresis. *Soil Sci.* 137:283-291.
- Mualem, Y. 1986. Hydraulic conductivity of unsaturated soils: Prediction and formulas. p. 799–823. In A. Klute (ed.) *Methods of soil analysis. Part 1*. 2nd ed. Agron. Mongor. 9. ASA and SSSA, Madison, WI.
- Mualem, Y. and A. Beriozkin. 2009. General scaling rules of the hysteretic water retention function based on Mualem's domain theory. *Eur. J. Soil Sci.* 60:652–661. doi:10.1111/j.1365-2389.2009.01130.x
- Nanzyo, M., S. Shoji, and R. Dahlgren. 1993. Physical characteristics of volcanic ash soils. In: Shoji, S., M. Nanzyo, R.A. Dahlgren. *Volcanic ash soils: Genesis, properties, and utilization*. Elsevier Amsterdam, the Netherlands. p:89-207. doi:10.1016/S0166-2481(08)70268-X
- Nanzyo, M. 2002. Unique properties of volcanic ash soils. *Glob. Environ. Res.* 6: 99-112.

- Parker, J.C. and R.J. Lenhard. 1987. A model for hysteretic constitutive relations governing multiphase flow: 1. Saturation-pressure relations. *Water Resour. Res.* 23:2187–2196. doi:10.1029/WR023i012p02187.
- Plagge, R., G. Scheffler, and J. Grunewald. 2006. On the hysteresis in moisture storage and conductivity measured by the instantaneous profile method. *J. Buil. Phys.* 29: 247-259. doi:10.1177/1744259106060706
- Priesack, E., and W. Durner. 2006. Closed-form expression for the multi-modal unsaturated conductivity function. *Vadose Zone J.* 5:121–124. doi:10.2136/vzj2005.0066
- Radcliffe, D., and J. Šimůnek. 2010. *Soil Physics with HYDRUS: Modeling and Applications*, CRC Press, Taylor & Francis Group, ISBN-10: 142007380X, ISBN-13: 9781420073805, pp. 373.
- Romano, N., and A. Santini. 1999. Determining soil hydraulic functions from evaporation experiments by a parameter estimation approach: Experimental verifications and numerical studies. *Water Resour. Res.* 35:3343–3359. doi:10.1029/1999WR900155
- Romano, N., P. Nasta, G. Severino, and J.W. Hopmans. 2011. Using bimodal log-normal functions to describe the hydraulic properties of soils. *Soil Sci. Soc. Am. J.* 75:468-480. doi:10.2136/sssaj2010.0084
- Ross, P.J., and K.R.J. Smettem. 1993. Describing Soil Hydraulic Properties with Sums of Simple Functions. *Soil Sci. Soc. Am. J.* 57:26-29. doi:10.2136/sssaj1993.03615995005700010006x
- Scanlon, B.R., B.J. Andrasky, and J. Bilskie. 2002. Miscellaneous methods for measuring matric or water potential. p. 643–670. In J.H. Dane, and G.C. Topp (ed.) *Methods of soil analysis. Part 4. Physical methods*. SSSA Book Ser. 5. SSSA, Madison, WI
- Schelle H., S. C. Iden, A. Peters, and W. Durner. 2010. Analysis of the agreement of soil hydraulic properties obtained from multistep-outflow and evaporation methods. *Vadose Zone J.* 9:1080–1091. doi: 10.2136/vzj2010.0050
- Schindler, U., and L. Müller. 2006. Simplifying the evaporation method for quantifying soil hydraulic properties. *J. Plant Nutr. Soil Sci.* 169:623–629. doi:10.1002/jpln.200521895

- Schindler, U., W. Durner, G. von Unold, and L. Müller. 2010. Evaporation Method for Measuring Unsaturated Hydraulic Properties of Soils: Extending the Measurement Range, *Soil Sci. Soc. Am. J.*, 74:1071-1083. doi:10.2136/sssaj2008.0358
- Schwarzel K., and J. Punzel. 2007. Hood infiltrometer - A new type of tension infiltrometer. *Soil Soil Sci. Soc. Am. J.* 71:1438-1447. doi:10.2136/sssaj2006.0104
- Scott, P.S., G.J. Farquhar, and N. Kouwen. 1983. Hysteretic effects on net infiltration. In: *Advances in Infiltration, Proceedings of the National Conference on Advances in Infiltration*, pp. 163–170. Publication 11–83, American Society of Agricultural Engineers, St Joseph, MI.
- Seki, K. 2007. SWRC fit—a nonlinear fitting program with a water retention curve for soils having unimodal and bimodal pore structure. *Hydrol. Earth Syst. Sci. Discuss.* 4:407–437. doi:10.5194/hessd-4-407-2007
- Shoji, S., M. Nanzyo, and R.A. Dahlgren. 1993. Productivity and utilization of volcanic ash soils. In: Shoji, S., M. Nanzyo, R.A. Dahlgren. *Volcanic ash soils: Genesis, properties, and utilization*. Elsevier Amsterdam, the Netherlands. p:209-251. doi:10.1016/S0166-2481(08)70269-1
- Shoji, S., and T. Takahashi. 2002. Environmental and agricultural significance of volcanic ash soils. *Glob. Environ. Res.* 6: 113-135.
- Šimůnek, J., O. Wendroth, and M.Th. van Genuchten. 1998. Parameter estimation analysis of the evaporation method for determining soil hydraulic properties. *Soil Sci. Soc. Am. J.* 62:894–905. doi:10.2136/sssaj1998.03615995006200040007x
- Šimůnek, J., R. Kodešová, M. M. Gribb, and M. Th. van Genuchten. 1999. Estimating hysteresis in the soil water retention function from cone permeameter experiments. *Water Resour. Res.* 35:1329–1345. doi:10.1029/1998WR900110
- Šimůnek, J., and J.W. Hopmans. 2002. Parameter Optimization and Nonlinear Fitting, In: *Methods of Soil Analysis, Part 1, Physical Methods, Chapter 1.7*, Eds. J. H. Dane and G. C. Topp, Third edition, SSSA, Madison, WI, 139-157.
- Šimůnek, J., M. Šejna, H. Saito, M. Sakai, and M. Th. van Genuchten. 2008. The Hydrus-1D Software Package for Simulating the Movement of Water, Heat, and Multiple Solutes in Variably Saturated Media, Version 4.0, HYDRUS Software

## 2 Literature review

- Series 3, Department of Environmental Sciences, University of California Riverside, Riverside, California, USA, pp. 315.
- Spohrer, K., L. Herrmann, J. Ingwersen, and K. Stahr. 2006. Applicability of uni- and bimodal retention functions for water flow method in a tropical Acrisol. *Vadose Zone J.* 5:48-58. doi:10.2136/vzj2005.0047
- van Genuchten, M. T. A closed-form equation for predicting the hydraulic conductivity of unsaturated soils. *Soil Sci. Soc. Am. J.* 44:892–898. doi:10.2136/sssaj1980.03615995004400050002x
- Warkentin, B.P., and T. Maeda. 1974. Physical properties of allophanesols from the West Indies and Japan. *Soil Sci. Soc. Am. J.* 38:372–377. doi:10.2136/sssaj1974.03615995003800020042x
- Weller, U., O. Ippisch, M. Köhne, and H.-J. Vogel. 2011. Direct measurement of unsaturated conductivity including hydraulic nonequilibrium and hysteresis. *Vadose Zone J.* 10:654-661. doi:10.2136/vzj2010.0074
- Werner, A.D., and D.A. Lockington. 2006. Artificial pumping errors in the Kool-Parker scaling model of soil moisture hysteresis. *J. Hydrol.* 325:118–133. doi:10.1016/j.jhydrol.2005.10.012.
- Zurmühl, T., and W. Durner. 1998. Determination of parameters for bimodal hydraulic functions by inverse method. *Soil Sci. Soc. Am. J.* 62:874-880. doi:10.2136/sssaj1998.03615995006200040004x
- Zurmühl, T. 1998. Capability of convection dispersion transport models to predict transient water and solute movement in undisturbed soil columns. *J. Contam. Hydrol.* 30:99–126. doi:10.1016/S0169-7722(97)00034-X

## CHAPTER 3

# ESTIMATING THE UNSATURATED HYDRAULIC CONDUCTIVITY OF ANDISOLS USING THE EVAPORATION METHOD

### 3.1 INTRODUCTION

Andisols generally are developed from volcanic ash consisting of noncrystalline materials such as allophone, imogolite, Al-humus complexes, and ferrihydrite (Shoji et al., 1993; Nanzo, 2002). Andisols cover 17% of the land surface in Japan, where they are widely used for agriculture. Water flow and solute transport processes in Andisols are of considerable interest because of their unique physical and chemical properties. They typically have a very low bulk density and a well-developed aggregated structure. Because of this, Andisols usually exhibit a composite (stepwise) water retention function reflecting distinct but interacting inter-aggregate and intra-aggregate pore regions (Miyamoto et al., 2003).

Several bimodal or multimodal functions have been proposed over the years to account for the additive effects of inter- and intra-aggregate pore regions to the overall soil hydraulic properties (Peters and Klavetter, 1988; Othmer et al., 1991; Gerke and van Genuchten, 1993; Mallants et al., 1997; Mohanty et al., 1997). One frequently used multimodal formulation stems from Durner (1992, 1994) who developed a composite retention function by summing multiple van Genuchten (VG) models (van Genuchten, 1980). The bimodal form of this function has been used in several recent studies (e.g., Coppola, 2000; Peters and Durner, 2008; Schelle et al., 2010), including for the water retention properties of Andisols (Miyamoto et al., 2003; Hamamoto et al., 2009; Chamindu Deepagoda et al., 2012). Most of these studies were concerned with the water retention properties of soils. By comparison, very few studies have applied the bimodal VG model to the unsaturated hydraulic conductivity function of aggregated soils. When used also for the hydraulic conductivity, most applications were concerned with improved descriptions of the unsaturated conductivity function near saturation in

attempts to account for the effects of macropores or rock fractures (Peters and Klavetter, 1988; Zurmühl and Durner, 1998; Iden and Durner, 2007; Durner and Iden, 2011).

The bimodal VG model has considerable flexibility in describing the hydraulic properties of aggregated media. Unfortunately, optimization of the large number of parameters in the model against transient flow data (such as from multistep outflow or evaporation methods) is a major challenge. Since several of the hydraulic parameters are often correlated (Zurmühl and Durner, 1998), it is inherently difficult to find the global minimum of the objective function in the optimization process. Zurmühl and Durner (1998) showed that convergence of the parameter optimization process depends very much on the initial estimates of the unknown parameters. In addition to the transient measurements, the objective function could also include independently measured soil water retention or unsaturated hydraulic conductivity data points. Parameter uncertainty (i.e., the reliable range of the optimized parameter values) generally will be reduced by including independently measured soil hydraulic property data in the objective function, but this may affect the goodness of fit between modeled and experimental data (Šimůnek et al., 1998; Hopmans et al., 2002). More rapid minimization of the objective function may be achieved by using as initial estimates water retention parameters fitted to observed retention data. For example, Spohrer et al. (2006) succeeded in estimating 25 parameters of the bimodal VG model for four soil layers of a tropical Acrisol from transient field data using initial values of the fitted water retention parameters.

When the hydraulic properties are estimated inversely using the evaporation method, the optimized hydraulic functions are generally assumed to be representative only within the range of the tensiometer data. No guarantee exists that the hydraulic functions can be extrapolated beyond the invoked pressure measurement range. Šimůnek et al. (1998) and Hopmans et al. (2002) suggested the applicable range of the model predictions could be extended by including independently measured hydraulic data in the objective function. Sakai and Toride (2007b) estimated the unsaturated conductivity of the model of Fayer and Simmons (1995) for a dune sand, as well as the bimodal VG model for an Andisol, using the evaporation method in combination with water retention data from close to saturation to very dry conditions down to pressure heads of approximately  $-10^5$  cm. They showed that the observed pressure heads agreed



well with the model predictions when an appropriate hydraulic function was used to describe the water retention data over a wide range of pressure heads. The validity of the estimated unsaturated hydraulic conductivity beyond the pressure measurement range, however, was not discussed in detail in their study.

The objective of this study was to determine parameters of the bimodal VG model for Andisols over a wide range of pressure heads as determined using the evaporation method. In addition to the pressure heads we also used water retention data in the objective function. The saturated hydraulic conductivity,  $K_s$ , and the pore-connectivity factor,  $\ell$ , in the VG hydraulic conductivity function, along with several water retention parameters, were optimized. Different sets of optimizations were conducted by restricting the pressure head range of the water retention and tensiometer measurements in the objective function. We were especially interested in the role of water retention data at very at low (negative) pressure heads in the objective function. We furthermore used the measured pressure head profiles of the samples at the end of the evaporation experiment to confirm the shape of the estimated hydraulic functions beyond the tensiometer measurement range.

## 3.2 MATERIALS AND METHODS

### 3.2.1 Evaporation experiment

For the evaporation experiments we used two different Japanese Andisols collected from the surface horizons of two sites. One set of soil samples was obtained from the NARO Kyushu Okinawa Agricultural Research Center in Kumamoto, and one from the NARO Institute of Vegetable and Tea Science in Mie, Japan. Collected soil samples were sieved using a 2 mm mesh. The disturbed Andisols were packed uniformly in 16-cm long, 3.8-cm diameter acrylic columns to bulk densities,  $\rho_b$ , of 0.48 and 0.75 g cm<sup>-3</sup> for the Kumamoto and Mie soils, respectively. The saturated hydraulic conductivity,  $K_s$ , based on the falling head method was estimated to be approximately 200 cm d<sup>-1</sup> for the Kumamoto Andisol, and 1000 cm d<sup>-1</sup> for the Mie Andisol. Fig. 3.1 shows water retention curves as measured using a hanging water column for the pressure head ( $h$ ) range  $-200 < h < -5$  cm, using a pressure plate for  $-1.2 \times 10^4 < h < -250$  cm, and a WP4 dew point potentiometer (Decagon Devices, Pullman, WA) based on relative humidity

### 3 Estimating the unsaturated hydraulic conductivity

measurements equilibrated with the soil water pressure for the range  $-10^5 < h < -3 \times 10^3$  cm. Although WP4 measurements are generally used for pressure heads below  $-10^4$  cm, we applied the WP4 potentiometer to the higher pressure heads up to approximately  $-3 \times 10^3$  cm with considerable care as suggested by Maček et al. (2013). Volumetric water contents for the WP4 measurements were determined from the gravimetric water contents and the bulk density of the soil.

After slowly saturating the soil samples from the bottom, the water supply was closed and evaporation was allowed to start using a fan to blow air away from the soil surface in a 25 °C constant temperature room. Pressure heads were monitored using five tensiometers connected to pressure transducers at 1, 2, 3, 5 and 10 cm depths. Cumulative amounts of evaporation were calculated from measurements of the soil column weights using an electrical balance connected to a data logger. The evaporation experiment for the Mie Andisol continued until the pressure head became less than -600 cm at 1 cm depth. The evaporation period for the Kumamoto Andisol was allowed to continue longer, until the pressure head at 10 cm depth became less than -500 cm. The valves connected to the tensiometers above 10 cm depth were closed at  $h$  values of about -500 cm to prevent water leakage from the tensiometer cups (Durner and Or, 2005; Schindler et al., 2010). Volumetric water content profiles at the end of experiments were determined gravimetrically by sectioning the soil columns. Pressure head profiles near the surface at the end of experiments for the Kumamoto Andisol were measured using the WP4 potentiometer.

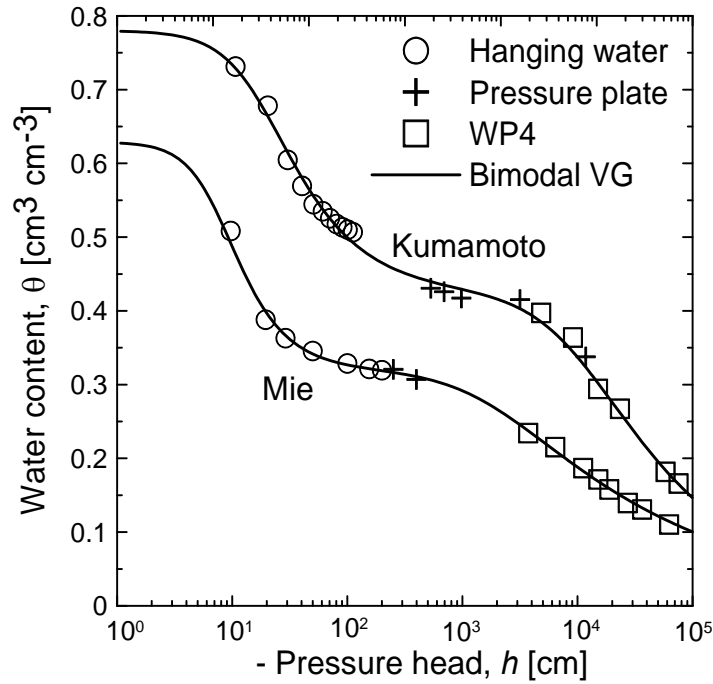


Fig. 3.1 Water retention curves for the Kumamoto and Mie Andisols fitted with the bimodal VG model (solid line). Retention data were obtained with a hanging water column (open circles), a pressure plate (crosses), and a WP4 dewpoint potentiometer (open squares).

### 3.2.2 Bimodal van Genuchten model

The bimodal water retention (Durner, 1992, 1994) and unsaturated hydraulic conductivity (Priesack and Durner, 2006) functions based on the van Genuchten-Mualem model (van Genuchten, 1980; Mualem, 1976) were used to describe the hydraulic properties of the two Andisols:

$$S = \frac{\theta(h) - \theta_r}{\theta_s - \theta_r} = w_1 S_1 + w_2 S_2 \quad [3.1]$$

where  $S_i$  is given by:

$$S_i = \left[ 1 + (\alpha_i |h|)^{n_i} \right]^{-m_i} \quad [3.2]$$

$$K(h) = K_s (w_1 S_1 + w_2 S_2)^\ell \frac{\left( w_1 \alpha_1 \left[ 1 - (1 - S_1^{1/m_1})^{m_1} \right] + w_2 \alpha_2 \left[ 1 - (1 - S_2^{1/m_2})^{m_2} \right] \right)^2}{(w_1 \alpha_1 + w_2 \alpha_2)^2} \quad [3.3]$$

### 3 Estimating the unsaturated hydraulic conductivity

The subscript  $i$  in these equations represents the number of subregions ( $i = 1, 2$  in our application),  $S_i$  is effective saturation [-] of the  $i$ -th subregion,  $h$  is the soil water pressure head [L],  $\theta$  is the volumetric water content [ $L^3L^{-3}$ ],  $\theta_s$  and  $\theta_r$  are the saturated and residual water contents [ $L^3L^{-3}$ ], respectively,  $n_i$  [-],  $\alpha_i$  [ $L^{-1}$ ], and  $m_i (=1-1/n_i)$  are shape parameters subject to  $\alpha_i > 0$  and  $n_i > 1$ ,  $w_1$  and  $w_2$  are the weighing factors subject to  $0 < w_i < 1$  and  $w_1 + w_2 = 1$ ,  $K$  is the hydraulic conductivity [ $LT^{-1}$ ],  $K_s$  is the saturated hydraulic conductivity [ $LT^{-1}$ ], and  $\ell$  is a pore-connectivity coefficient [-]. The  $S_1$  variable (subject to  $\alpha_1 > \alpha_2$ ) is associated with the first subregion of  $\theta(h)$  at the higher water contents, while  $S_2$  corresponds to the second subregion at the lower water contents. The hydraulic functions given by Eq. [3.1] to [3.3] are further referred to here as the bimodal VG model. Note that the hydraulic functions contain a total of nine parameters. Seven of these parameters ( $\theta_s$ ,  $\theta_r$ ,  $\alpha_1$ ,  $n_1$ ,  $w_2$ ,  $\alpha_2$ ,  $n_2$ ) relate primarily to the water retention curve, and two additional parameters ( $K_s$ ,  $\ell$ ) to the unsaturated hydraulic conductivity function.

#### 3.2.3 Parameter optimization

Parameters of the bimodal VG model for our two Andisols were optimized using version 4.08 of the HYDRUS-1D software package (<http://www.pc-progress.com/en/Default.aspx?hydrus-1d>) of Šimůnek et al. (2008). The calculations assumed applicability of the Richards equation to one-dimensional vertical water flow under isothermal condition as follows:

$$\frac{\partial \theta(h)}{\partial t} = \frac{\partial}{\partial z} \left( K(h) \frac{\partial h}{\partial z} + K(h) \right) \quad [3.4]$$

where  $z$  is the vertical coordinate [L] positive upward, and  $t$  is time [T].

The initial and boundary conditions for the evaporation experiment are given by (e.g., Šimůnek et al., 1998):

$$h(z, 0) = h_i(z) \quad [3.5]$$

$$-K(h) \left( \frac{\partial h}{\partial z} + 1 \right) = q_{\text{evap}}(L, t) \quad [3.6]$$

$$q(0, t) = -K(h) \left( \frac{\partial h}{\partial z} + 1 \right) = 0 \quad [3.7]$$

### 3 Estimating the unsaturated hydraulic conductivity

where  $h_i(z)$  is the initial pressure head [L] distribution in the column,  $q_{\text{evap}}(t)$  is the time-variable evaporation rate [ $\text{LT}^{-1}$ ] at the soil surface, and  $L$  is the  $z$  coordinate of the soil surface [L]. The initial condition,  $h_i(z)$ , was linearly interpolated using the initial tensiometer readings, while  $q_{\text{evap}}(t)$  was described with a polynomial function fitted to the observed evaporation rate as shown in Fig. 3.2. A no-flow boundary condition was imposed at the bottom boundary. We note that vapor flow was not included in the flow model, thus assuming that the effects of vapor flow on the parameter optimization process using the evaporation method can be neglected (Sakai and Toride, 2007b).

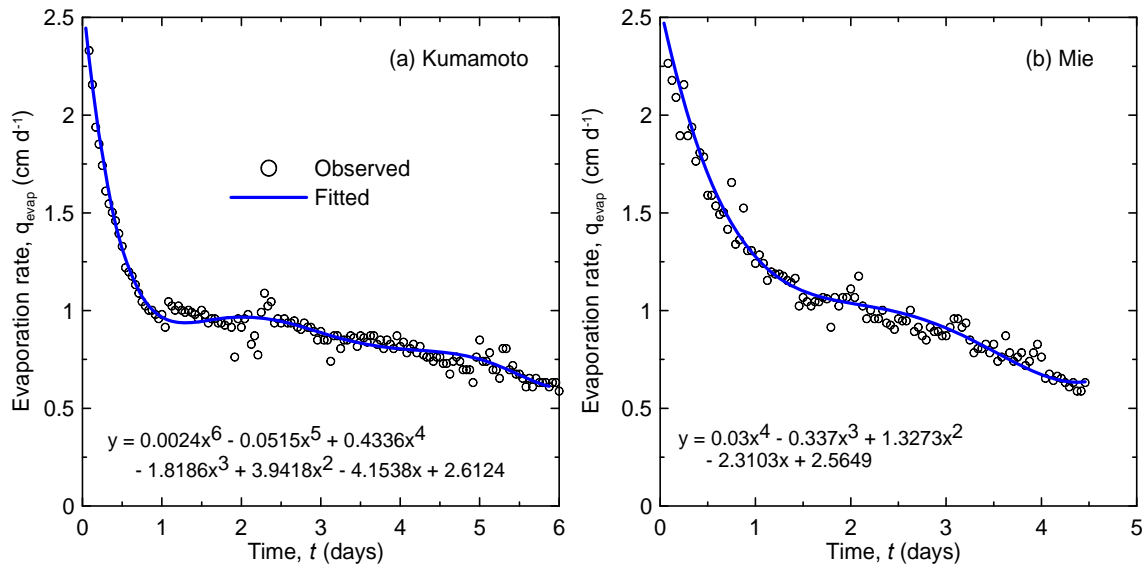


Fig.3.2 Evaporation rate from the surface of the Kumamoto (a) and Mie (b) Andisol soils samples. Shown are the observed evaporation rate data (open circles) and the fitted polynomial equation (solid line).

### 3 Estimating the unsaturated hydraulic conductivity

The objective function,  $\Phi$ , to be minimized during the parameter estimation process consisted of pressure heads measured at several depths as well as the independently measured water retention data shown in Fig. 3.1 (Hopmans et al., 2002; Šimůnek et al., 2008):

$$\Phi = v_h \sum_{i=1}^{n_h} [h_{\text{obs}}(t_i) - h_{\text{fit}}(t_i)]^2 + v_\theta \sum_{i=1}^{n_\theta} [\theta_{\text{obs}}(h_i) - \theta_{\text{fit}}(h_i)]^2 \quad [3.8]$$

where  $n_h$  and  $n_\theta$  are the number of observed pressure heads (in the column) and independently measured water retention data, respectively,  $v_h = 1/(n_h \sigma_h^2)$  and  $v_\theta = 1/(n_\theta \sigma_\theta^2)$  are weights for each data type (in which  $\sigma$  is the variance of the observed data), while the subscripts obs and fit indicate observed and model fitted values, respectively, at time  $t_i$ .

Šimůnek et al. (1998) recommended including the final water content of the evaporation experiment in the objective function in order to anchor the retention curve along the  $\theta$  axis. Instead of including the final water content in the objective function, we fixed the value of  $\theta_s$  by applying a mass balance to the column. The value of  $\theta_s$  was estimated from the final water content of the column and the cumulative amount of evaporation during the evaporation experiment as determined from the loss of weight of the sample after the experiment. Estimates of the remaining water retention parameters ( $\theta_r$ ,  $\alpha_1$ ,  $n_1$ ,  $w_2$ ,  $\alpha_2$ ,  $n_2$ ) in Eqs. [3.1] to [3.3] were determined first from the observed water retention data in Fig. 3.1 using version 6.02 of the RETC code (<http://www.pc-progress.com/en/Default.aspx?retc>) of van Genuchten et al. (1991). In order to reduce the number of optimized parameters, the value of  $\theta_r$  was assumed to be zero for our two Andisols since we found that optimization of  $\theta_r$  did not improve the fit of the data in Fig. 3.1. We similarly found that the restrictions  $m_i = 1 - 1/n_i$  in the bimodal VG model did not affect the goodness of fit. Fig. 3.1 shows excellent visual matches of the bimodal VG soil water retention functions to the data.

Following Spohrer et al. (2006) and Sakai and Toride (2007b), the fitted retention parameter values were used next as initial estimates in the overall optimization of the evaporation experiment. In our study we optimized the hydraulic conductivity parameters  $K_s$  and  $\ell$  since these two parameters are generally difficult to measure directly. The initial value for  $K_s$  was fixed at the value obtained with the falling head method, while  $\ell$  was initially assumed to be 0.5 as suggested by Mualem (1976). The

values of  $\theta_s$  and  $K_s$  in an evaporation experiment may be slightly different from observed static water retention measurements and the falling head method because of entrapped air during saturation or the length of soil column used (Hopmans and Dane, 1986; Dane and Hopmans, 2002. Sakaguchi et al., 2005). The value of  $K_s$  can easily change with very small variations in  $\theta_s$ . Since Andisols have a large porosity (especially the Kumamoto soil in our study), direct measurement of saturation can be quite vulnerable also to small measurement errors. Since we fixed  $\theta_s$  based on water mass balances of the sample,  $K_s$  is probably best treated as fitting parameter in the evaporation method. Initial values of all of the parameters used in the optimizations for the two Andisols are listed in Table 1.

We optimized the  $K_s$  and  $\ell$  values for three cases involving different combinations with the water retention parameters: (1) only two hydraulic conductivity parameters (i.e.,  $K_s$ ,  $\ell$ ) while keeping the water retention parameters fixed according to the independently measured water retention functions, (2) adding the water retention parameters of the first subregion (i.e.,  $K_s$ ,  $\ell$ ,  $\alpha_1$ ,  $n_1$ ,  $w_2$ ) in the optimization, and (3) further including the retention parameters of the second subregion (i.e.,  $K_s$ ,  $\ell$ ,  $\alpha_1$ ,  $n_1$ ,  $w_2$ ,  $\alpha_2$ ,  $n_2$ ). The values of  $\theta_s$  and  $\theta_r$  ( $= 0$ ) remained fixed in all optimizations.

## 3.3 RESULTS AND DISCUSSION

### 3.3.1 Parameter estimation

In earlier work, Šimůnek et al. (1998) showed that a single set of tensiometer readings near the sample surface was sufficient to yield accurate estimates of the soil hydraulic parameters using the evaporation method. Our experiments confirmed this in that similar results were obtained irrespective of including pressure head data from points deeper in the columns. Sakai and Toride (2007a) found that using pressure heads at two different depths in the objective function produced smaller standard errors for  $K_s$  and  $\ell$  than when data from only one depth were used. Since  $K_s$  and  $\ell$  were our primary concern, we will show below results when using pressure heads at 1 and 3 cm depths in the objective function given by Eq. [3.8]. Still, obtaining additional tensiometer measurements at other depths may well be useful for backup information in case some of tensiometers failed to work properly (Hopmans et al., 2002).

### 3 Estimating the unsaturated hydraulic conductivity

Fig. 3.3 shows fitted and observed pressure heads as a function of time at the 1 and 3 cm depths for the Kumamoto and Mie Andisols. Estimated water retention and unsaturated hydraulic conductivity functions corresponding to the three optimization cases of our study are shown in Fig. 3.4. The optimized parameter values and their standard errors, as well as the coefficients of variations (defined as the optimized values divided by the standard errors) for the bimodal VG model are listed in Table 1.

For the Kumamoto Andisol, all three optimization scenarios (i.e., case 1 with  $(K_s, \ell)$  optimized, case 2 with  $(K_s, \ell, \alpha_1, n_1, w_2)$  optimized, and case 3 with  $(K_s, \ell, \alpha_1, n_1, w_2, \alpha_2, n_2)$  optimized) gave almost identical results. All three cases produced excellent agreement with the observed pressure heads at the 1 and 3 cm depths (Fig. 3.3a). Predicted pressure heads for cases 2 and 3 were almost identical. The three cases also produced close agreement with the observed water retention data (Fig. 3.4a). In fact, as shown in Fig. 3.4b, the estimated hydraulic conductivities were almost identical for all three Kumamoto optimizations. In addition, all of the optimized parameters had small standard errors as reflected by the narrow confidence intervals shown in Table 1. These results suggest that when reliable water retention data are available and used in the objective function, it is possible to predict  $K(h)$  by optimizing only the two conductivity parameters  $(K_s, \ell)$ . This implies that as long as the water retention parameters can be properly determined using observed water retention data, the number of parameters in Mualem-type soil hydraulic functions, even for the bimodal VG model as given by Eq. [3.3], should not pose a problem in the optimization.

Results for the Mie Andisol were different. Case 1 for this soil failed to fit the sudden pressure drop at  $h = -50$  cm after about 3.5 days in Fig. 3.3b, with the fitted pressure heads being greater than the observations. Cases 2 and 3 improved the agreement between observed and fitted pressure heads. As the number of optimized parameter increases, the bimodal VG model clearly has more flexibility in fitting the pressure head data. Improved fitting of the pressure head data could be achieved also by sacrificing the close fit of the water retention data. However, compared to the differences between the fitted and observed pressure heads in Fig. 3.3b, the fitted water retention curves in Fig. 3.4c were very similar for all three cases. The bimodal water retention curve of Fig. 3.4c has a relatively flat region between about -50 cm and -10<sup>3</sup> cm. Since the soil water capacity ( $d\theta/dh$ ) is small in that flat region, the abrupt pressure



### 3 Estimating the unsaturated hydraulic conductivity

drop below  $h = -50$  cm in Fig. 3.3b should not change the water content very much. This explains why the small change in the water retention curve obtained by additionally optimizing the first subregion retention parameters ( $\alpha_1$ ,  $n_1$ ,  $w_2$ ) still produced a significant improvement in the pressure head simulations. By comparison, the pressure range of the flat region of the Mie Andisol is wider and the soil water capacity smaller than of the Kumamoto Andisol (Fig. 3.4a versus and 3.4c). We emphasize that the discrepancies in the pressure head were apparent when optimizing only the conductivity parameters (case 1), and then only for the Mie Andisol, but not for the Kumamoto soil.

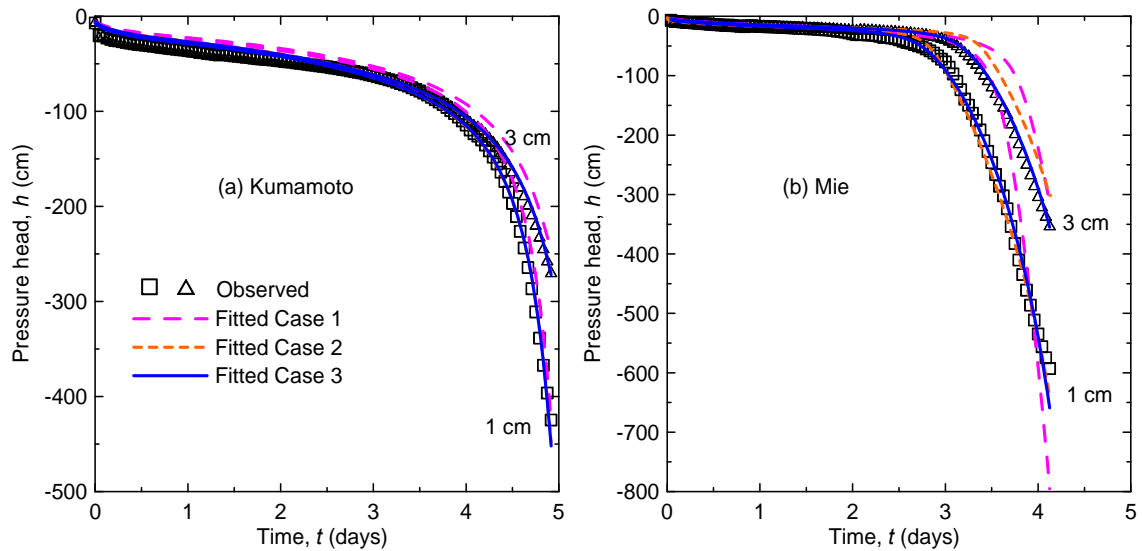


Fig. 3.3 Observed and fitted pressure heads as a function of time for the Kumamoto (a) and Mie (b) Andisols. Case 1 (pink long dash line), case 2 (orange short dash line) and case 3 (blue solid line).

### 3 Estimating the unsaturated hydraulic conductivity

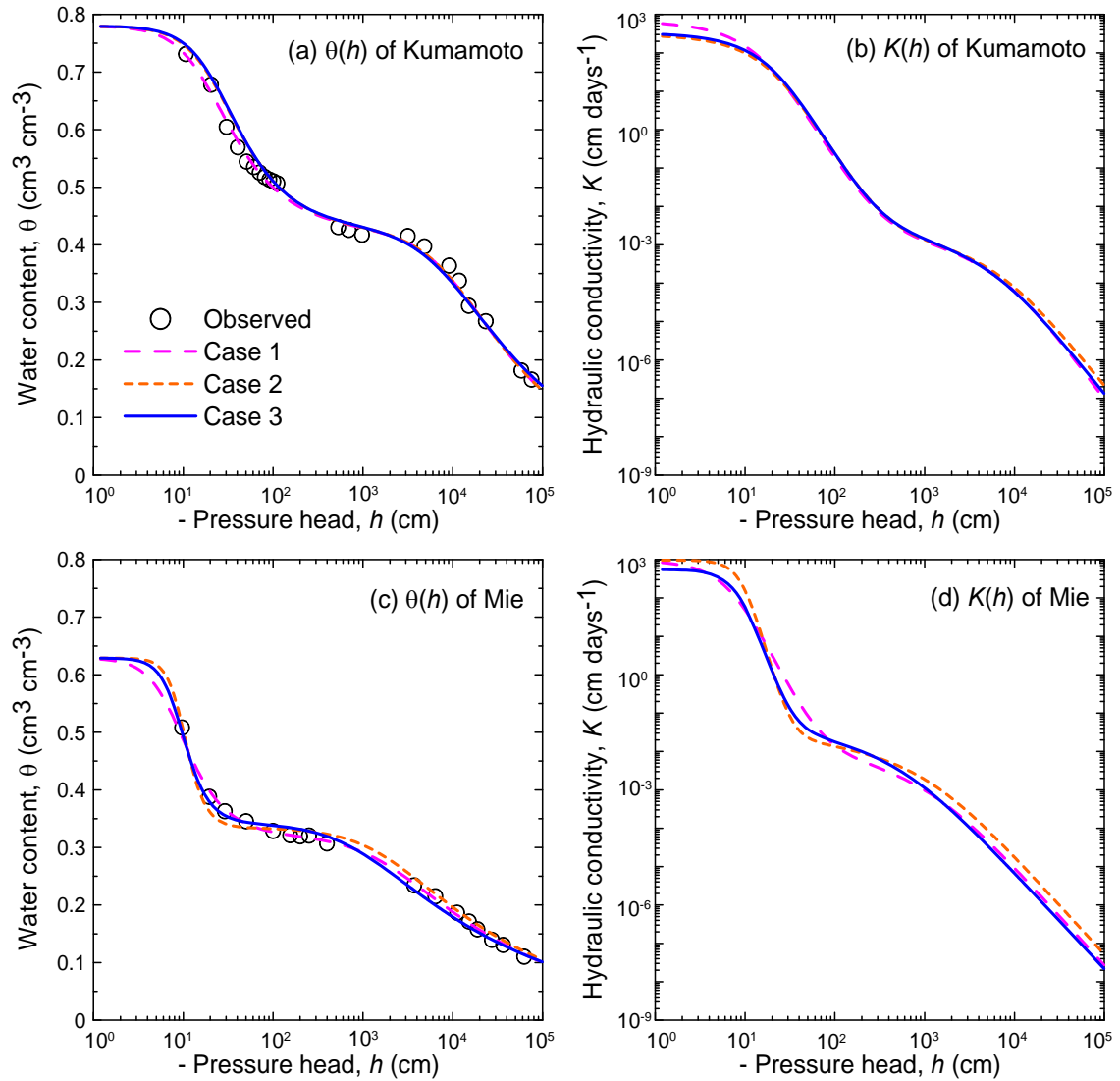


Fig. 3.4 Estimated water retention (a, c) and unsaturated hydraulic conductivity (b, d) curves for the Kumamoto (top) and Mie (bottom) Andisols: case 1 (pink long dash lines), case 2 (orange short dash lines) and case 3 (blue solid lines).

Table 3.1. Values of the optimized hydraulic parameters of the bimodal VG model, and their standard errors (SE) and coefficients of variation (CV), obtained with the evaporation method for cases 1, through 7 of the Kumamoto and Mie Andisols. .

### 3 Estimating the unsaturated hydraulic conductivity

Case	$\theta_r$	$\theta_s$	$\alpha_1$	$n_1$	$K_s$	$\ell$	$w_2$	$\alpha_2$	$n_2$
	(cm <sup>3</sup> cm <sup>-3</sup> )		(cm <sup>-1</sup> )	(-)	(cm d <sup>-1</sup> )	(-)	(-)	(cm <sup>-1</sup> )	(-)
<b>Kumamoto</b>									
initial	0	0.78	0.057	1.88	200	0.5	0.544	0.00011	1.44
1	-	-	-	-	703	0.751	-	-	-
SE	-	-	-	-	11	0.107	-	-	-
CV	-	-	-	-	0.016	0.142	-	-	-
2	-	-	0.045	1.92	312	0.054	0.544	-	-
SE	-	-	0.001	0.03	26	0.022	0.003	-	-
CV	-	-	0.022	0.015	0.083	0.418	0.005	-	-
3	-	-	0.044	1.96	343	0.436	0.549	0.00013	1.39
SE	-	-	0.001	0.03	32	0.214	0.003	0.00001	0.02
CV	-	-	0.023	0.017	0.093	0.492	0.006	0.076	0.011
4	-	-	0.055	1.87	312	0.614	0.541	0.00025	1.55
s.e.	-	-	0.001	0.04	38	0.231	0.008	0.00006	0.31
CV	-	-	0.018	0.020	0.122	0.377	0.014	0.232	0.203
5	-	-	-	-	971	2.301	-	-	-
SE	-	-	-	-	18	0.227	-	-	-
CV	-	-	-	-	0.019	0.099	-	-	-
6	-	-	-	-	208	0.007	-	-	-
SE	-	-	-	-	42	0.016	-	-	-
CV	-	-	-	-	0.202	2.167	-	-	-
7	-	-	-	-	28	0.001	-	-	-
SE	-	-	-	-	6	0.012	-	-	-
CV	-	-	-	-	0.214	15.250	-	-	-
<b>Mie</b>									
initial	0	0.629	0.129	2.41	1000	0.5	0.509	0.00062	1.28
1	-	-	-	-	969	0.040	-	-	-
SE	-	-	-	-	66	0.016	-	-	-
CV	-	-	-	-	0.068	0.389	-	-	-
2	-	-	0.101	4.36	968	0.044	0.532	-	-
SE	-	-	0.002	0.06	50	0.006	0.003	-	-
CV	-	-	0.020	0.013	0.052	0.145	0.005	-	-
3	-	-	0.111	3.57	555	0.011	0.545	0.00125	1.25
SE	-	-	0.002	0.07	34	0.004	0.003	0.00009	0.01
CV	-	-	0.018	0.020	0.061	0.381	0.005	0.072	0.005
4	-	-	0.131	2.42	507	0.330	0.513	0.00072	1.74
s.e.	-	-	0.002	0.04	176	0.608	0.002	0.00004	0.07
CV	-	-	0.015	0.016	0.347	1.844	0.005	0.056	0.043
5	-	-	-	-	850	0.620	-	-	-
SE	-	-	-	-	223	0.378	-	-	-
CV	-	-	-	-	0.262	0.610	-	-	-
6	-	-	-	-	617	0.407	-	-	-
SE	-	-	-	-	39	0.059	-	-	-
CV	-	-	-	-	0.063	0.145	-	-	-
7	-	-	-	-	391	0.018	-	-	-
SE	-	-	-	-	22	0.014	-	-	-
CV	-	-	-	-	0.056	0.765	-	-	-

Note: Entries indicated by - were not included in the optimization but fixed at the initial values

### 3 Estimating the unsaturated hydraulic conductivity

We also note that measurements of water retention data in the flat part of the retention function are often subject to errors. It is not easy to precisely determine the water content and pressure head relationships when the soil water capacity is very small. Pressure plates are generally used to measure water retention in this region. Nonequilibrium conditions, poor contact between the soil sample and the plate (Cresswell et al., 2008; Bittelli and Flury, 2009), and hysteresis in the sample preparation often affect the measurements. For this reason it may be better to optimize at least the first subregion parameters ( $\alpha_1$ ,  $n_1$ ,  $w_2$ ) also. But as long as water retention data over a wide range of pressure heads are available and can be used in the objective function, as Durner (1994) also suggested, case 3 optimization should yield the best overall results.

We mention some concern about the value of the pore-connectivity coefficient,  $\ell$ , which is often fixed at 0.5 following Mualem (1976). As pointed out in several studies (e.g., Wösten and van Genuchten, 1988; Kaveh and van Genuchten, 1992; Schaap and Leij, 2000; Spohrer et al., 2006),  $\ell$  can be quite variable depending upon soil type. Using the case 3 optimization,  $\ell$  was found to be 0.436 for the Kumamoto Andisol and 0.011 for the Mie Andisol. More data are clearly needed to obtain a better definition of possible  $\ell$  values for Andisols.

Our parameter optimizations were found to converge quickly, in all cases less than 10 iterations (5, 8 and 8 iterations for cases 1 to 3, respectively, of the Kumamoto Andisol and 8, 9 and 9 iterations for cases 1 to 3 of the Mie Andisol). This included case 3 which had the largest number of optimized parameters. Our results suggests that using water retention parameters fitted to independently observed retention data as initial estimates will facilitate convergence.

### 3.3.2 Water retention data at low pressure heads

In addition to the pressure head measurements obtained during the evaporation experiments for  $h > -600$  cm, we included in the objective function thus far also all of the independently measured water retention data between  $-10^5$  and  $-5$  cm (Fig. 3.1). This is to obtain reliable estimates of  $K(h)$  in the low pressure head range as recommended by Šimůnek et al. (1998) and Hopmans et al. (2002). To test the need for retention data in the dry range, we compared hydraulic functions optimized with (case 3) and without (case 4) including the independent water retention data at the low pressure heads in the objective function. The optimized conditions for case 4 were the same as for case 3, including the initial estimates, except that case 4 considered only water retention data for  $h > -10^3$  cm. The estimated parameter values for case 4 are also listed in Table 1. For both Andisols, good agreement between the observed and fitted pressure heads in the columns was obtained, very similar to case 3 as shown in Fig. 3.3.

Fig. 3.5 shows the observed and fitted water retention curves and the estimated unsaturated hydraulic conductivity functions for cases 3 and 4. The observed water retention data in the dry range were severely underestimated using case 4 relative to case 3. Since no information was given for  $h < -10^3$  cm for the case 4 optimizations, it is not surprising that this case converged to different values of the second subregion parameter ( $\alpha_2$ ,  $n_2$ ). The discrepancies shown in Fig. 3.5 for case 4 are a reason why optimized hydraulic functions are generally assumed to be reliable only within the range of the tensiometer measurements (Šimůnek et al., 1998; Hopmans et al., 2002). Table 1 shows that most of the standard errors of the estimated parameters for case 3 were smaller than those for case 4, which indicates that including water retention data at the lower pressure heads in the objective function will reduce parameter uncertainty and lead to more reliable parameter values.

Although observed pressure head data over a 5-day period were used for parameter optimization of the Kumamoto Andisol (Fig. 3.3a), the evaporation experiments continued for 6 days until the pressure heads at 10 cm depth reached approximately  $-500$  cm. To confirm the accuracy of the hydraulic properties of cases 3 and 4 for the Kumamoto Andisol, pressure heads were simulated for a longer time period using case 3 and 4 properties. Fig. 3.6 shows observed WP4 data near the surface with one tensiometer datum at the 10-cm depth, and predicted final pressure head

### 3 Estimating the unsaturated hydraulic conductivity

profiles after 6 days. The simulation using case 3 parameters agreed well with the observed pressure profile near the surface, whereas the prediction using case 4 parameters overestimated the pressure heads. These results again indicate that including water retention data at pressure heads below the tensiometer range (about -500 cm) will improve the estimates of the soil hydraulic parameters.

Since water retention at low pressure heads now can be measured relatively easily and accurately using dew point potentiometers (e.g., WP4), we strongly recommended to include in the optimization also water retention data in the measurement range of the dew point potentiometer ( $-10^5 < h < -3 \times 10^3$  cm) to extend the applicable range of the model predictions. On the other hand, estimates of the hydraulic conductivity at the very low pressure heads (e.g.,  $h < -10^4$ ) may require further investigations because of the possible effects of film flow (Peters and Durner, 2008), diffusion of water vapor (Saito et al., 2006; Peters and Durner, 2010) and the effect of shrinkage (Dorel et al., 2000).

### 3 Estimating the unsaturated hydraulic conductivity

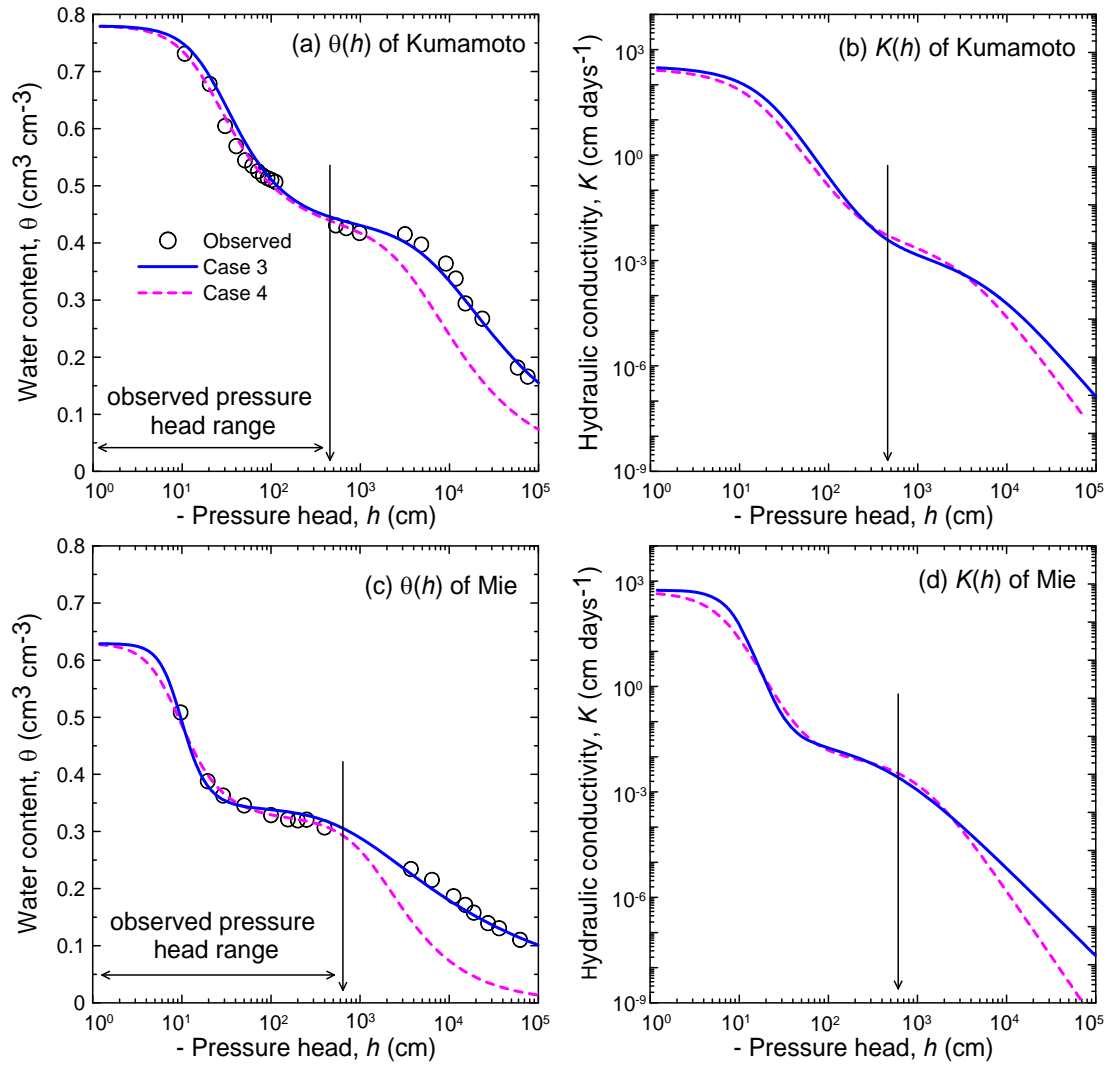


Fig. 3.5 Estimated water retention (a, c) and unsaturated hydraulic conductivity (b, d) curves for the Kumamoto (top) and Mie (bottom) Andisols. Results were obtained with (solid lines) and without (dashed lines) including water retention data at the low pressure heads in the objective function.

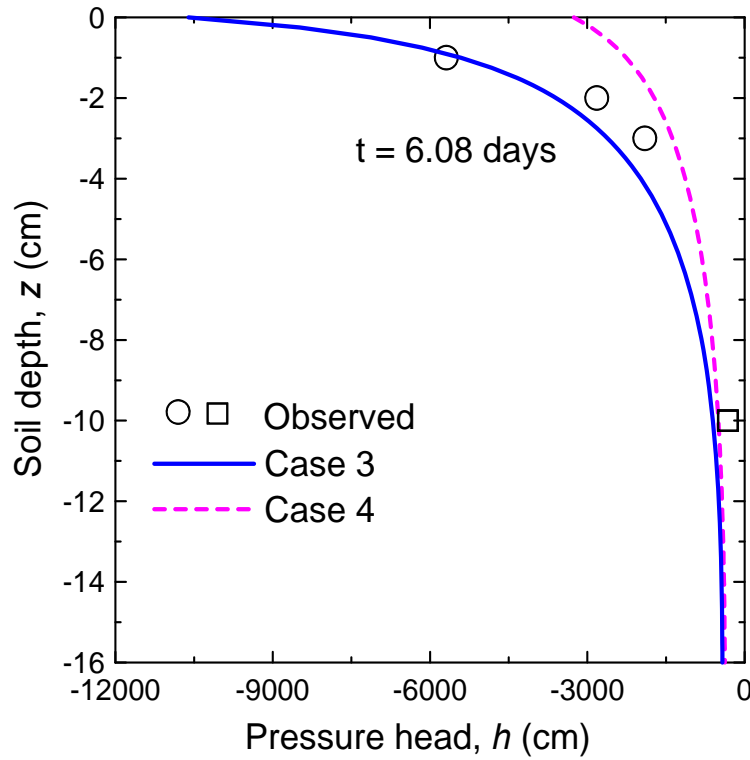


Fig. 3.6. Observed and predicted pressure head profiles after 6.08 days for the evaporation experiment of the Kumamoto Andisol. Results were obtained with (solid lines, case 3) and without (dashed lines, case 4) including water retention data at the low pressure heads in the objective function. Circles represent WP4 data and the square a tensiometer datum.

### 3.3.4 Pressure head measurement range

We next demonstrate the effect of using different ranges of the pressure head data measured in the columns during the evaporation experiments in the inverse analysis, while fixing in the objective function the bimodal water retention parameters ( $\square_r$ ,  $\square_s$ ,  $\alpha_1$ ,  $n_1$ ,  $w_2$ ,  $\alpha_2$ ,  $n_2$ ) as determined from the independently measured retention data. These scenarios are the same as case 1 in that only the conductivity parameters ( $K_s$ ,  $\ell$ ) are optimized, except that we used different ranges of the measured pressure heads in the optimizations: only data for which  $h > -200$  cm (case 5),  $h > -100$  cm (case 6), and  $h > -50$  cm (case 7). The estimated parameter values for these three cases (5 to 7) are given in Table 1.



### 3 Estimating the unsaturated hydraulic conductivity

Fig. 3.7 shows the estimated  $K(h)$  plots for the Kumamoto and Mie Andisols obtained with the different pressure head measurement ranges. The conductivity function for case 1 is the same as shown in Fig. 3.4. Except for the much lower  $K(h)$  curve for case 7 of the Kumamoto Andisol, the plots neglecting the lower pressure data did not affect the  $K(h)$  results very much; they produced almost identical  $K(h)$  curves as for case 1. For the Mie Andisol, even case 7 did give a good estimate of  $K(h)$ , likely because  $h > -50$  cm covered the entire region of the first slope of the water retention curve (Fig. 3.1). We conclude that independently measured water retention data covering a wide range of pressure heads provide very useful information to the parameter estimation process, leading to a much more robust optimization of the remaining parameters ( $K_s$ ,  $\ell$  in this case). Note that the standard errors and coefficients of variation have a tendency to increase as the pressure range becomes narrower (Table 1). This means that one should still use all available tensiometer data in the objective function.

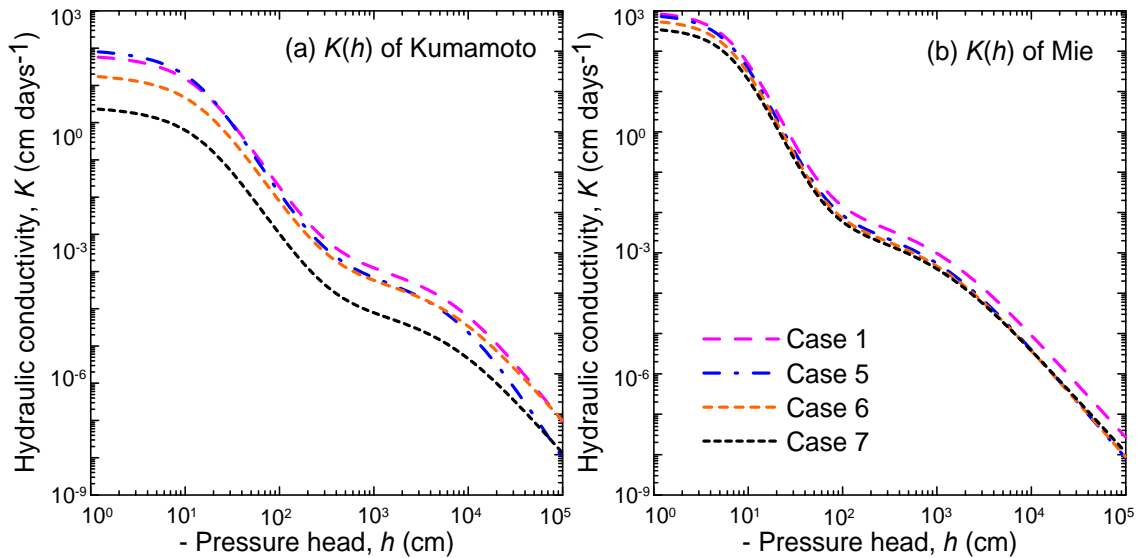


Fig. 3.7 Impacts of the pressure head range in the objective function on the estimated unsaturated hydraulic conductivity for the Kumamoto (a) and Mie (b) Andisols: case 1 used all data, case 5 only  $h > -200$  cm, case 6 only  $h > -100$  cm, and case 7 only  $h > -50$  cm.

### 3.4 CONCLUSIONS

Parameters of the bimodal VG model for two aggregated Andisols were inversely determined using the evaporation method. Independently measured water retention data from near saturation to very low pressure heads down to  $-10^5$  cm were included in the objective function in addition to soil pressure head data at two depths measured during the evaporation experiments. The saturated hydraulic parameter,  $K_s$ , and the pore-connectivity factor,  $\ell$ , along with several sets of water retention parameters were optimized. Since direct  $\theta_s$  measurements are often quite variable for high-porosity Andisols, the saturated water content was determined from the final water content and the measured cumulative amount of evaporation. When the value of  $\theta_s$  is fixed from these water mass balance considerations,  $K_s$  should be estimated in the evaporation method.

Since the initial estimates of the water retention parameters were determined from the independently measured water retention data, parameter estimation succeeded to converge quickly regardless of the number of optimized parameters. When water retention data from near saturation to very low pressure heads are available and used in the objective function, it is possible to predict  $K(h)$  by optimizing only two conductivity parameters ( $K_s$ ,  $\ell$ ). Since the flat region of the bimodal water retention curve is difficult to measure precisely, we recommend optimizing all of the bimodal VG parameters except  $\theta_s$  and  $\theta_r$  to yield the best overall fit.

In order to demonstrate the role of water retention data at low pressure heads in the objective function, we compared hydraulic functions optimized with and without water retention data at low pressure heads. Although almost similar matches to observed pressure heads were obtained with or without the low pressure data in the dry range, the second subregion parameter ( $\alpha_2$ ,  $n_2$ ) converged to different values if the low pressure data were omitted from the objective function. Predictions based on the hydraulic functions optimized with the low pressure data agreed well with observed pressure heads near the surface after a longer period of evaporation than used for the tensiometer measurements. The results indicate that including water retention data at low pressure heads can extend the applicable range of the model predictions, at least down to approximately  $-10^4$  cm.

The benefit of using independently measured water retention data was further studied by including different pressure head measurement ranges in the objective function. Neglecting the lower pressure data did not affect the  $K(h)$  estimation process very much, leading to almost similar  $K(h)$  functions. This confirms that collecting water retention data over a wide range of pressure heads will give very useful prior information to the parameter estimation process.

### 3.5 REFERENCES

- Bittelli, M., and M. Flury. 2009. Errors in water retention curves determined with pressure plates and their effect on soil hydraulic functions. *Soil Sci. Soc. Am. J.* 73:1453-1460. doi:10.2136/sssaj2008.0082
- Chamindu Deepagoda, T.K.K., P. Moldrup, M.P. Jensen, S.B. Jones, L.W. de Jonge, P. Schjønning, K. Scow, J.W. Hopmans, D.E. Rolston, K. Kawamoto, and T. Komatsu. 2012. Diffusion aspects of designing porous growth media for earth and space. *Soil Sci. Soc. Am. J.* 76:1564-1578. doi:10.2136/sssaj2011.0438
- Cresswell, H.P., T.W. Green, and N.J. McKenzie. 2008. The adequacy of pressure plate apparatus for determining soil water retention. *Soil Sci. Soc. Am. J.* 72:41–49. doi:10.2136/sssaj2006.0182
- Coppola, A. 2000. Unimodal and bimodal descriptions of hydraulic properties for aggregated soils. *Soil Sci. Soc. Am. J.* 64:1252-1262. doi:10.2136/sssaj2000.6441252x
- Dane, J.H., and J.W. Hopmans. 2002. Water retention storage. p. 675–680. In J.H. Dane and G.C. Topp (ed.) *Methods of soil analysis. Part 4. SSSA Book Ser. 5. SSSA, Madison WI.*
- Dorel, M., J.Roger-Estrade, H. Manichon, B. Delvaux. 2000. Porosity and soil water properties of Caribbean volcanic ash soils. *Soil Use Manage.* 16:133-140. doi:10.1111/j.1475-2743.2000.tb00188.x
- Durner, W. 1992. Predicting the unsaturated hydraulic conductivity using multi-porosity water retention curves. In: M.Th. van Genuchten et al. (ed.) *Indirect methods for estimating the hydraulic properties of unsaturated soils: Proceedings of the International Workshop, Riverside, CA. 11–13 Oct. 1989. U.S. Salinity Lab., Riverside, CA. p. 185–202.*

- Durner, W. 1994. Hydraulic conductivity estimation for soils with heterogeneous pore structure. *Water Resour. Res.* 30:211–223. doi:10.1029/93WR02676
- Durner, W., and Or, D. 2005. Soil water potential measurement, in: Anderson M. G. and J. J. McDonnell (ed), *Encyclopedia of Hydrological Sciences*, Chapter 73, 1089–1102, John Wiley & Sons, Ltd. doi:10.1002/0470848944.hsa077a
- Durner, W., and S.C. Iden. 2011. Extended multistep outflow method for the accurate determination of soil hydraulic properties near water saturation. *Water Resour. Res.* 47:W08526. doi:10.1029/2011WR010632
- Fayer, M.H., and C.S. Simmons. 1995. Modified soil water retention functions for all matric suctions. *Water Resour. Res.* 31:1233–1238. doi:10.1029/95WR00173
- Gerke, H.H., and M.Th. van Genuchten. 1993. A dual-porosity model for simulating the preferential movement of water and solutes in structured porous media. *Water Resour. Res.* 29:305–319, doi:10.1029/92WR02339
- Hamamoto, S., M.S.A. Perera, A.C. Resurreccion, K. Kawamoto, S. Hasegawa, T. Komatsu, and P. Moldrup. 2009. The solute diffusion coefficient in variably compacted, unsaturated volcanic ash soils. *Vadose Zone J.* 8:942–952. doi:10.2136/vzj2008.0184.
- Hopmans, J. W., and J. H. Dane. 1986. Temperature dependence of soil water retention curves. *Soil Sci. Soc. Am. J.* 50:562–567. doi:10.2136/sssaj1986.03615995005000030004x
- Hopmans, J.W., J. Šimůnek, N. Romano, and W. Durner. 2002. Simultaneous determination of water transmission and retention properties. Inverse methods. p. 963–1008. In J.H. Dane and G.C. Topp (ed.) *Methods of soil analysis. Part 4.* SSSA Book Ser. 5. SSSA, Madison WI.
- Iden, S.C., and W. Durner. 2007. Free-Form estimation of the unsaturated soil hydraulic properties by inverse modelling using global optimization, *Water Resour. Res.* 43: W07451. doi:10.1029/2006WR005845
- Kaveh, F., and M.Th. van Genuchten. 1992. A further look at a new unsaturated hydraulic conductivity equation. *Iranian J. Agric. Sciences.* 23: 24–32.
- Maček, M., J. Smolar, and A. Petkovšek. 2013. Extension of measurement range of dew-point potentiometer and evaporation method. *Proc. 18th Int. Conf. on Soil Mechanics and Geotechnical Engineering*, pp. 1137–1142, Paris.

- Mallants, D., D. Jacques, P.H. Tseng, M.Th. van Genuchten, and J. Feyen. 1997. Comparison of three hydraulic property measurement methods. *J. Hydrol.* 199:295-318. doi:10.1016/S0022-1694(96)03331-8
- Miyamoto, T., T. Annaka, and J. Chikusi. 2003. Soil aggregate structure effects on dielectric permittivity of an Andisol measured by time domain reflectometry. *Vadose Zone J.* 2:90-97. doi:10.2136/vzj2003.9000
- Mohanty, B.P., R.S. Bowman, J.M.H. Hendrickx, and M.Th. van Genuchten. 1997. New piecewise-continuous hydraulic functions for modeling preferential flow in an intermittent flood-irrigated field. *Water Resour. Res.* 33:2049-2063. doi:10.1029/97WR01701
- Mualem, Y. 1976. A new model for predicting the hydraulic conductivity of unsaturated porous media. *Water Resour. Res.* 12:513-522. doi:10.1029/WR012i003p00513
- Nanzyo, M. 2002. Unique properties of volcanic ash soils. *Glob. Environ. Res.* 6:99-112.
- Othmer, H., B. Diekkrüger, and M. Kutilek, 1991. Bimodal porosity and unsaturated hydraulic conductivity. *Soil Sci.* 152:139-150. doi:10.1097/00010694-199109000-00001
- Peters, A., and W. Durner. 2008. A simple model for describing hydraulic conductivity in unsaturated porous media accounting for film and capillary flow. *Water Resour. Res.* 44: W11417. doi:10.1029/2008WR007136
- Peters, A., and W. Durner. 2010. Reply to comment by N. Shokri and D. or on "a simple model for describing hydraulic conductivity in unsaturated porous media accounting for film and capillary flow". *Water Resour. Res.* 46:W06802. doi:10.1029/2010WR009181
- Peters, R.R., and E.A. Klavetter. 1988. A continuum model for water movement in an unsaturated fractured rock mass. *Water Resour. Res.* 24:416-430. doi:10.1029/WR024i003p00416
- Priesack, E., and W. Durner. 2006. Closed-form expression for the multi-modal unsaturated conductivity function. *Vadose Zone J.* 5:121-124. doi:10.2136/vzj2005.0066

- Saito, H., J. Šimůnek, and B. Mohanty. 2006. Numerical analyses of coupled water, vapor and heat transport in the vadose zone. *Vadose Zone J.* 5:784–800. doi:10.2136/vzj2006.0007
- Sakaguchi, A., T. Nishimura, and M. Kato. 2005. The effect of entrapped air on the quasi-saturated soil hydraulic conductivity and comparison with the unsaturated hydraulic conductivity. *Vadose Zone J.* 4:139–144. doi: 10.2136/vzj2005.0139
- Sakai, M., and N. Toride. 2007a. Optimum conditions for predicting unsaturated hydraulic properties using the evaporation method. *J. Jpn. Soc. Soil Phys.* 106:33–46. (in Japanese with English abstract).
- Sakai, M., and N. Toride. 2007b. Soil water hydraulic functions for a sandy soil and an aggregated soil. *J. Jpn. Soc. Soil Phys.* 107:63–77. (in Japanese with English abstract).
- Schaap, M.G., and F.J. Leij. 2000. Improved prediction of unsaturated hydraulic conductivity with the Mualem-van Genuchten model. *Soil Sci. Soc. Am. J.* 64:843–851. doi:10.2136/sssaj2000.643843x
- Schelle, H., S.C. Iden, A. Peters, and W. Durner. 2010. Analysis of the agreement of soil hydraulic properties obtained from multistep-outflow and evaporation methods. *Vadose Zone J.* 9:1080–1091. doi: 10.2136/vzj2010.0050
- Schindler, U., W. Durner, G. von Unold, L. Mueller, and R. Wieland. 2010. The evaporation method – Extending the measurement range of soil hydraulic properties using the air-entry pressure of the ceramic cup. *J. Plant Nutr. Soil Sci.* 173:563–572, doi:10.1002.jpln200900210
- Shoji, S., M. Nanzyo, and R.A. Dahlgren. 1993. Volcanic ash soils: Genesis, properties, and utilization. Elsevier Amsterdam, the Netherlands. p. 1–288.
- Šimůnek, J., O. Wendroth, and M.Th. van Genuchten. 1998. Parameter estimation analysis of the evaporation method for determining soil hydraulic properties. *Soil Sci. Soc. Am. J.* 62:894–905. doi:10.2136/sssaj1998.03615995006200040007x
- Šimůnek, J., M. Šejna, H. Saito, M. Sakai, and M.Th. van Genuchten. 2008a. The Hydrus-1D software package for simulating the movement of water, heat, and multiple solutes in variably saturated media. Version 4.0. HYDRUS Softw. Ser. 3. Dep. of Environ. Sci., Univ. of California, Riverside.

- Spohrer, K., L. Herrmann, J. Ingwersen, and K. Stahr. 2005. Applicability of uni- and bimodal retention functions for water flow method in a tropical Acrisol. *Vadose Zone J.* 5: 48-58. doi:10.2136/vzj2005.0047
- van Genuchten, M.Th. 1980. A closed-form equation for predicting the hydraulic conductivity of unsaturated soils. *Soil Sci. Soc. Am. J.* 44:892–898. doi:10.2136/sssaj1980.03615995004400050002x
- van Genuchten, M. Th., F.J. Leij, and S.R. Yates. 1991. The RETC Code for Quantifying the Hydraulic Functions of Unsaturated Soils, Version 1.0. EPA Report 600/2-91/065, R. S. Kerr Environmental Research Laboratory, U. S. Environmental Protection Agency, Ada, OK, 85 p. (<http://www.pc-progress.com/en/Default.aspx?retc>).
- Wösten, J. H. M., and M.Th. van Genuchten. 1988. Using texture and other soil properties to predict the unsaturated soil hydraulic properties. *Soil Sci. Soc. Am. J.* 52: 1762-1770. doi:10.2136/sssaj1988.03615995005200060045x
- Zurmühl, T. and W. Durner. 1998. Determination of parameters for bimodal hydraulic functions by inverse method. *Soil Sci. Soc. Am. J.* 62:874-880. doi:10.2136/sssaj1998.03615995006200040004x

#### 4 A hysteretic model of hydraulic properties



## CHAPTER 4

# A HYSTERETIC MODEL OF HYDRAULIC PROPERTIES FOR DUAL POROSITY SOILS

### 4.1 INTRODUCTION

Water retention in aggregated soils is often described as a dual-porosity (or bimodal) system consisting of inter- and intra-aggregated pore domains, each having their own hydraulic properties. Durner (1992, 1994) developed a multimodal retention function as a summation of multiple van Genuchten (VG) models (van Genuchten, 1980) to describe a stepwise water retention curve. This function, which may be reduced to a bimodal function, has been used quite widely in recent years (e.g., Coppola, 2000, Peters and Durner, 2008; Schindler et al., 2010; Schelle et al, 2010, 2011; Durner and Iden, 2011; Diamantopoulos et al., 2012).

Miyamoto et al. (2004) applied the bimodal VG model to highly aggregated Japanese volcanic-ash soils, which exhibited a distinct stepwise water retention curve. Similar to the capillary water retention of coarse textured sandy soils, hysteresis may also exist for water retained in inter-aggregated pores, which are represented by the first part of the bimodal water retention curve in the near-saturation range. Although remarkable hysteresis loops were observed in the retention curve near saturation for baked ceramic aggregates (Steinberg et al., 2005), only limited effort has been made to develop a hysteretic model for dual porosity soils.

Kool and Parker (1987) proposed a hysteretic model based on the formulations introduced by Scott et al. (1983) for the unimodal VG model. The Kool and Parker (K&P) model describes the main drying and wetting curves using different values of the unimodal VG model parameter,  $\alpha$ . The K&P model estimates drying and wetting scanning curves based on the scaling of the main drying and wetting curves, respectively. Since it is relatively flexible in describing hysteretic loops, the K&P model is widely used in numerical water flow simulation codes such as HYDRUS (Šimůnek et al., 2008b), SWAP (Kroes et al., 2008), and UNSAT-H (Fayer, 2000), regardless of its simple assumptions and formulations. Minor modifications of the K&P model have

been suggested by Lenhard et al. (1991) and Lenhard and Parker (1989) to eliminate the so-called ‘pumping’, or unclosed hysteretic loops, by keeping track of historical reversal points.

The objective of this study is to introduce hysteretic water retention into the bimodal VG model based on the K&P model. The applicability of the proposed hysteretic model is demonstrated using observed hysteretic water retention curves and scanning curves for an Andisol. The unsaturated conductivity function based on the Mualem model (Mualem, 1976) is discussed for the main wetting and drying retention curves. An additional constraint for a nonhysteretic hydraulic conductivity function, when expressed as a function of the water content, is proposed.

## 4.2 MATERIAL AND METHODS

### 4.2.1 Observed Hysteretic Water Retention Curves

Because of a well-developed and stable aggregate structure made up of noncrystalline minerals (e.g., allophane, imogolite, ferrihydrite), Andisols exhibit unique physical properties such as a low bulk density, a high porosity, and a stepwise water retention curve reflecting inter- and intra-aggregate pores (Miyamoto et al., 2004). Hysteretic water retention curves were observed for an Andisol from an upland field at the National Institute of Vegetable and Tea Science in Mie, Japan, using a multistep outflow-inflow experiment. The soil sieved through a 2-mm mesh was packed in a 5-cm-depth and 5-cm-diameter soil column with a bulk density of  $0.75 \text{ g cm}^{-3}$ . A fritted glass filter of a 6-mm thickness was used at the bottom of the soil column. The bottom pressure head was controlled using a Mariotte bottle during sample wetting and by decreasing the position of a drip point during its draining. A tensiometer was horizontally installed at a 2.5-cm depth. Cumulative water inflow and drainage were monitored by regularly weighting the soil column. .

After saturating the soil with a Mariotte bottle supply, the bottom pressure head was gradually decreased to -80.5 cm to obtain the main drying retention curve. Then after switching back to the Mariotte bottle supply, the main wetting retention curve was monitored by increasing the bottom pressure head until saturation. Subsequently, draining and wetting processes were repeated in the intermediate pressure head range to obtain drying and wetting scanning curves. Average water contents of the soil column

#### 4 A hysteretic model of hydraulic properties

were determined based on the cumulative inflow-drainage and the final water content at the end of the experiment. Hysteretic water retention curves were obtained from the average water contents and the corresponding tensiometer readings. Figure 4.1 shows collected hysteretic water retention curves as well as their fit using the hysteretic model described below.

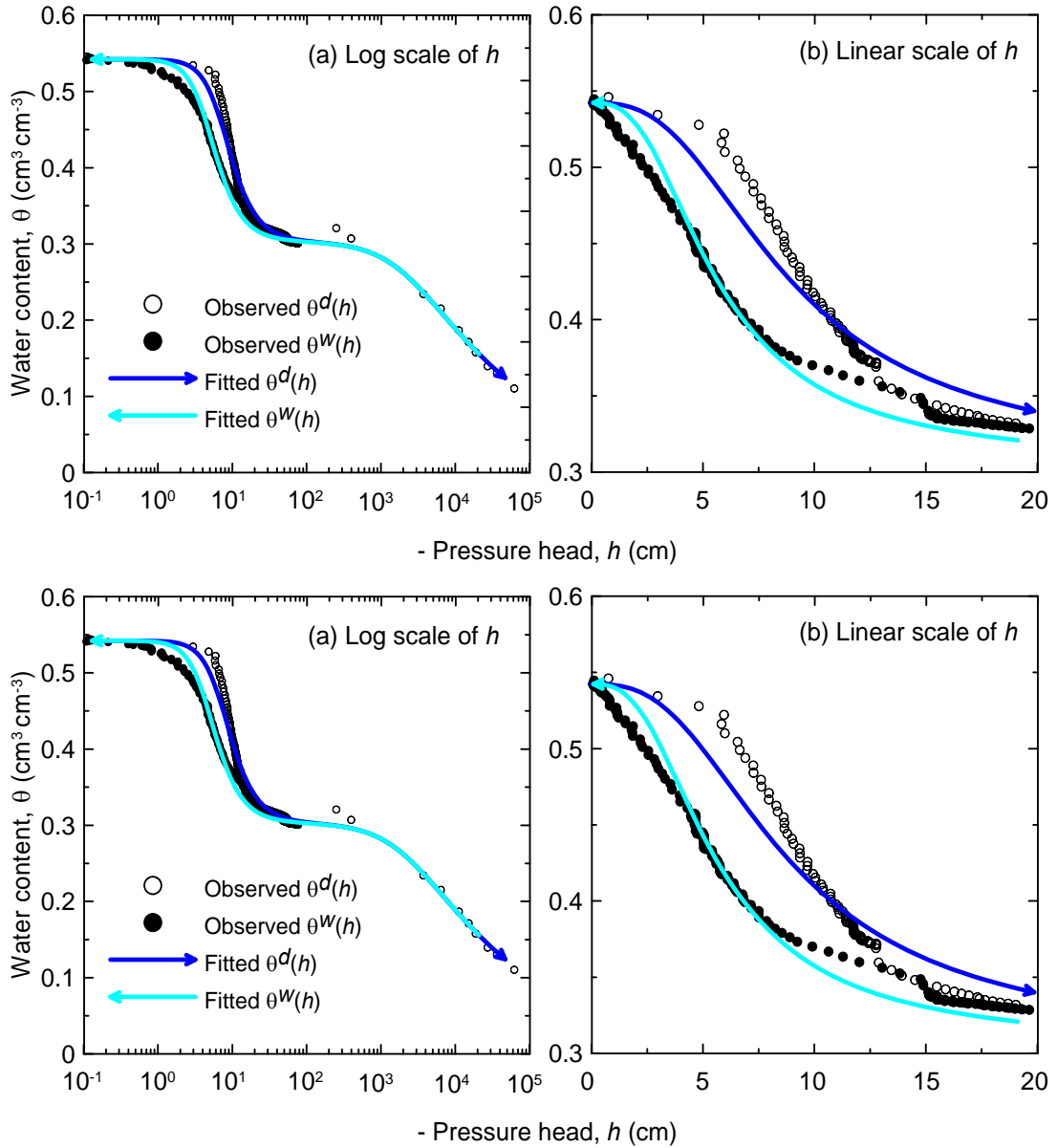


Fig. 4.1. Observed and fitted hysteretic water retention curves of Mie Andisol on (a) a logarithmic scale of the pressure head,  $h$ , and (b) a linear scale of the pressure head,  $h$ . Observed drainage data points are displayed as open circles and observed wetting data points as solid circles. Dark blue lines represent drying curves and light blue lines represent wetting curves.

#### 4.2.2 Hysteretic Model

##### *Dual-Porosity Hydraulic Functions*

The dual-porosity retention function introduced by Durner (1992, 1994) is expressed as a linear superposition of the unimodal VG model for each subregion:

$$S = \frac{\theta(h) - \theta_r}{\theta_s - \theta_r} = w_1 S_1 + w_2 S_2 \quad [4.1]$$

in which  $S_i$  is given by:

$$S_i = \left[ 1 + (\alpha_i |h|)^{n_i} \right]^{-m_i} \quad [4.2]$$

where the subscript  $i$  represents the number of subregions ( $i = 1, 2$ ),  $S$  is the effective saturation (-),  $h$  is the soil water pressure head (L),  $\theta_s$  and  $\theta_r$  are the saturated and residual water contents ( $\text{L}^3 \text{L}^{-3}$ ), respectively,  $n_i$  (-),  $\alpha_i$  ( $\text{L}^{-1}$ ), and  $m_i$  ( $=1-1/n_i$ ) are shape parameters subject to  $\alpha_i > 0$  and  $n_i > 1$ , and  $w_1$  and  $w_2$  are the weighing factors subject to  $0 < w_i < 1$  and  $w_1 + w_2 = 1$ . In the following discussion,  $S_1$ , subject to  $\alpha_1 > \alpha_2$ , corresponds to the first part of  $\theta(h)$  in the higher water content range, while  $S_2$  corresponds to the second part of  $\theta(h)$  in the lower water content range. In the case of  $w_2 = 0$ , Eq. [4.1] is reduced to the unimodal VG model. A closed-form expression of the unsaturated hydraulic conductivity function for the dual-porosity retention function (1) based on the Mualem model (Mualem, 1976) is given by Priesack and Durner (2006):

$$K(\theta) = K_s (w_1 S_1 + w_2 S_2)^\ell \frac{\left( w_1 \alpha_1 \left[ 1 - (1 - S_1^{1/m_1})^{m_1} \right] + w_2 \alpha_2 \left[ 1 - (1 - S_2^{1/m_2})^{m_2} \right] \right)^2}{(w_1 \alpha_1 + w_2 \alpha_2)^2} \quad [4.3]$$

where  $K_s$  is the saturated hydraulic conductivity ( $\text{L T}^{-1}$ ), and  $\ell$  is the pore-connectivity coefficient (-). Hereafter, the dual-porosity hydraulic functions of Eq. [4.4–4.3] are referred to as the bimodal VG model.

##### *Hysteretic Retention Functions*

When  $\theta_i(h)$  is defined as

$$\theta_i(h) = [\theta_s - \theta_r] w_i S_i + \theta_{ri} \quad [4.4]$$

the total water content in Eq. [4.1] can be simply expressed as a sum of three components:

$$\theta(h) = \theta_r + (\theta_1(h) - \theta_{r1}) + (\theta_2(h) - \theta_{r2}) \quad [4.5]$$

Since  $\theta_{s1} - \theta_{r1} = [\theta_s - \theta_r]w_1$  and  $\theta_{s2} - \theta_{r2} = [\theta_s - \theta_r]w_2$  for  $h = 0$  in Eq. [4.4], the effective saturation of the subregion  $i$  can be defined similarly to Eq. [4.1]:

$$S_i = \frac{\theta_i(h) - \theta_{ri}}{\theta_{si} - \theta_{ri}} \quad [4.6]$$

Since  $\theta_r$  is independently defined, in addition to the water contents of the subregions in Eq. [4.5],  $\theta_{ri}$  is assumed to be zero in this study.

Since Fig. 4.1 shows that hysteresis may occur only in the first, high-saturation part of the dual-porosity retention function, we apply the K&P model (Kool and Parker, 1987) to  $\theta_1(h)$  while assuming nonhysteretic  $\theta_2(h)$ . The main hysteretic loop is described with  $\alpha_1^d$  for the main drying curve,  $\theta_1^d(h)$ , and  $\alpha_1^w$  for the main wetting curve,  $\theta_1^w(h)$ . Remaining parameters ( $\theta_s$ ,  $\theta_r$ ,  $n_1$ ,  $w_2$ ,  $\alpha_2$ ,  $n_2$ ) are the same for both curves.

### Scanning Retention Curves

The K&P model is also applied to  $\theta_1(h)$  to describe the scanning curves of  $\theta(h)$ . Drying scanning curves are scaled using the main drying curve,  $\theta_1^d(h)$ , and can be expressed as (Šimůnek et al., 2008a):

$$\theta_1(h) = \theta_{r1} + \alpha_{\theta 1} [\theta_1^d(h) - \theta_{r1}^d] \quad [4.7]$$

where  $\alpha_{\theta 1}$  is the scaling factor for the drying scanning curve passing through the latest reversal point ( $\theta_{\Delta 1}$ ,  $h_{\Delta}$ ) from wetting to drying. The scaling factor  $\alpha_{\theta 1}$  is obtained by substituting ( $\theta_{\Delta 1}$ ,  $h_{\Delta}$ ) into Eq. [4.7] assuming  $\theta_{r1} = \theta_{r1}^d$ :

$$\alpha_{\theta 1} = \frac{\theta_{\Delta 1} - \theta_{r1}}{\theta_1^d(h_{\Delta}) - \theta_{r1}} \quad [4.8]$$

Note that we keep a nonzero  $\theta_{r1}$  in the above scaling Eq. [4.7–4.8] despite assuming  $\theta_{r1}=0$ . This is because a similar scaling procedure for wetting scanning curves based on the main wetting curve is used, as shown below. The scaling procedure results in a fictitious value of the parameter  $\theta_{s1}^*$ , which can be obtained by substituting the full saturation point ( $\theta_{s1}$ , 0) into Eq. [4.7] (Šimůnek et al., 2008a; Kool and Parker, 1987):

$$\theta_{s1}^* = \theta_{r1} + \alpha_{\theta 1} (\theta_{s1}^d - \theta_{r1}) = \frac{\theta_{\Delta 1} - \theta_{r1} [1 - S_1^d(h_{\Delta})]}{S_1^d(h_{\Delta})} \quad [4.9]$$

#### 4 A hysteretic model of hydraulic properties

Note that an identical drying scanning curve as in Eq. [4.7] can be derived by replacing  $\theta_{s1}$  with  $\theta_{s1}^*$  in the main drying curve described with Eq. [4.2] and [4.6] (Kool and Parker, 1987). Since the main hysteresis loop is closed at saturation,  $\theta_{s1}^d$  and  $\theta_{s1}^w$  are equal to  $\theta_{s1}$ .

Similarly, wetting scanning curves are scaled using the main wetting curve,  $\theta_1^w(h)$ , and can be described as:

$$\theta_1(h) = \theta_{r1}^* + \alpha_{\theta 1} [\theta_1^w(h) - \theta_{r1}^w] \quad [4.10]$$

in which the fictitious residual water content,  $\theta_{r1}^*$ , and the scaling factor for a particular wetting scanning curve. Substituting the reversal point  $(\theta_{\Delta 1}, h_{\Delta})$  and the full saturation point  $(\theta_{s1}, 0)$  into Eq. [4.10] lead to:

$$\theta_{\Delta 1} = \theta_{r1}^* + \alpha_{\theta 1} [\theta_1^w(h_{\Delta}) - \theta_{r1}^w] \quad [4.11]$$

$$\theta_{s1} = \theta_{r1}^* + \alpha_{\theta 1} [\theta_{s1}^w - \theta_{r1}^w] \quad [4.12]$$

Subtracting Eq. [4.12] from Eq. [4.11] results in:

$$\alpha_{\theta 1} = \frac{\theta_{\Delta 1} - \theta_{s1}}{\theta_1^w(h_{\Delta}) - \theta_{s1}^w} \quad [4.13]$$

The fictitious residual water content,  $\theta_{r1}^*$ , can be obtained by substituting Eq. [4.13] into Eq. [4.12] (Šimůnek et al., 2008a; Kool and Parker, 1987):

$$\theta_{r1}^* = \theta_{s1} - \alpha_{\theta 1} [\theta_{s1}^w - \theta_{r1}^w] = \frac{\theta_{\Delta 1} - \theta_{s1} S_1^w(h_{\Delta})}{1 - S_1^w(h_{\Delta})} \quad [4.14]$$

Note again that the identical wetting scanning curve as Eq. [4.10] can be also derived by replacing  $\theta_{r1}$  with  $\theta_{r1}^*$  in the main wetting curve described with Eq. [4.2] and [4.6] (Kool and Parker, 1987). Also note that it is possible to formulate the scanning curve model to describe unclosed hysteretic loops as done for the unimodal VG model by Lenhard et al. (1991) and Lenhard and Parker (1989).

### 4.3 RESULTS AND DISCUSSION

#### 4.3.1 Main Wetting and Drying Branches of Hysteretic Retention Curves

Figures 4.1a and 4.1b show observed hysteretic water retention curves on a logarithmic scale for  $-10^{-1} > h > -10^5$  cm and on a linear scale for  $0 > h > -20$  cm, respectively. Drying retention data measured with a pressure plate for  $-100 > h > -1000$  cm and a dew point potentiometer (WP4, Decagon Devices, Pullman, WA) for  $h < -1000$  cm are also plotted in Fig. 1a. The wetting curve data range between the pressure head of -76 cm up to saturation. Since the drying and wetting curves practically merged for pressure heads below  $h = -20$  cm (Fig. 4.1b), we assume that the observed retention curves can represent both main drying and wetting curves, confirming our assumption made above that the distinct hysteretic behaviour occurs only in the first part of the retention curve near saturation.

In order to test the hysteretic model, all data from the main drying and wetting curves including data for  $h < -100$  cm in Fig. 4.1a were fitted simultaneously by minimizing the root-mean-square error between the fitted and observed data sets ( $\text{RMSE}_\theta$ ) using Solver add-in in Microsoft Excel<sup>®</sup>. Parameters of  $\theta_s$ ,  $\alpha_1^d$ ,  $\alpha_1^w$ ,  $n_1$ ,  $w_2$ ,  $\alpha_2$ ,  $n_2$  were optimized assuming  $\theta_r = 0$  for the sake of simplicity (Durner, 1994). Figures 4.1a and 4.1b also show the main drying and wetting curves with optimized parameter values listed in Table 4.1. Since the water retention curve exhibits a distinct air entry near saturation with a steep gradient of  $d\theta/dh$ ,  $n_1$  is quite large ( $= 2.8$ ). However, the fitted drying curve underestimates and the fitted wetting curve overestimates experimental retention data near saturation because  $n_1$  is identical for both curves. While the fitted main loop closes at around  $h = -100$  cm, the observed loop closes at around  $h = -20$  cm. This disagreement comes from the fitting for the entire range of pressure head (Fig. 4.1a). Although certain discrepancies still exist at the beginning and the end of the loop, the hysteretic water retention model can describe reasonably well both the drying and wetting retention curves as a whole for Andisols.

Figures 4.2a and 4.2b show the main hysteretic loop for two hypothetical soils having different  $n_1$  values. Drying and wetting processes are indicated with the direction of arrows. Parameters for both hypothetical soils are given in Table 4.1. The gradient of the water content decrease close to saturation is steeper for  $n_1 = 2.56$ , representing a

narrower pore-size distribution. On the other hand,  $n_1 = 1.2$ , reflecting a wider pore-size distribution, results in the smaller gradient.

For  $n_1 = 2.56$ , hysteresis appears only in  $\theta(h)$  near saturation because  $\theta_1(h)$  approaches zero for  $h < -100$  cm (Fig. 4.2a). As in the case of the unimodal VG model, the larger  $n_1$  results in the greater gradient of  $d\theta/dh$  near saturation and a distinct air entry. Note that the gradient of the first part of  $\theta^d(h)$  is the same as for  $\theta^w(h)$  because  $n_1$  is identical for both curves. For  $n_1 = 1.2$ , hysteresis also occurs at lower pressure heads, extending even to the second section of  $\theta(h)$  because  $\theta_1(h)$  decreases gradually with the decreasing pressure head, as shown in Fig. 4.2b. The difference between  $\theta^d(h)$  and  $\theta^w(h)$  at a certain pressure head,  $h$ , is larger for the soil with  $n_1 = 2.56$  than for the soil with  $n_1 = 1.2$ .



#### 4 A hysteretic model of hydraulic properties

Table 4.1 Parameter values of the hysteretic bimodal VG model for two types of hypothetical soils having different  $n_1$  value, and fitted parameter values for observed main drying and wetting retention curves for Mie Andisol.

	$\theta_r$ (cm <sup>3</sup> cm <sup>-3</sup> )	$\theta_s$	$\alpha_1^d$ (cm <sup>-1</sup> )	$\alpha_1^w$ (cm <sup>-1</sup> )	$n_1$ (-)	$w_2$ (-)	$\alpha_2$ (cm <sup>-1</sup> )	$n_2$ (-)
Soil with $n_1 = 2.56$	0	0.57	0.121	0.543	2.56	0.52	0.00035	1.3
Soil with $n_1 = 1.20$	0	0.57	0.121	0.543	1.2	0.52	0.00001	1.3
Mie Andisol	0	0.542	0.139	0.219	2.8	0.559	0.00047	1.29

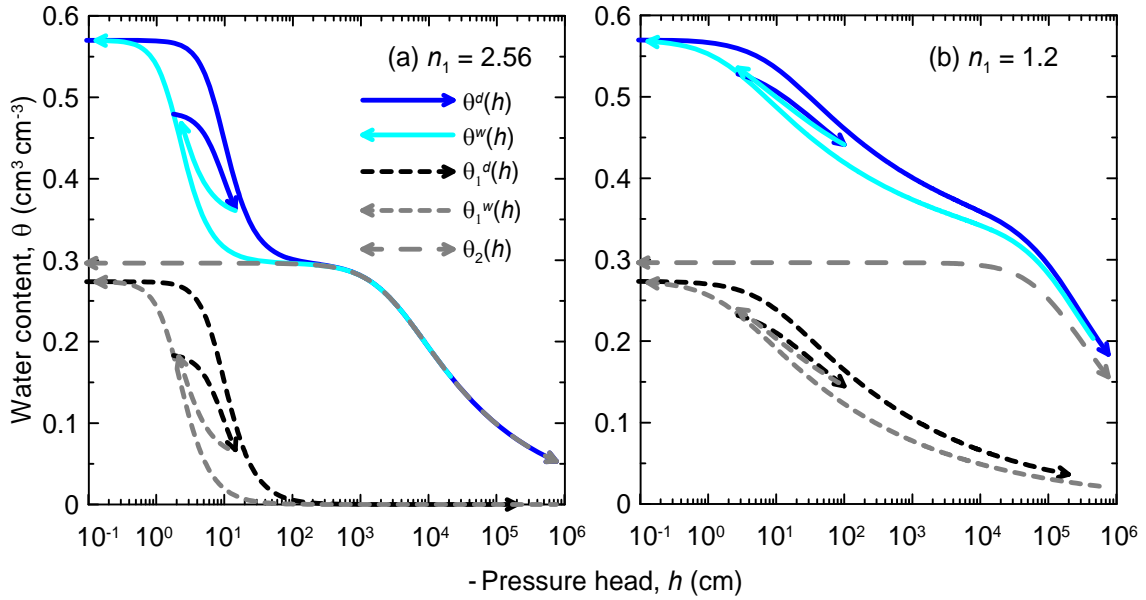


Fig. 4.2. Main hysteretic loop, primary drying and subsequent wetting scanning curves of  $\theta(h)$  for soils with (a)  $n_1 = 2.56$  and (b)  $n_1 = 1.2$ . Dashed lines are for retention curves of the two subdomains, solid lines are for the composite retention functions, dark blue lines represent drying curves, and light blue lines represent wetting curves.

### 4.3.2 Scanning Retention Curves

Figure 4.2 also shows a primary drying scanning curve and a subsequent secondary wetting scanning curve. The reversal points ( $h_\Delta$ ,  $\theta_\Delta$ ) used in Fig. 4.2 are (-1.8 cm, 0.479  $\text{cm}^3 \text{cm}^{-3}$ ) and (-15.1 cm, 0.360  $\text{cm}^3 \text{cm}^{-3}$ ) for the soil with  $n_1 = 2.56$ , and (-1.8 cm, 0.541  $\text{cm}^3 \text{cm}^{-3}$ ) and (-100.2 cm, 0.447  $\text{cm}^3 \text{cm}^{-3}$ ) for the soil with  $n_1 = 1.2$ .

Figure 4.3 presents observed and predicted scanning wetting and drying curves for Andisol. A reversal point for the drying scanning curve in Fig. 4.3a is (-3.4 cm, 0.485  $\text{cm}^3 \text{cm}^{-3}$ ), while a reversal point for the wetting scanning curve in Fig. 4.3b is (-10.3 cm, 0.408  $\text{cm}^3 \text{cm}^{-3}$ ). A good agreement between the observed and predicted scanning curves can be found especially for the wetting scanning curve (Fig. 4.3b).

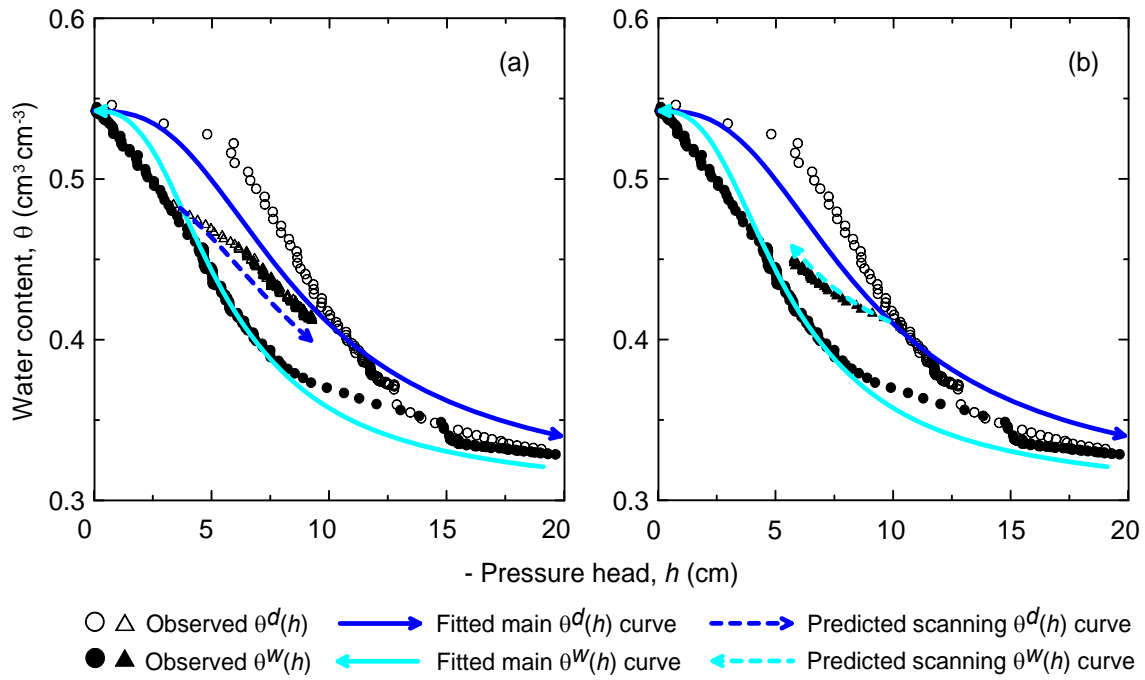


Fig. 4.3. Main branches of wetting and drying retention curves as shown in Fig. 4.1b (see a description given there), as well as observed (open and solid triangles) and predicted (dark and light blue dash lines) scanning curves. (a) Drying scanning curve departing from the main wetting curve and (b) wetting scanning curve departing from main the main drying curve.

### 4.3.3 Unsaturated Hydraulic Conductivity

Figure 4 presents the unsaturated hydraulic conductivity,  $K$ , (dashed lines) as a function of the pressure head,  $h$ , and water content,  $\theta$ , derived from the main drying and wetting water retention curves using Eq. [4.3]. Parameter values are  $K_s = 1000 \text{ cm days}^{-1}$  and  $\ell = 0.5$ , while the remaining parameters are the same as in the water retention curves in Fig. 4.2. For both soils, the drying  $K^d(h)$  function is larger than the wetting  $K^w(h)$  function for the entire range of  $h$ . On the other hand, the  $K^d(\theta)$  and  $K^w(\theta)$  functions are almost identical for high water contents ( $\theta > 0.3$  for  $n_1 = 2.56$  and  $\theta > 0.36$  for  $n_1 = 1.2$ ). However,  $K^d(\theta)$  is larger than  $K^w(\theta)$  for low water contents in both soils.

For high water contents, since  $S_2$  is close to 1 and  $\alpha_1$  is significantly greater than  $\alpha_2$  (Table 1), Eq. [4.3] can be reduced to

$$K(\theta) \approx K_s (w_1 S_1 + w_2)^\ell \left( \left[ 1 - \left( 1 - S_1^{1/m_1} \right)^{m_1} \right] \right)^2 \quad [4.15]$$

Hence,  $K$  as a function of  $\theta$  is almost identical for higher water contents, regardless of an  $\alpha_1$  value. Conversely,  $S_1$  becomes close to zero for lower water contents. In this case, Eq. [4.3] can be reduced to

$$K(\theta) \approx K_s (w_2 S_2)^\ell \frac{\left( w_2 \alpha_2 \left[ 1 - \left( 1 - S_2^{1/m_2} \right)^{m_2} \right] \right)^2}{(w_1 \alpha_1 + w_2 \alpha_2)^2} \quad [4.16]$$

Since  $\alpha_1$  remains in the denominator of Eq. [4.16] and  $\alpha_1^d$  is different from  $\alpha_1^w$ , unrealistic hysteresis in  $K$  as a function of  $\theta$  occurs between  $K^d(\theta)$  and  $K^w(\theta)$  for lower water contents. Note that in the case of  $w_2 = 0$  for the unimodal VG model,  $\alpha_1$  in Eq. [4.3] cancels out and  $K$  is independent from  $\alpha_1$  (van Genuchten, 1980).

The unsaturated hydraulic conductivity is generally assumed to be nonhysteretic when expressed as a function of the water content (van Genuchten, 1980; Mualem, 1986; and Plagge et al., 2005). When the K&P model for the unimodal VG model is used, nonhysteretic  $K(\theta)$  is obtained using the same  $n$  value for both wetting and drying curves (Kool and Parker, 1987). Since  $K(\theta)$  is a function of  $\alpha_1$  for the bimodal VG model, as shown in Eq. [4.16], it is possible to obtain a nonhysteretic  $K(\theta)$  function, if an additional constraint in terms of  $\alpha_1$  in Eq. [4.3] is imposed. In this study, a single value of  $\alpha_1^k$  is used for both  $K^d(\theta)$  and  $K^w(\theta)$ , while using  $\alpha_1^d$  for  $\theta^d(h)$  and  $\alpha_1^w$  for  $\theta^w(h)$ .

We demonstrate the effects of this additional constraint on  $K^d$  and  $K^w$  curves in Fig. 4.4. For example, the  $\alpha_1^k$  value is defined here as an average value of  $\alpha_1^d$  and  $\alpha_1^w$  on the logarithmic scale, i.e.,  $\log \alpha_1^k = (\log \alpha_1^d + \log \alpha_1^w)/2$ . As shown in Fig. 4.4a and 4.4c for both soils (solid lines),  $K^d(h)$  is larger than  $K^w(h)$  for higher pressure heads, whereas  $K^d(h)$  and  $K^w(h)$  are almost identical for lower pressure heads. This additional constraint in terms of the  $\alpha_1^k$  value resulted in an almost nonhysteretic  $K(\theta)$  function in the entire range of water contents, as shown in Fig. 4b and 4d.

Although in Fig. 4.4 we demonstrated the  $K(\theta)$  function with an intermediate value of  $\alpha_1^k$  (between  $\alpha_1^d$  and  $\alpha_1^w$ ), in an ideal case,  $\alpha_1^k$  would be a fitting parameter obtained from an experimentally determined  $K(\theta)$  for low water contents. However, such experimental data are rarely, if ever, available. Further experimental investigations will be needed to evaluate  $K(\theta)$  in a relatively dry range.

#### 4 A hysteretic model of hydraulic properties

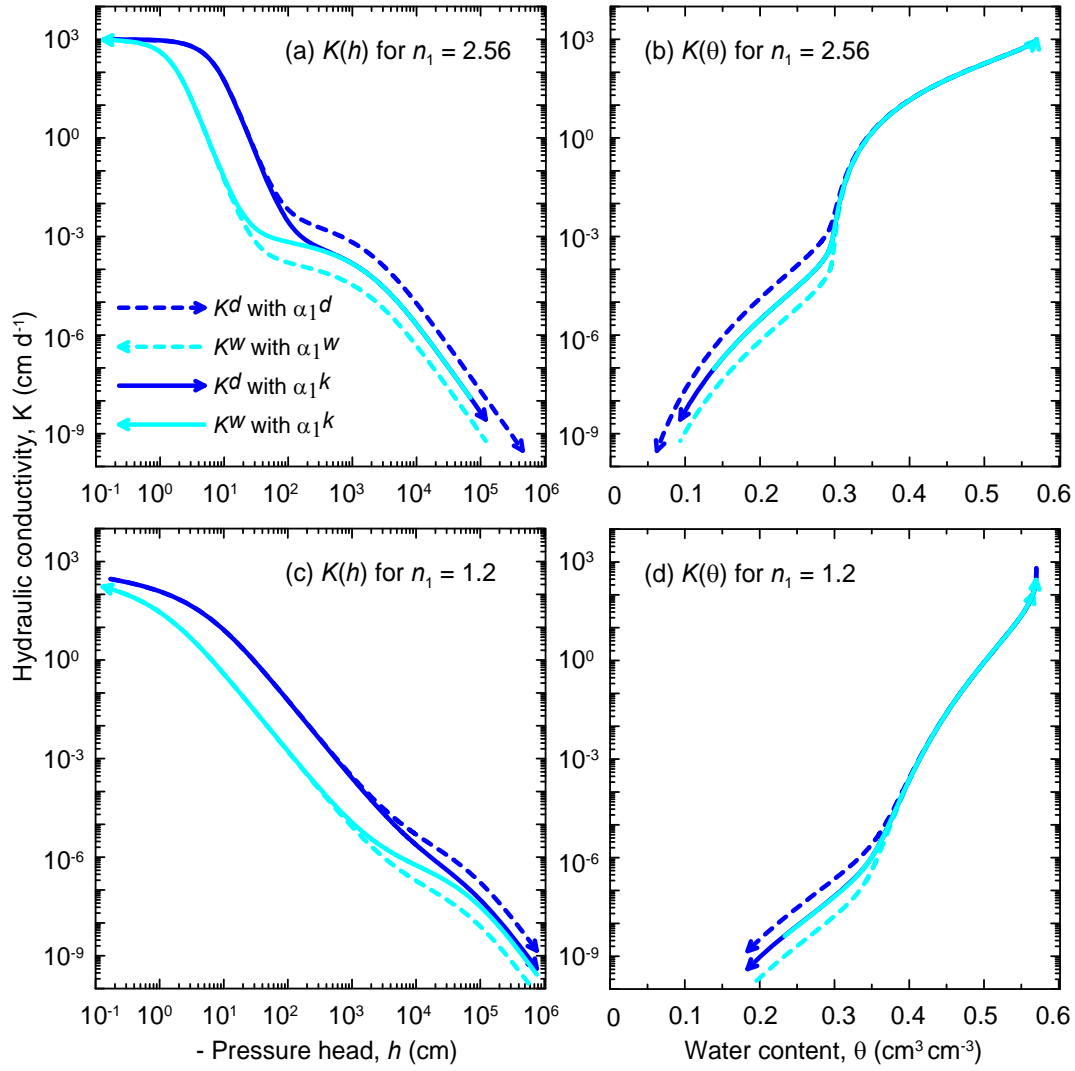


Fig. 4.4 The unsaturated hydraulic conductivity functions (dashed lines) for the main drying and wetting water retention curves shown in Fig. 4.2: (a)  $K(h)$  and (b)  $K(\theta)$  for the soil with  $n_1 = 2.56$ , and (c)  $K(h)$  and (d)  $K(\theta)$  for the soil with  $n_1 = 1.2$ . The  $K(h)$  and  $K(\theta)$  functions with a single value of  $\alpha_1^k$  are also plotted as solid lines in each figure. Dark blue lines represent drying curves and light blue lines represent wetting curves.

#### 4.4 CONCLUSIONS

We proposed here a hysteretic model of soil hydraulic properties for dual-porosity soils. The model is based on a bimodal VG model (Durner, 1994) and the K&P hysteresis model (Kool and Parker, 1987). Hysteresis is considered only in the first subregion,  $\theta_1(h)$ , affecting mainly higher water contents, while a nonhysteretic behaviour is assumed in the second subregion,  $\theta_2(h)$ , affecting mainly lower water contents. The main hysteretic loop is described with  $\alpha_1^d$  for the main drying curve,  $\theta_1^d(h)$ , and  $\alpha_1^w (>\alpha_1^d)$  for the main wetting curve,  $\theta_1^w(h)$ . Remaining parameter values are the same for the main drying and wetting curves. For soils with the larger  $n_1$  (e.g.,  $n_1 = 2.56$ ), hysteresis affects mainly the first part of the retention curve  $\theta(h)$  near saturation. On the other hand, for soils with the smaller  $n_1$  (e.g.,  $n_1 = 1.2$ ), some hysteresis extends from the full saturation to lower pressure heads, also affecting the second part of the retention curve  $\theta(h)$ . Scanning curves of  $\theta(h)$  can also be successfully described using the K&P model in the first subregion of  $\theta_1(h)$ . The observed main hysteretic loop and scanning curves for Andisols aggregates could be reasonably well described using this proposed hysteretic model.

The drying and wetting unsaturated hydraulic conductivity functions  $K^d(\theta)$  and  $K^w(\theta)$ , respectively, are almost identical for higher water contents. However,  $K^d(\theta)$  is greater than  $K^w(\theta)$  for lower water contents. To overcome this unrealistic phenomenon in the conductivity function, we use an additional constraint on the value of the  $\alpha_1$  parameter and use a single value  $\alpha_1^k$  for both drying and wetting functions. As a result, an almost nonhysteretic  $K(\theta)$  function is obtained for the entire range of water contents. It is necessary to experimentally investigate  $K(\theta)$  for low water contents to determine the  $\alpha_1^k$  value.

#### 4.5 REFERENCES

- Coppola, A. 2000. Unimodal and bimodal descriptions of hydraulic properties for aggregated soils. *Soil Sci. Soc. Am. J.* 64:1252-1262. doi:10.2136/sssaj2000.6441252x
- Diamantopoulos, E., S.C. Iden, and W. Durner. 2012. Inverse modeling of dynamic nonequilibrium in water flow with an effective approach. *Water Resour. Res.* 48:W03503. doi:10.1029/2011WR010717
- Durner, W. 1992. Predicting the unsaturated hydraulic conductivity using multi-porosity water retention curves. p. 185-202. In M.Th. van Genuchten et al. (ed.) *Proceedings of the International Workshop on Indirect Methods for Estimating the Hydraulic Properties of Unsaturated Soils*. University of California, Riverside.
- Durner, W. 1994. Hydraulic conductivity estimation for soils with heterogeneous pore structure. *Water Resour. Res.* 30:211-223. doi:10.1029/93WR02676
- Durner, W., and S.C. Iden. 2011. Extended multistep outflow method for the accurate determination of soil hydraulic properties near water saturation. *Water Resour. Res.* 47:W08526. doi:10.1029/2011WR010632
- Fayer, M.J. 2000. UNSAT-H version 3.0: unsaturated soil water and heat flow model theory, user manual, and examples. Pacific Northwest National Laboratory Richland, Washington.
- Kool, J.B., and J.C. Parker. 1987. Development and evaluation of closed-form expressions for hysteretic properties. *Water Resour. Res.* 23:105-114. doi:10.1029/WR023i001p00105
- Kroes, J.G., J.C. Van Dam, P. Groenendijk, R.F.A. Hendriks, and C.M.J. Jacobs. 2008. SWAP version 3.2. Theory description and user manual. Alterra, Wageningen.
- Lenhard, R.J., J.C. Parker, and J.J. Kaluarachchi. 1991. Comparing simulated and experimental hysteretic two-phase transient fluid flow phenomena. *Water Resour. Res.* 27:2113-2124. doi:10.1029/91WR01272
- Lenhard, R.J., and J.C. Parker. 1989. Modeling multiphase fluid hysteresis and comparing results to laboratory investigations. In M.Th. van Genuchten, F.J. Leij, and L.J. Lund (ed.), *Proc. Intl. Workshop on Indirect Methods for Estimating the Hydraulic Properties of Unsaturated Soils*. October 11-13, 1989, University of California, Riverside. p. 233-248.

- Miyamoto, T., T. Annaka, and J. Chikusi. 2003. Soil aggregate structure effects on dielectric permittivity of an andisol measured by time domain reflectometry. *Vadose Zone J.* 2:90-97. doi: 10.2136/vzj2003.9000
- Mualem, Y. 1976. A new model for predicting the hydraulic conductivity of unsaturated porous media. *Water Resour. Res.* 12:513-522. doi:10.1029/WR012i003p00513.
- Mualem, Y. 1986. Hydraulic conductivity of unsaturated soils: Prediction and formulas. p. 799-824. In A. Klute (ed.), *Methods in soil analysis. Part 1. Agron. Monogr.* 9. ASA and SSSA, Madison, WI.
- Peters, A., and W. Durner. 2008. A simple model for describing hydraulic conductivity in unsaturated porous media accounting for film and capillary flow. *Water Resour. Res.* 44:W11417. doi:10.1029/2008WR007136
- Plagge, R., G. Scheffler, J. Grunewald, and M. Funk. 2006. On the hysteresis in moisture storage and conductivity measured by the instantaneous profile method. *J. Bldg. Phys.* 29:247-259. doi: 10.1177/1744259106060706
- Priesack, E., and W. Durner. 2006. Closed-form expression for the multi-modal unsaturated conductivity function. *Vadose Zone J.* 5:121-124. doi:10.2136/vzj2005.0066
- Schelle, H., S.C. Iden, A. Peters, and W. Durner. 2010. Analysis of the agreement of soil hydraulic properties obtained from multistep-outflow and evaporation methods. *Vadose Zone J.* 9:1080-1091. doi: 10.2136/vzj2010.0050
- Schelle, H., S.C. Iden, and W. Durner. 2011. Combined transient method for determining soil hydraulic properties in a wide pressure head range. *Soil Sci. Soc. Am. J.* 75:1681-1693. doi: 10.2136/sssaj2010.0374
- Schindler, J., W. Durner, G. von Unold, and L. Müller. 2010. Evaporation method for measuring unsaturated hydraulic properties of soils: Extending the measurement range. *Soil Sci. Soc. Am. J.* 74:1071-1083. doi: 10.2136/sssaj2008.0358
- Scott, P.S., G.J. Farquhar, and N. Kouwen. 1983. Hysteresis effects on net infiltration. *Publ.* 11-83. p. 163-170. In *Advances in Infiltration*. Am. Soc. of Agric. Eng. St. Joseph, Mich.
- Šimůnek, J., M. Šejna, H. Saito, M. Sakai, and M.Th. van Genuchten. 2008a. The Hydrus-1D software package for simulating the movement of water, heat, and



- multiple solutes in variably saturated media. Version 4.0. HYDRUS Softw. Ser. 3. Dep. of Environ. Sci., Univ. of California, Riverside.
- Šimůnek, J., M. Th. van Genuchten, and M. Šejna. 2008b. Development and applications of the HYDRUS and STANMOD software packages, and related codes. *Vadose Zone J.* 7:587–600. doi:10.2136/vzj2007.0077
- Steinberg, S.L, G.J. Kluitenberg, S.B.Jones, N.E. Daidzic, L.N. Reddi, M. Xiao, M. Tuller, R.M. Newman, D. Or, and J.I.D. Alexander. 2005. Physical and hydraulic properties of baked ceramic aggregates used for plant growth medium. *J. Amer. Soc. Hort. Sci.* 130:767-774.
- van Genuchten, M.Th. 1980. A closed-form equation for predicting the hydraulic conductivity of unsaturated soils. *Soil Sci. Soc. Am. J.* 44:892-898. doi:10.2136/sssaj1980.03615995004400050002x

#### 4 A hysteretic model of hydraulic properties

## CHAPTER 5

# ROLES OF AGGREGATE STRUCTURE OF ANDISOLS IN WATER FLOW IN THE ROOT ZONE

### 5.1 INTRODUCTION

Soil productivity is a soil capacity to produce a certain yield for a specific crop under optimum condition (Shoji et al., 1993). From soil physics point of view, soil productivity strongly depends on sufficient water and oxygen in the root zone of plant. Those key factors are corresponding to plant available water (PAW) and soil aeration at the root zone.

PAW is controlled by water retention. PAW is generally defined as the difference between -33 kPa water content,  $\theta_{fc}$  (water content at the field capacity) and -1500 kPa water content,  $\theta_{wp}$  (water content at the permanent wilting point) (Nanzyo et al., 1993). Soil texture and structure will effect on water retention, thereby PAW and soil productivity. Coarse textured soils have low PAW because water held in large pores has drained before the field capacity reaches. Fine textured soils also have low PAW because large the specific surface gives large water content in the wilting point. Large PAW is obtained in medium textured soils (Radcliffe and Šimůnek, 2010).

In twin fluids-water and air, their volume fractions are inversely correlated where an increase of the one causes a decrease the other (Hillel, 1998). Thus, soil aeration and free drainage have a strong relationship which also depends on soil texture and soil structure. Coarse textured and strong aggregate soils which have large pores are typically well aerated soils because a lot of water drains quickly and subsequently, air fills the open pores. Conversely, fine textured soils which hold the most water and are difficult to release gravitational water are typically poor aeration soils.

Andisols are known the most productive soil in the earth because Andisols could provide favorable condition for plant root growth such as large water storage and PAW, large drainage rate and good aeration (Nanzyo et al., 1993; Shoji et al., 1993; Shoji and

Takahashi, 2002; Nanzyo, 2002; and Dahlgren et al., 2004). Moreover, Andisols also reduce runoff (flood) and hence to soil erosion due to high water infiltration. Schematically, those valueable properties of Andisols are shown in Fig. 5.1. Those properties are resulted in by aggregate structure that well developed in Andisols. Noncrystalline materials (e.g., allophane, imogolite, ferrihydrite) and organic C content (humus), the soil moisture or alternate wetting and drying contribute highly on the formation of interaggregate and intraaggregate pores and low bulk density of Andisols. Interaggregate and intraaggregate pores are created within and between aggregates, respectively. That pore system produce stepwise (two sub-curves) soil water retention, high porosity and wide range of pore size distribution that retain large amount of water with varying pressure head (Miyamoto et al., 2003). The intraaggregate pores retain water tightly for PAW, while interaggregate pores play important role in soil aeration and water infiltration (Shoji et al., 1993; Shoji and Takahashi, 2002; Dahlgren et al., 2004).

Recently, Chamindu Deepagoda et al. (2012) analyzed oxygen and nutrients supply and water availability in a Japanese Andisol as a candidate of porous growth media for future space-based applications using the critical windows of diffusivity and the critical water storage window or PAW. They concluded that Andisol is better than the tested four commercial growth media such as: Pumice, Turface, Profile, and Zeoponic; and shows large perspectives for Martian outpost missions, since NASA has found that Martian dust/soil mostly resembles volcanic ash soil among terrestrial materials.

Mostly previous studies used water retention curve to analyze PAW in Andisols (Chamindu Deepagoda et al., 2012; Ahmed et al., 2009; Armas-Espinel et al., 2003; Arnalds et al., 1995; Nanzyo et al., 1993). The PAW based on the different  $\theta_{fc}$  and  $\theta_{wp}$  from soil water retention represents maximum value because the actual water content,  $\theta$  of soil in the field might be varied. Therefore, we define the difference between  $\theta_{fc}$  and  $\theta_{wp}$  as “the potential PAW” (PAWo) while the difference between the actual water content and the wilting point water content is defined as “the actual PAW”.

## 5 Roles of aggregate structure

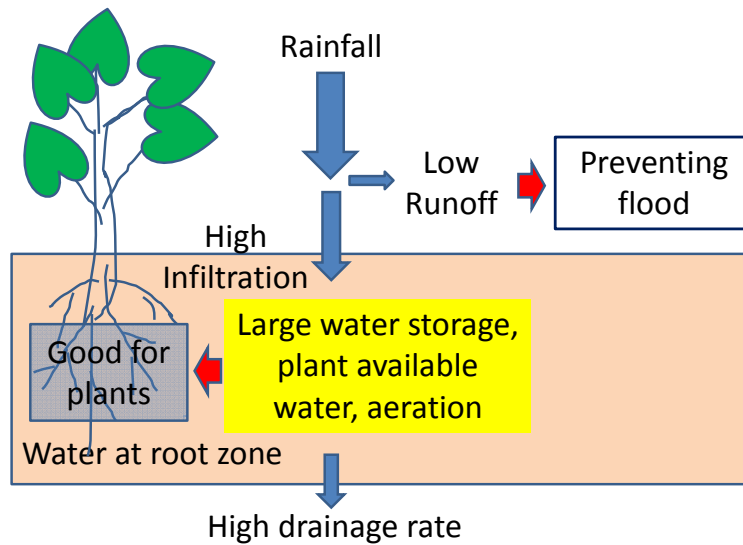


Fig. 5.1. Valuable properties of Andisols for agriculture and environment

Evaluation of the actual PAW can be conducted using transient water flow to represent the actual water content at the root zone. The transient water flow will account the effect of not only water retention but also unsaturated hydraulic conductivity on the actual PAW.

The objective of this study is to evaluate the roles of aggregate structure of Andisols for the infiltration, surface runoff, redistribution, water and air storage, and drainage from the root zone and the potential and actual PAW based on numerical analysis of water flow. Infiltration followed by redistribution was carried out in Andisols, sandy loam and clay soils and subsequently the results were compared.

## 5.2 THEORETICAL CONSIDERATION

### 5.2.1 Governing equation of water flow.

In unsaturated zone, vertical water flux may be expressed based on the Buckingham-Darcy flux law (Jury and Horton, 2004 and Radcliffe and Šimůnek, 2010):

$$J_w = -K(h) \frac{\partial h}{\partial z} - K(h) \quad [5.1]$$

Where  $J_w$  is the total water flux ( $L \ T^{-1}$ ),  $h$  is the soil-water pressure head (L),  $K$  is the unsaturated hydraulic conductivity ( $L \ T^{-1}$ ). The first term in the right side,  $-K(h)\partial h/\partial z$  is the capillary flux, that is water flux due to the capillarity, while the second one,  $-K(h)$  is the gravity flux, that is water flux due to the gravity.

Water flow is assumed in an equilibrium condition. The Richard equation in vertical direction of one dimensional flow without sinks and sources is given by (Jury and Horton, 2004 and Radcliffe and Šimůnek, 2010):

$$\frac{\partial \theta(h)}{\partial t} = -\frac{\partial J_w}{\partial z} = \frac{\partial}{\partial z} \left( K(h) \frac{\partial h}{\partial z} + K(h) \right) \quad [5.2]$$

The initial condition and the upper and bottom boundary condition for infiltration followed by redistribution processes are as follows

$$h(z, t) = h_o \quad t = 0, 0 \leq z \leq L \quad [5.3]$$

$$-K(h) \left[ \frac{\partial h}{\partial z} + 1 \right] = \begin{cases} q_{in}(t) & 0 < t < t_1, z = L \\ 0 & t > t_1, z = L \end{cases} \quad [5.4]$$

$$-K(h) \left[ \frac{\partial h}{\partial z} + 1 \right] = -K(h) \quad t > 0, z = 0 \quad [5.5]$$

where  $\theta$  is the volumetric water content ( $L^3 L^{-3}$ ),  $z$  is a vertical coordinate (L) positive upward,  $t$  is time (T),  $q_{in}(t)$  is the rainfall rate ( $L T^{-1}$ ), and  $t_1$  is final time for infiltration (T). Note that, surface runoff will occur when pressure head at the soil surface is equal to zero, and  $|-K(h)\partial h/\partial z - K(h)| < q_{in}(t)$ . In this case, a prescribed head boundary condition will be used to calculate the actual surface flux (Šimůnek et al., 2008).

### 5.2.2 Soil hydraulic functions

Soil water retention is described by the bimodal VG model (Durner, 1994):

$$S = \frac{\theta(h) - \theta_r}{\theta_s - \theta_r} = w_1 S_1 + w_2 S_2 \quad [5.6]$$

where  $S_i$  is given by:

$$S_i = \left[ 1 + (\alpha_i h)^{n_i} \right]^{-m_i} \quad [5.7]$$

the subscript  $i$  represents the number of subregion ( $i = 1, 2$ ),  $S$  is the effective saturation,  $h$  is the soil water pressure head,  $\theta_s$  and  $\theta_r$  are the saturated and residual water contents, respectively,  $n_i$ ,  $\alpha_i$ , and  $m_i$  ( $=1-1/n_i$ ) are shape parameters subject to  $\alpha_i > 0$ ,  $\alpha_1 > \alpha_2$  and  $n_i > 1$ . Parameter  $w_i$  are weighing factor subject to  $0 < w_i < 1$  and  $w_1 + w_2 = 1$ .

A closed form expression of unsaturated hydraulic conductivity for the bimodal VG model based on the Mualem model (Mualem, 1976) is given by Priesack and Durner (2006):

$$K(\theta) = K_s (w_1 S_1 + w_2 S_2)^\ell \frac{\left( w_1 \alpha_1 \left[ 1 - \left( 1 - S_1^{1/m_1} \right)^{m_1} \right] + w_2 \alpha_2 \left[ 1 - \left( 1 - S_2^{1/m_2} \right)^{m_2} \right] \right)^2}{(w_1 \alpha_1 + w_2 \alpha_2)^2} \quad [5.8]$$

where  $K_s$  is the saturated hydraulic conductivity ( $\text{L T}^{-1}$ ), and  $\ell$  is the pore-connectivity coefficient (-). In case of  $w_2 = 0$ , Eqs. [5.6] and [5.7] are identical with the unimodal VG model (van Genuchten, 1980).

## 5.3 MATERIALS AND METHODS

### 5.3.1 Materials

Three soils were used in this study: (1) Kumamoto Andisol, (2) Sandy loam and (3) Clay. Kumamoto Andisol soil was collected from Kumamoto prefecture, Japan exhibits strong aggregated structure. Sandy loam and clay soils were used to represent contrasting soil texture. To describe soil hydraulic functions, the bimodal VG model was for Kumamoto Andisol and the unimodal VG model was for sandy loam and clay soils. The bimodal VG parameters for Kumamoto Andisol were obtained in **Chapter 3** (Rudiyanto et al., 2013<sup>b</sup>). The unimodal VG parameters for sandy loam and clay soils were set base on Hydrus-1D soil catalog (Carsel and Parrish, 1988). Figure 5.2 shows soil hydraulic properties for Kumamoto Andisol, sandy loam and clay soils, and parameter set for those soils were listed in Table 5.1.

Table 5.1. Soil hydraulic parameters of the bimodal VG model for Kumamoto Andisol and the unimodal VG model for sandy loam and clay soils.

Soils	$\theta_r$	$\theta_s$	$\alpha_1$	$n_1$	$K_s$	$\ell$	$w_2$	$\alpha_2$	$n_2$
	( $\text{cm}^3 \text{ cm}^{-3}$ )		( $\text{cm}^{-1}$ )	(-)	( $\text{cm d}^{-1}$ )	(-)	(-)	( $\text{cm}^{-1}$ )	(-)
Kumamoto Andisol	0.000	0.780	0.044	1.96	343.2	0.435	0.549	0.000132	1.39
Sandy Loam	0.065	0.410	0.075	1.89	106.1	0.5	0	-	-
Clay	0.068	0.380	0.008	1.09	4.8	0.5	0	-	-

## 5 Roles of aggregate structure

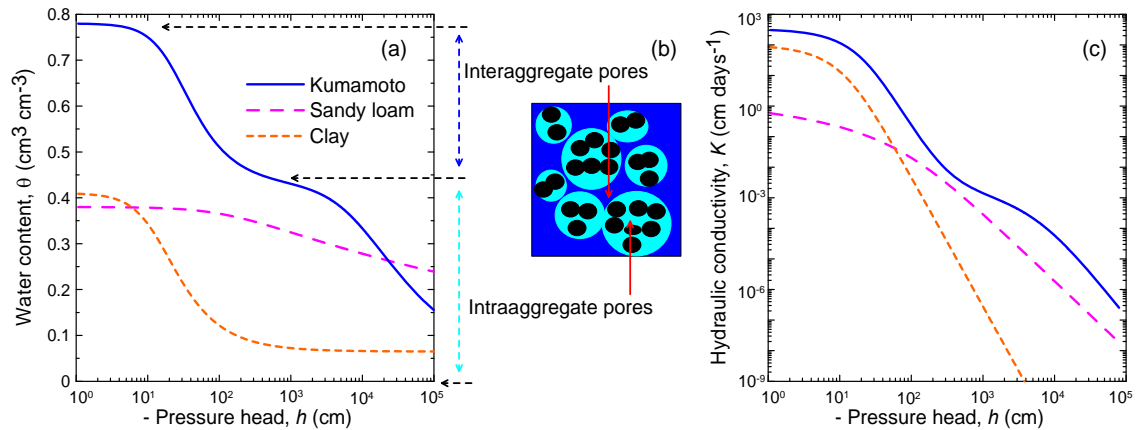


Fig.5.2. Hydraulic properties for Kumamoto Andisol, sandy loam, and clay soils, (a) water retention curves, (b) schematic soil pore system (interaggregate and intraaggregate pores) in Andisol soils and (c) unsaturated hydraulic conductivity curves.

### 5.3.2 Numerical analysis of water flow

The numerical analysis of water flow was conducted using Hydrus-1D (Šimůnek et al., 2008) in 200 cm soil depth. Depth of the root zone was 50 cm. To represent infiltration and followed by redistribution process, upper boundary condition (BC) was set as atmospheric BC with surface runoff (no ponding) where rainfall rate is 10 cm d<sup>-1</sup> for 1 day and subsequently equal to be zero for 29 days. Evapotranspiration was zero and there was no root water uptake. Lower boundary condition was free drainage. Initial condition was uniform pressure head,  $h = -15000$  cm which is the wilting point. To calculate water drainage from the root zone two observation points were put at 50 and 51 cm. Hysteresis on soil hydraulic properties was neglected.

Calculation of the actual *PAW* at the root zone requires the field capacity and the wilting points. Romano and Santini (2002) suggested using water content of field capacity at pressure head of -10 kPa for sandy soils, -35 kPa for medium-textured soils, and -50 kPa for clay soils. Table 5.2 shows the field capacity, the wilting point and the potential available water for Kumamoto Andisol, sandy loam and clay that used in this study.



Table 5.2. Field capacity, wilting point and potential available water for Kumamoto Andisol, sandy loam and clay soils.

Soils	Field Capacity		Wilting Point		Potential PAW
	$h_{fc}$	$\theta_{fc}$	$h_{wp}$	$\theta_{wp}$	$\theta_{PAW}$
	(cm)	(cm <sup>3</sup> cm <sup>-3</sup> )	(cm)	(cm <sup>3</sup> cm <sup>-3</sup> )	(cm <sup>3</sup> cm <sup>-3</sup> )
Kumamoto Andisol	-350	0.454	-15000	0.300	0.154
Sandy Loam	-100	0.122	-15000	0.066	0.056
Clay	-500	0.339	-15000	0.271	0.068

## 5.4 RESULTS AND DISCUSSION

### 5.4.1 Soil water infiltration and surface runoff

Amount water that infiltrated into soil is represented by cumulative infiltration, while surface runoff is represented portion of the water supply that not enters into the soil (Hillel, 1998). Cumulative infiltration and surface runoff during infiltration process (0 - 1 day) for sandy loam, clay and Kumamoto Andisol soils are shown in Fig. 5.3. Cumulative infiltration for sandy loam and Kumamoto Andisol soils were same where it increased linearly and reached 10 cm at 1 day (Fig. 5.3a). Since the rainfall rate (10 cm d<sup>-1</sup>) was less than the final gravity- dominated infiltration rate  $\approx K_s$  (Jury and Horton, 2004), for sandy loam (106.1 cm d<sup>-1</sup>) and Kumamoto Andisol soil (343.2 cm d<sup>-1</sup>), all water in both soils will infiltrate into the soil and there was no runoff as shown in Fig. 5.3b. Contrary for clay soil, it was not all amount of water infiltrated into soil because the rainfall rate (10 cm d<sup>-1</sup>) exceeded the final gravity- dominated infiltration rate  $\approx K_s$  (4.8 cm d<sup>-1</sup>). Therefore, surface runoff occurred for clay soil as shown in Fig. 5.3b.

Above examples suggested that Andisols are able to prevent flood due to large  $K_s$  which resulted in by interaggregate pores (see Fig. 5.2). Moreover, there was no soil water erosion owing to no-surface runoff (Radcliffe and Šimůnek, 2010). Poulenard et al. (2001) also reported that natural plots of Andisols from the Ecuadorian *Púravlzo* had very high infiltration rate and very low sediment loss.

Figure 5.4 shows profiles water content for sandy loam, clay and Kumamoto Andisol during infiltration process,  $t = 0, 0.5$  and 1 day. The profiles show depths of wetting front were 43, 32 and 37 cm for sandy loam, clay and Kumamoto Andisol,

## 5 Roles of aggregate structure

respectively. Although, the infiltration rate (=the rainfall rate) was the same, penetrating wetting front for sandy loam was deeper than that of Kumamoto Andisol soil because Kumamoto Andisol soil has more pores space at certain pressure head than that of sandy loam soil as shown by soil water retention (see Fig. 5.2a) and larger difference between the wetted surface water content and initial water content,  $0.324 \text{ cm}^3 \text{ cm}^{-3}$  for Kumamoto Andisol soil and  $0.263 \text{ cm}^3 \text{ cm}^{-3}$  for sandy loam soil. Water filled more pores space in Kumamoto Andisol, thus, the wetting front of Kumamoto Andisol soil moved downward slower than that of sandy loam soil. Clay soil exhibited shallowest wetting front due to lowest  $K_s$ .

## 5 Roles of aggregate structure

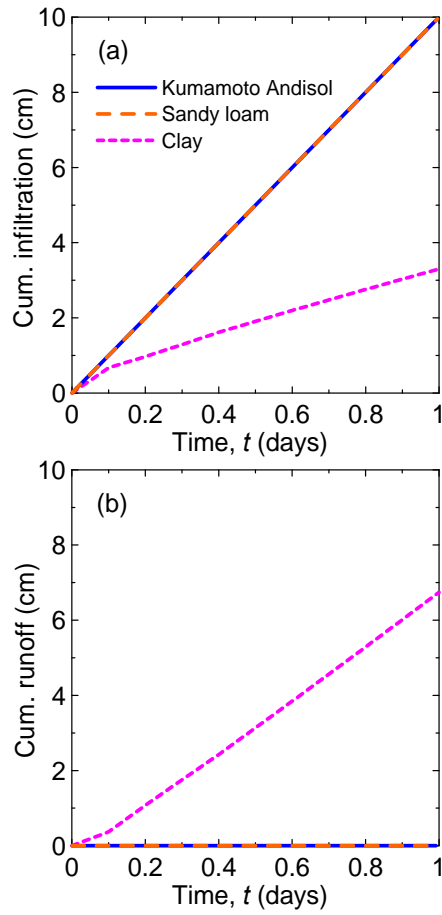


Fig. 5.3. (a) Cumulative infiltration and (b) Surface runoff for Kumamoto Andisol, sandy loam, and clay soils.

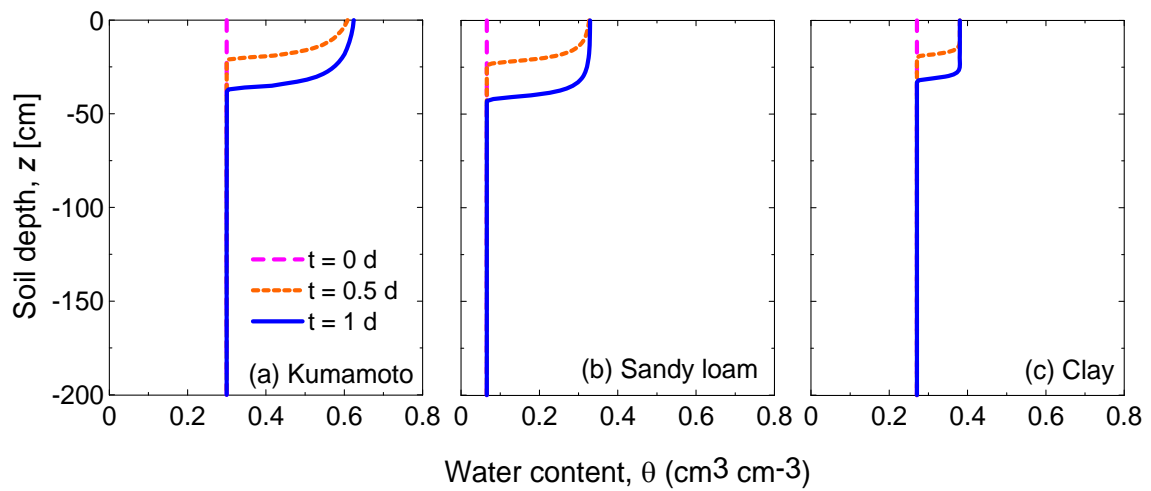


Fig. 5.4. Water content profiles during infiltration period ( $t = 0$ -1 day) for (a) Kumamoto Andisol, (b) sandy loam, and (c) clay soils.

#### 5.4.2 Redistribution of water in soil

When rain have ceased and there is no free water on the soil surface, part of water from the wetted soil at the upper soil moves downward into the lower soil layer because of the gravity and probably also the capillarity. If groundwater is absence or the water table is too deep to affect the relevant depth zone, and the profile is initially dry, this movement is referred to redistribution (Hillel, 1998).

Figure 5.5 and 5.6 show water content and pressure head profiles during redistribution,  $t = 1, 6$  and 30 days. Wetting front for sandy loam soil moved downward fastest followed by Kumamoto Andisol and then clay soil because total water flux at wetting front for sandy loam is greatest, for example water flux profiles at  $t = 6$  days as shown in Fig. 5.7 that calculated from pressure head profile  $t = 6$  days (Fig. 5.6) using Eq.(5.1).

For clay and Kumamoto Andisol soils, water content at wetted soil profiles decreased almost uniform near surface (Fig 5.5a and 5.5c) and then, tail was developed at wetting front because the peak of capillary flux at wetting front was larger than the peak of gravity flux at behind water front as shown in Fig. 5.7a and 5.7c. For Kumamoto Andisol soil, it was found that water filled intraaggregate pores at wetting front (Fig. 5.5a) which suggests that intraaggregate pores are responsible on the capillary flux profile, thereby total water flux profile during redistribution (Fig. 5.7a).

For sandy loam soil, water content near soil surface dropped slightly faster than the wetted soil profile behind the wetting front, thus water content at wetted soil profile slightly increased with depth (Fig 5.5b). Furthermore, shape of wetting front was slightly sharp because peak of gravity flux behind wetting front was larger than peak of capillary flux at wetting front as shown in Fig. 5.6b.

## 5 Roles of aggregate structure

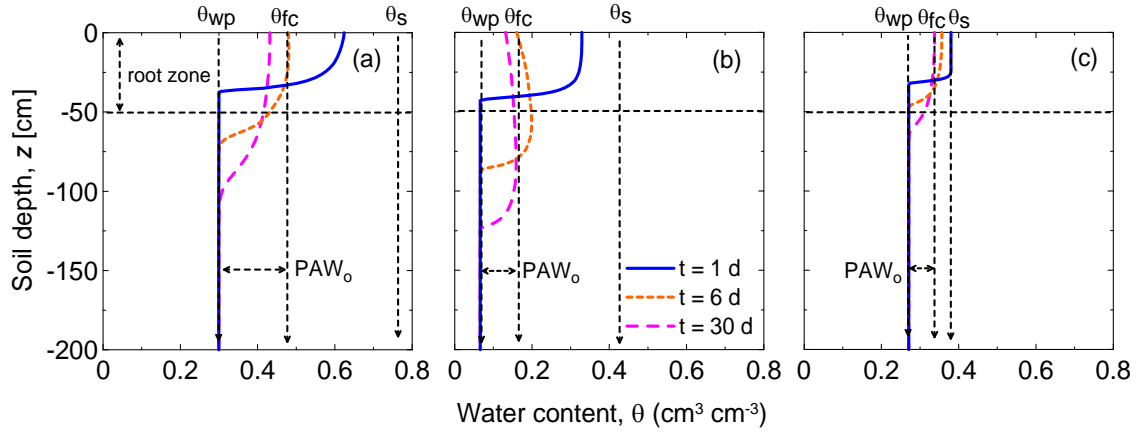


Fig. 5.5. Water content profiles during redistribution period,  $t = 1$  (starting redistribution), 6 and 30 days, for (a) Kumamoto Andisol, (b) sandy loam, and (c) clay soils.  $PAW_o$  is the potential plant available water which is  $\theta_{fc} - \theta_{wp}$ ;  $\theta_{wp}$  and  $\theta_{fc}$  are the wilting point water content and the field capacity water content, respectively.

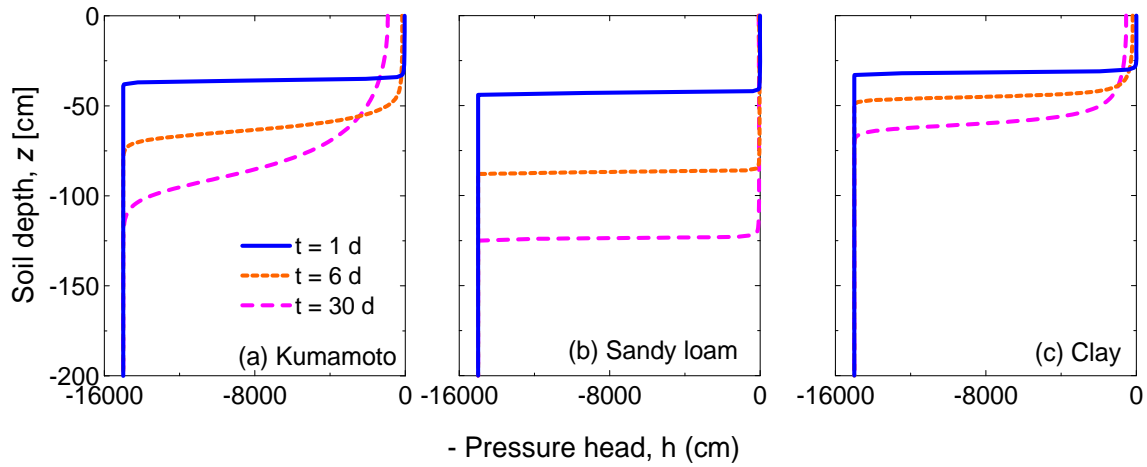


Fig. 5.6. Pressure head profiles during redistribution period,  $t = 1$  (starting redistribution), 6 and 30 days, for (a) Kumamoto Andisol, (b) sandy loam, and (c) clay soils.

## 5 Roles of aggregate structure

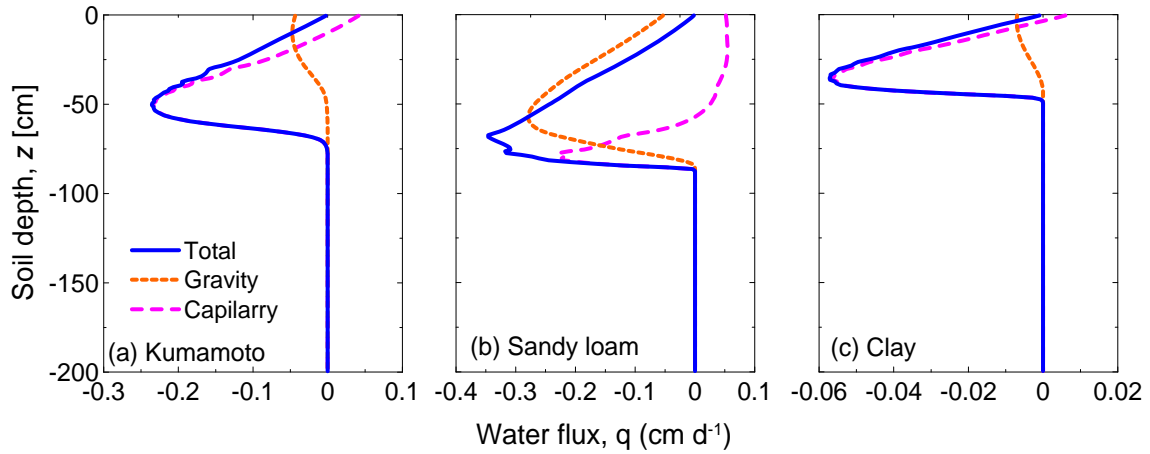


Fig. 5.7. Total, gravity and capillary flux profiles during redistribution period,  $t = 6$  days, for (a) Kumamoto Andisol, (b) sandy loam, and (c) clay soils.

### 5.4.3 Drainage from the root zone

Drainage flux ( $D_i$ ) from the root zone was calculated using the Buckingham-Darcy flux law, Eq. [5.9] from observation nodes at 50 and 51 cm depths:

$$D_i(t) = - \left[ \frac{K(h_{zr}) + K(h_{zr-1})}{2} \right] \left[ \left( \frac{h_{zr} - h_{zr-1}}{\Delta z} \right) + 1 \right] \quad [5.9]$$

Where  $h_{zr}$  is the pressure head at a node  $zr = 50$  cm, and  $zr-1$  is a node below  $zr$ . Then, cumulative drainage ( $CD_i$ ) from the root zone was obtained by integrating the flux over the time, Eq. [5.10]:

$$CD_i(t) = \int_{t=0}^{t=t_f} D_i dt \quad [5.10]$$

Drainage flux and cumulative drainage from the root zone for Kumamoto Andisol, sandy loam, and clay soils are presented in Fig. 5.8a and 5.8b, respectively. When drainage flux started to increase, it indicated that the wetting front started to reach the bottom root zone. It showed that the wetting front for sandy soil was fastest to reach the bottom root zone ( $t =$  about 1.2 days) followed by Kumamoto Andisol ( $t =$  about 2 days) and then clay ( $t =$  about 17.5 days). It is confirmed by water content and pressure head profiles during redistribution (Fig. 5.4 and 5.5) that wetting front of sandy loam move downward fastest followed by Kumamoto and clay soils. Drainage flux for sandy loam soil increased suddenly because of sharp wetting front. On the other hand, drainage flux for clay soil increased gradually because of tail in wetting front. For those three soils,

after the drainage fluxes reached the peak, it decreased gradually because pressure head profile at the root zone decreased continually as water moved downward to reach equilibrium (Fig. 5.5).

The peak of drainage flux for sandy loam was largest followed by those of Kumamoto Andisol and clay soils (Fig. 5.8a). Thus, Sandy loam exhibited large cumulative drainage (5.6 cm) followed by those of Kumamoto Andisol (3.6 cm) and clay soils (0.3) at 30 days as shown in Fig. 5.8b. As also reported by Nanzyo et al. (1993); Shoji et al. (1993); Shoji and Takahashi (2002); and Dahlgren et al. (2004), this study also showed that Kumamoto Andisol exhibited large drainage rate, albeit not as large as that in sandy loam soil. Large drainage rate is important for soil aeration, however, large drainage rate will effect on nutrient leaching in Andisol. Maeda et al. (2003) reported that application of large amount of N from chemical fertilizers in Andisols can cause substantial  $\text{NO}_3$  leaching. Sansoulet et al. (2007) and Sansoulet et al. (2008) also showed that large drainage volume and fast leaching of nutrients from Andisols occurred under the banana stem due to stemflow.

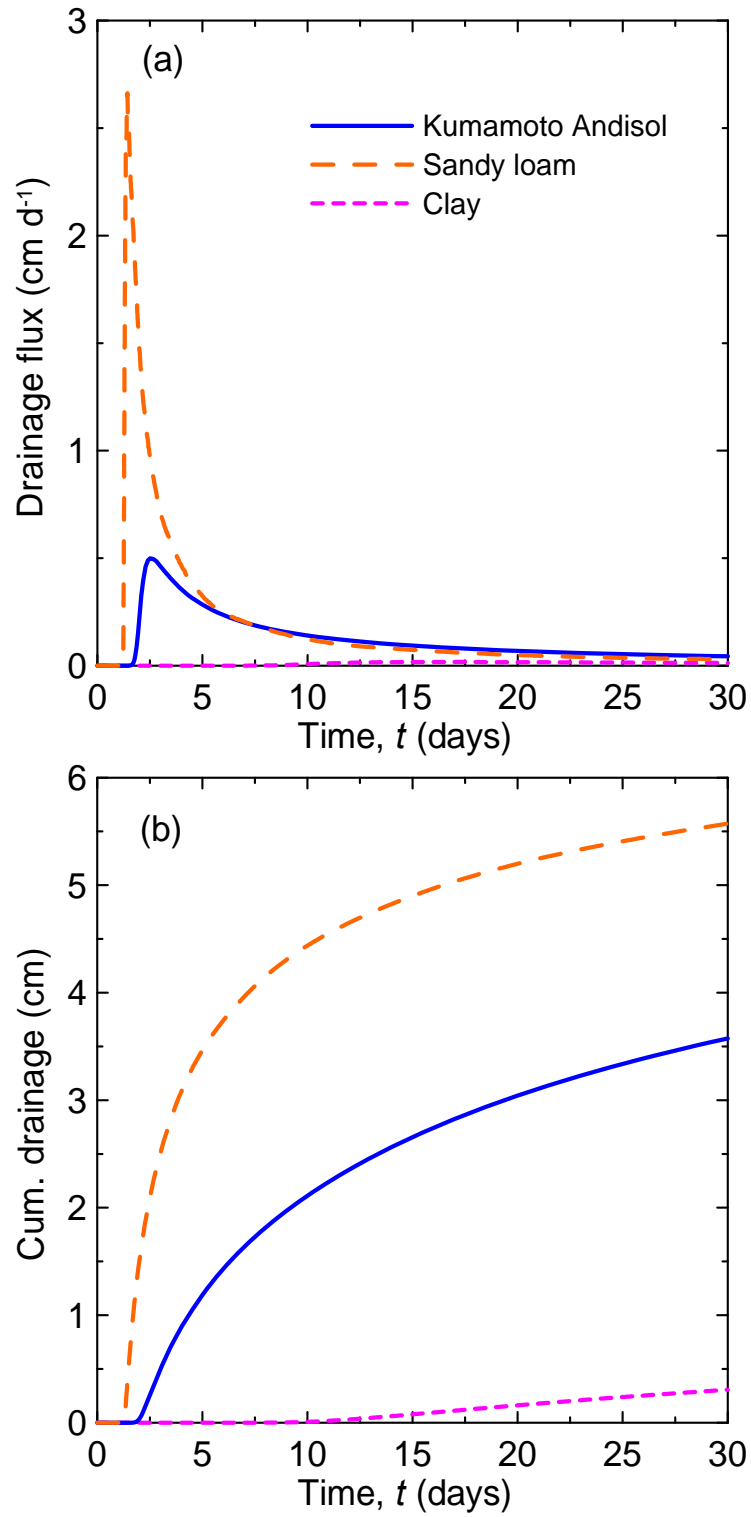


Fig. 5.8. (a) Drainage flux and (b) cumulative drainage at the bottom root zone for Kumamoto Andisol, sandy loam, and clay soils.



#### 5.4.4 Water and air storage and PAW

Figure 5.9 shows twin-fluid system (water and air content) profiles for Kumamoto Andisol  $t = 0, 1$  and 30 days. Thus, based on those schematic, water and air storage and actual PAW at the root zone were calculated as a function of time using Eqs. [5.11 - 5.14]:

(a) Water storage ( $WS$ ) at the root zone

$$WS(t) = \int_{z=0}^{z=zr} \theta(z, t) dz \quad [5.11]$$

(b) Air content ( $AC$ ) at the root zone, for simplification, twin liquid phase (water and air) is used and assumed  $\theta_s$  is equal to porosity,  $\phi$ .

$$AC(t) = \int_{z=0}^{z=zr} \theta_s(z) dz - \int_{z=0}^{z=zr} \theta(z, t) dz \quad [5.12]$$

(c) Potential plant available water (the potential  $PAW$ ) at the root zone

$$Potential\ PAW(t) = \int_{z=0}^{z=zr} (\theta_{fc} - \theta_{wp}) dz \quad [5.13]$$

where  $\theta_{wp}$  is the water content at the wilting point, and  $\theta_{fc}$  is the water content at the field capacity.

(d) Actual plant available water (the actual  $PAW$ ) at the root zone

$$Act\ PAW(t) = \int_{z=0}^{z=zr} (p(z)) dz \begin{cases} p(z, t) = 0 & (h(z, t) \geq h_{fc}) \\ p(z, t) = (\theta(z, t) - \theta_{wp}) & (h_{wp} \leq h(z, t) \leq h_{fc}) \\ p(z, t) = 0 & (h(z, t) \leq h_{wp}) \end{cases} \quad [5.14]$$

where  $\theta_{wp}$  is the water content at the permanent wilting point,  $h_{fc}$  is the pressure head at the field capacity and  $h_{wp}$  is the pressure head at the permanent wilting point.

The calculation results of those properties are presented in Fig. 5.10 for sandy loam, clay and Kumamoto Andisol soils. In Fig. 5.10a, during infiltration ( $t = 0-1$  day), water storage at the root zone (0-50 cm of depth) increased for all three soils. After that

it's were slightly constant because wetting front still remained within the root zone. It started to decrease when wetting front leaved the root zone.

The air storages at the root zone for those soils are presented in Fig. 5.10b. Because of twin fluids-water and air system, it shows that when water storage increased; air storage decreased, and vice versa. It also shows that Kumamoto Andisol soil exhibited largest both water and air storage. Water storage for clay soil was larger than that of sandy loam soil. In contrast, air storage for clay soil was smaller than that in sandy loam soil. Drainage rate from the root zone had a positive correlation to air storage in the root zone. Large drainage rate yields great air storage as shown in sandy loam and Kumamoto Andisol soils.

Figure 5.10c shows the potential and actual PAW at root zone for sandy loam, clay, and Kumamoto Andisol soils. Kumamoto Andisol exhibited largest the potential PAW, PAW<sub>o</sub> at the root zone (7.7 cm) followed by clay soil (3.4 cm) and sandy loam soil (2.8 cm). For the actual PAW at the root zone, Kumamoto Andisol soil also had the largest one followed by clay and sandy loam soils. The actual PAW at the root zone increased with increasing time and then reached the peak for Kumamoto Andisol soil (7.04 cm) at  $t = 18$  days and for clay soil (3.06 cm) at  $t = 27$  days. The actual PAW at the root zone for sandy loam soil was zero from  $t = 0$  to 30 days because water content profiles at root zone was still larger than water content of the field capacity during those times (see Fig. 5.5b).

Those results show that the presence of intra interaggregate and interaggregate pores in Kumamoto Andisol (Fig. 5.9) lead to large porosity as also shown in water retention (Fig. 5.2) thereby large water and air storage and the potential and actual PAW at the root zone. Thus Kumamoto Andisol exhibits excellent physical properties for plant growth such as (1) large air storage which is good for soil aeration (oxygen availability) in the root zone and (2) large PAW which is good for water availability in the root zone.

## 5 Roles of aggregate structure

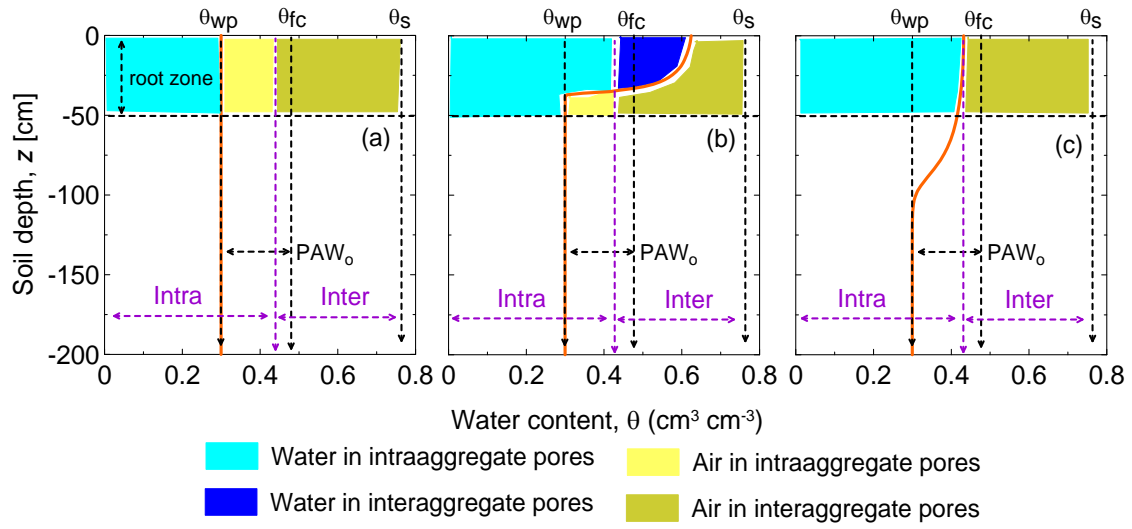


Fig. 5.9. Twin fluids-water and air system in the root zone. Water content and air content profiles at (a) initial condition  $t = 0$ , (b) final infiltration  $t = 1$  day and (c) final redistribution  $t = 30$  days corresponding to interaggregate and intraaggregate pores of Kumamoto Andisol.

## 5 Roles of aggregate structure

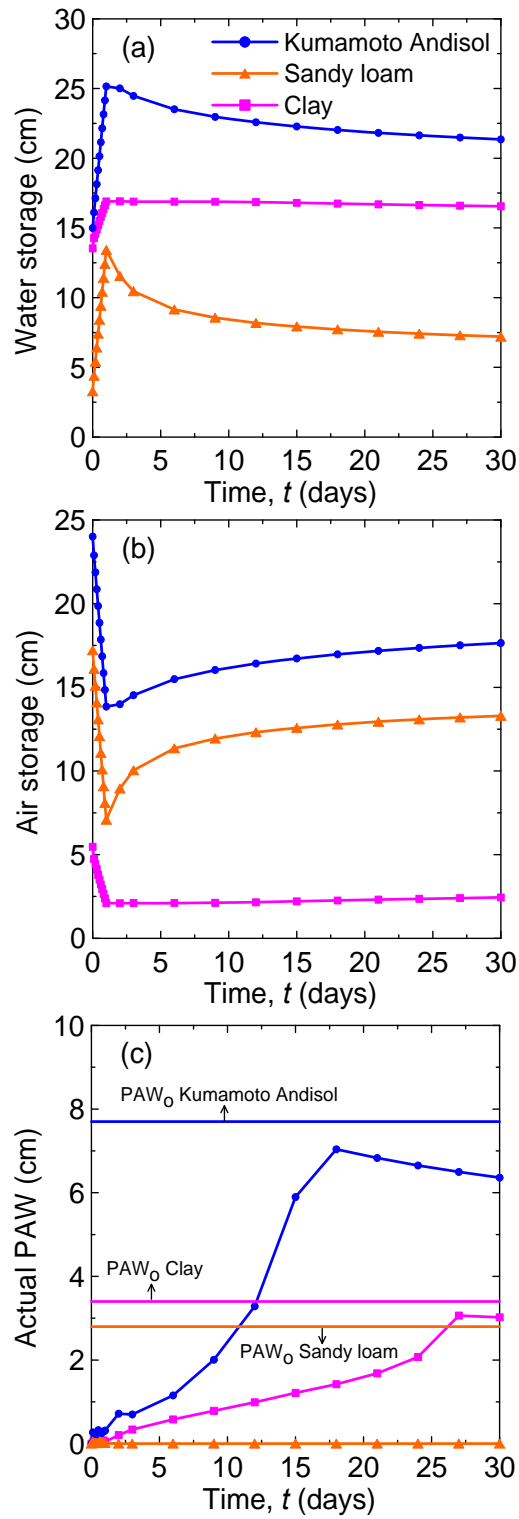


Fig. 5.10. (a) Water storage, (b) air storage and (c) the potential PAW (PAW<sub>0</sub>) and actual PAW at the root zone as a function of time for Kumamoto Andisol, sandy loam, and clay soils.

#### 5.4.5 Roles of interaggregate and intraaggregate pores in water and air storage

Figure 5.9 also shows schematic how to split water and air storage into intra interaggregate and interaggregate pores. As shown in Fig. 2b, we defined saturated intraaggregate pores as  $\theta_{s2} = w_2 (\theta_s - \theta_r)$ , whereas saturated interaggregate pores as  $\theta_{s1} = (1 - w_2) (\theta_s - \theta_r)$ . Thus,  $\theta_s = \theta_{s1} + \theta_{s2} + \theta_r$ . In this study,  $\theta_r = 0$ . Those definitions were used to split water and air storage, the potential and actual PAW at the root zone into intraaggregate and interaggregate pores in Andisol, as follows:

(a) Water storage within intraaggregate pores ( $WS_2$ ) at the root zone:

$$WS_2(t) = \int_{z=0}^{z=zr} \theta_2(z,t) dz \begin{cases} \theta_2(z,t) = \theta_{s2} & \theta(z,t) > \theta_{s2} \\ \theta_2(z,t) = \theta(z,t) & \theta(z,t) \leq \theta_{s2} \end{cases} \quad [5.15]$$

$\theta_2$  is the water content in intraaggregate pores.

(b) Water storage within interaggregate pores ( $WS_1$ ) at the root zone:

$$WS_1(t) = \int_{z=0}^{z=zr} \theta_1(z,t) dz \begin{cases} \theta_1(z,t) = \theta(z,t) - \theta_{s2} & \theta(z,t) > \theta_{s2} \\ \theta_1(z,t) = 0 & \theta(z,t) \leq \theta_{s2} \end{cases} \quad [5.16]$$

$\theta_1$  is the water content in intraaggregate pores.

(c) Air content within intraaggregate pores ( $AC_2$ ) at the root zone, for simplification, twin liquid phase (water and air) is used and assumed  $\theta_s$  is equal to porosity,  $\phi$ :

$$AC_2(t) = \int_{z=0}^{z=zr} \theta_{s2}(z) dz - \int_{z=0}^{z=zr} \theta_2(z,t) dz \quad [5.17]$$

(d) Air content within interaggregate pores ( $AC_1$ ) at the root zone, for simplification, twin liquid phase (water and air) is used and assumed  $\theta_s$  is equal to porosity,  $\phi$ .

$$AC_1(t) = \int_{z=0}^{z=zr} \theta_{s1}(z) dz - \int_{z=0}^{z=zr} \theta_1(z,t) dz \quad [5.18]$$

(e) Potential plant available water within intraaggregate pores (the potential PAW<sub>2</sub>) at the root zone:

$$Potential\ PAW_2(t) = \int_{z=0}^{z=zr} (\theta_{s2} - \theta_{wp}) dz \quad [5.19]$$

## 5 Roles of aggregate structure

(f) Potential plant available water within interaggregate pores (the potential PAW<sub>1</sub>) at the root zone:

$$Potential\ PAW_1(t) = \int_{z=0}^{z=z_r} (\theta_{fc} - \theta_{s2}) dz \quad [5.20]$$

(g) Actual plant available water within intraaggregate pores (the actual PAW<sub>2</sub>) at the root zone:

$$ActPAW_2(t) = \int_{z=0}^{z=z_r} (p(z)) dz \begin{cases} p(z,t) = 0 & (h(z,t) \geq h_{fc}) \\ p(z,t) = (\theta_{s2} - \theta_{wp}) & (h_{wp} \leq h(z,t) \leq h_{fc}) \text{ and } \theta(z,t) > \theta_{s2} \\ p(z,t) = (\theta(z,t) - \theta_{wp}) & (h_{wp} \leq h(z,t) \leq h_{fc}) \text{ and } \theta(z,t) \leq \theta_{s2} \\ p(z,t) = 0 & (h(z,t) \leq h_{wp}) \end{cases} \quad [5.21]$$

(h) Actual plant available water within interaggregate pores (the actual PAW<sub>1</sub>) at the root zone:

$$Act\ PAW_1(t) = \int_{z=0}^{z=z_r} (p(z)) dz \begin{cases} p(z,t) = 0 & (h(z,t) \geq h_{fc}) \\ p(z,t) = (\theta(z,t) - \theta_{s2}) & (h_{wp} \leq h(z,t) \leq h_{fc}) \text{ and } \theta(z,t) > \theta_{s2} \\ p(z,t) = 0 & (h_{wp} \leq h(z,t) \leq h_{fc}) \text{ and } \theta(z,t) \leq \theta_{s2} \\ p(z,t) = 0 & (h(z,t) \leq h_{wp}) \end{cases} \quad [5.22]$$

Figure 5.11 shows the roles of intraaggregate and interaggregate pores on water and air storage and the potential and actual PAW in Kumamoto Andisol during infiltration and then followed by redistribution. Figure 5.11a shows that much more water was stored in intraaggregate pores than interaggregate pores because intraaggregate pores have smaller pore size than interaggregate pores and the water flow is assumed in equilibrium condition which firstly water will fill smaller pore and then larger pores. Contrary, much more air was stored in interaggregate pores than intraaggregate pores as shown in Fig. 5.11b because water in larger pores will drain firstly and then followed by smaller pores. Figure 5.11c shows that the potential and actual PAW in intraaggregate pore is greater significantly than that interaggregate pore.

## 5 Roles of aggregate structure

These findings are agreed well with statements of Shoji et al. (1993), Shoji and Takahashi (2002) and Dahlgren et al. (2004).

Further studies are still needed by accounting hysteresis effect, root water and nutrient uptake model in the root zone to evaluate favorable physical properties of Andisols for plant growth. The hysteretic model for dual porosity soil (Rudiyanto et al., 2013a) might be able to use. Uncompensated root water uptake proposed by Feddes et al. (1978) or compensated root water uptake proposed by Jarvis (1989), and Jarvis (2011) and compensated root water and nutrient uptake model (Šimůnek and Hopmans, 2009) can be used for root water and nutrient uptake model.

## 5 Roles of aggregate structure

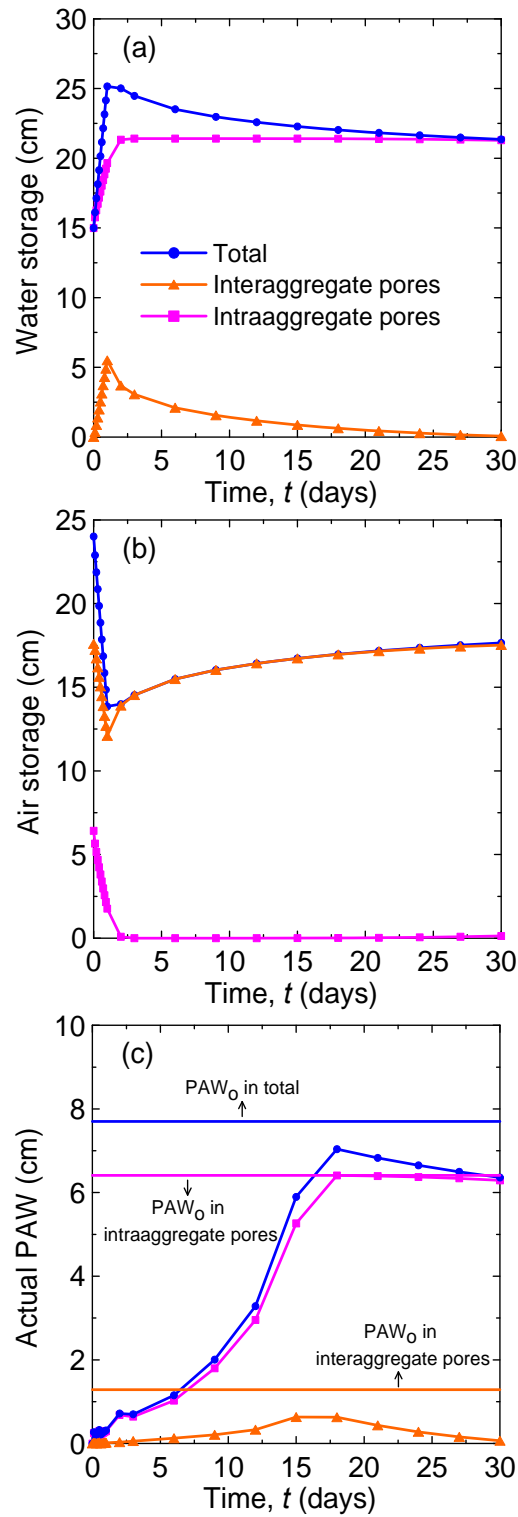


Fig. 5.11. Contribution of interaggregate and intraaggregate pores into (a) total water and (b) air storage and (c) the potential PAW (PAW<sub>0</sub>) and actual PAW at the root zone as a function of time in Kumamoto Andisol.



### 5.5 CONCLUSIONS

The evaluation of the roles of aggregated structure in Andisol was conducted using numerical analysis of water flow where soil water infiltration was followed by redistribution. The results were compared with those in sandy loam and clay soils. Kumamoto Andisol exhibits large infiltration which was similar to sandy loam soil because of large  $K_s$ . Interaggregate pores in Andisols is responsible on high  $K_s$ . During redistribution, tail is developed in the wetting front of Andisol and clay soils because capillary flux in Andisol is more dominant to total water flux than gravity flux. Drainage rate from the root zone showed that sandy loam soil and Andisol are large while clay soil was poor drainage.

Kumamoto Andisol exhibits greater water and air storage, the potential and actual PAW than those in those two soils. For water storage and the potential and actual PAW, Kumamoto Andisol is similar to clay soil, however, for air storage, Kumamoto Andisol has similarity to sandy loam soil. It is also reflected by shape of unsaturated hydraulic conductivity of Kumamoto Andisols which is similar to sandy loam in high pressure head and clay in low pressure head. Therefore, Kumamoto Andisol combines valuable properties in sandy loam and clay soils for plant growth.

Finally, intra interaggregates and interaggregates pores in Andisol have different roles for plant growth. Intraaggregate pores are responsible on water storage and the potential and actual PAW which corresponding to water supply for root water uptake. Conversely, interaggregate pores are responsible on soil aeration which corresponding to oxygen supply for root.

## 5.6 REFERENCES

- Ahmed, S.U., M. Senge, K. Ito and J.T. Adomako. 2009. Evaluation of the potentialities of different soil types to yield response of soybean under deficit irrigation. *J. Jpn. Soc. Soil Phys.* 113: 13-20.
- Armas-Espinel, S., J.M. Hernández-Moreno, R. Muñoz-Carpena, and C.M. Regalado. 2003. Physical properties of “sorriba” – cultivated volcanic soils from Tenerife in relation to andic diagnostic parameters. *Geoderma*. 117:297–311. doi:10.1016/S0016-7061(03)00130-7
- Arnalds, O., C.T. Hallmark, and L.P. Wilding. 1995. Andisols from four different regions of Iceland. *Soil Sci. Soc. Am.* 59:161–169. doi:10.2136/sssaj1995.03615995005900010025x
- Blonquist, J.M., Jr., S.B. Jones, I. Lebron, and D.A. Robinson. 2006. Microstructural and phase configurational effects determining water content: Dielectric relationships of aggregated porous media. *Water Resour. Res.* 42:W05424. doi:10.1029/2005WR004418
- Carsel, R.F., and R.S. Parrish. 1988. Developing joint probability distributions of soil water retention characteristics. *Water Resour. Res.* 24:755-769. doi:10.1029/WR024i005p00755.
- Chamindu Deepagoda, T.K.K., P. Moldrup, M.P. Jensen, S.B. Jones, L.W. de Jonge, P. Schjønning, K. Scow, J.W. Hopmans, D.E. Rolston, K. Kawamoto, and T. Komatsu. 2012. Diffusion aspects of designing porous growth media for earth and space. *Soil Sci. Soc. Am. J.* 76: 1564-1578. doi:10.2136/sssaj2011.0438
- Dahlgren, R.A., M. Saigusa, F.C. Ugolini. 2004. The nature, properties and management of volcanic soils. *Adv. Agron.* 82:113-182. doi:10.1016/S0065-2113(03)82003-5
- Durner, W. 1994. Hydraulic conductivity estimation for soils with heterogeneous pore structure. *Water Resour. Res.* 30:211-223. doi:10.1029/93WR02676
- Feddes, R.A., P.J. Kowalik, and H. Zaradny. 1978. Simulation of field water use and crop yield. John Wiley & Sons. New York, NY. p. 188.
- Hillel, D. 1998. Environmental soil physics. Academic Press, London. p.771.
- Jarvis, N.J. 1989. A simple empirical model of root water uptake. *J. Hydrol.* 107:57–72. doi:10.1016/0022-1694(89)90050-4

- Jarvis, N.J. 2011. Simple physics-based models of compensatory plant water uptake: concepts and eco-hydrological consequences. *Hydrol. Earth Syst. Sci.* 15:3431-3446. doi:10.5194/hess-15-3431-2011
- Jury, W. and R. Horton. 2004. *Soil Physics*. 6th Edition. John Wiley & Sons. New York. p. 390.
- Maeda, M., B. Zhao, Y. Ozaki, and T. Yoneyama. 2003. Nitrate leaching in an Andisol treated with different types of fertilizers. *Environ Pollut.* 121:477-87. doi:10.1016/S0269-7491(02)00233-6
- Miyamoto, T., T. Annaka, and J. Chikusi. 2003. Soil aggregate structure effects on dielectric permittivity of an andisol measured by time domain reflectometry. *Vadose Zone J.* 2:90-97. doi:10.2136/vzj2003.9000
- Mualem, Y. 1976. A new model for predicting the hydraulic conductivity of unsaturated porous media. *Water Resour. Res.* 12:513-522. doi:10.1029/WR012i003p00513
- Nanzoyo, M., S. Shoji, and R.A. Dahlgren. 1993. Physical characteristics of volcanic ash soils. In: Shoji, S., M. Nanzoyo, and R.A. Dahlgren. *Volcanic ash soils: Genesis, properties, and utilization*. Elsevier Amsterdam, the Netherlands. p:89-207. doi:10.1016/S0166-2481(08)70268-X
- Nanzoyo, M. 2002. Unique properties of volcanic ash soils. *Glob. Environ. Res.* 6: 99-112.
- Poulenard, J., P. Podwojewski, J. Janeau, and J. Collinet. 2001. Runoff and soil erosion under rainfall simulation of Andisols from the Ecuadorian Paramo: effect of tillage and burning. *Catena*. 45:185-207. doi:10.1016/S0341-8162(01)00148-5
- Radcliffe, D., and J. Šimůnek. 2010. *Soil Physics with HYDRUS: Modeling and Applications*. CRC Press, Taylor & Francis Group. p. 373.
- Romano, N., and A. Santini. 2002. Water retention and storage: Field. In: Dane, J.H. and G.C. Topp, eds. *Methods of Soil Analysis, Part 4, Physical Methods*. p. 721-738, SSSA Book Series N.5, Madison, WI, USA.
- Rudiyanto, N. Toride, M. Sakai, and J. Šimůnek. 2013<sup>a</sup>. A hysteretic model of hydraulic properties for dual-porosity soils. *Soil Sci. Soc. Am. J.* 77:1182-1188. doi:10.2136/sssaj2012.0339n

- Rudiyanto, N. Toride, M. Sakai, and M.Th. van Genuchten. 2013<sup>b</sup>. Estimating the unsaturated hydraulic conductivity of andisols using the evaporation method. *J. Jpn. Soc. Soil Physics*. 125:3-15.
- Sansoulet, J., Y.M. Cabidoche, and P. Cattan. 2007. Adsorption and transport of nitrate and potassium in an andosol under banana (Guadeloupe, French West Indies). *Eur. J. Soil Sci.* 58:478-489. doi:10.1111/j.1365-2389.2007.00904.x
- Sansoulet, J., Y.M. Cabidoche, P. Cattan, S. Ruy, and J. Šimůnek. 2008. Spatially distributed water fluxes in an andisol under banana plants: experiments and three-dimensional modeling. *Vadose Zone J.* 7:819-829. doi: 10.2136/vzj2007.0073
- Shoji, S., M. Nanzyo, and R.A. Dahlgren. 1993. Productivity and utilization of volcanic ash soils. In: Shoji, S., M. Nanzyo, R.A. Dahlgren. *Volcanic ash soils: Genesis, properties, and utilization*. Elsevier Amsterdam, the Netherlands. p:209-251. doi:10.1016/S0166-2481(08)70269-1
- Shoji, S., and T. Takahashi. 2002. Environmental and agricultural significance of volcanic ash soils. *Glob. Environ. Res.* 6:113-135.
- Šimůnek, J., and J. W. Hopmans. 2009. Modeling compensated root water and nutrient uptake, *Ecological Modeling*. 220:505-521. doi:10.1016/j.ecolmodel.2008.11.004
- Šimůnek, J., M. Šejna, H. Saito, M. Sakai, and M.Th. van Genuchten. 2008. The Hydrus-1D Software Package for Simulating the Movement of Water, Heat, and Multiple Solutes in Variably Saturated Media. Version 4.0. HYDRUS Softw. Ser. 3. Dep. of Environ. Sci., Univ. of California, Riverside.
- van Genuchten, M.Th. 1980. A closed-form equation for predicting the hydraulic conductivity of unsaturated soils. *Soil Sci. Soc. Am. J.* 44:892–898. doi:10.2136/sssaj1980.03615995004400050002x

## CHAPTER 6

# CONCLUDING REMARKS AND PERSPECTIVES

### 6.1 CONCLUSIONS

Andisols generally are developed from volcanic ash consisting of noncrystalline materials such as allophone, imogolite, Al-humus complexes, and ferrihydrite (Shoji et al., 1993; Nanzo, 2002). They typically have very low bulk density and well-developed aggregated structure. Because of this, Andisols usually exhibit a composite (stepwise) water retention function reflecting distinct but interacting interaggregate and intraaggregate pore regions (Miyamoto et al., 2003).

Those properties above lead to Andisols (volcanic ash soils) are known the most productive soil in the earth. Andisols provide favorable condition for plant root growth such as large water storage and PAW, large drainage rate and good aeration (Nanzzyo et al., 1993; Shoji et al., 1993; Shoji and Takahashi, 2002; Nanzzyo, 2002; and Dahlgren et al., 2004). Moreover, Andisols also reduce runoff (flood) and hence to soil erosion due to high water infiltration. One alternative that can be used to evaluate the roles of aggregate structure of Andisols is numerical analysis of water flow. It can be done since hydraulic properties (i.e., water retention,  $\theta(h)$  and unsaturated hydraulic conductivity,  $K(h)$ ) of Andisols are known.

The aims of this thesis are: (1) to estimate a wide range of the unsaturated hydraulic conductivity of Andisols based on the evaporation method; (2) to observe and propose a hysteretic model of hydraulic properties for Andisols; and (3) to evaluate roles of aggregate structure of Andisols, numerically in water flow in the root zone.

Parameters of the bimodal VG model for hydraulic properties of two aggregated Andisols were inversely determined using the evaporation method in **Chapter 3**. Independently measured water retention data from near saturation to very low pressure heads down to  $-10^5$  cm were included in the objective function in addition to soil pressure head data at two depths measured during the evaporation experiments. The saturated hydraulic parameter,  $K_s$ , and the pore-connectivity factor,  $\ell$ , along with several

sets of water retention parameters were optimized. Since direct  $\theta_s$  measurements are often quite variable for high-porosity Andisols, the saturated water content was determined from the final water content and the measured cumulative amount of evaporation. When the value of  $\theta_s$  is fixed from these water mass balance considerations,  $K_s$  should be estimated in the evaporation method.

Since the initial estimates of the water retention parameters were determined from the independently measured water retention data, parameter estimation succeeded to converge quickly regardless of the number of optimized parameters. When water retention data from near saturation to very low pressure heads are available and used in the objective function, it is possible to predict  $K(h)$  by optimizing only two conductivity parameters ( $K_s$ ,  $\ell$ ). Since the flat region of the bimodal water retention curve is difficult to measure precisely, we recommend optimizing all of the bimodal VG parameters except  $\theta_s$  and  $\theta_r$  to yield the best overall fit.

In order to demonstrate the role of water retention data at low pressure heads in the objective function, we compared hydraulic functions optimized with and without water retention data at low pressure heads. Although almost similar matches to observed pressure heads were obtained with or without the low pressure data in the dry range, the second subregion parameter ( $\alpha_2$ ,  $n_2$ ) converged to different values if the low pressure data were omitted from the objective function. Predictions based on the hydraulic functions optimized with the low pressure data agreed well with observed pressure heads near the surface after a longer period of evaporation than used for the tensiometer measurements. The results indicate that including water retention data at low pressure heads can extend the applicable range of the model predications, at least down to approximately  $-10^4$  cm.

The benefit of using independently measured water retention data was further studied by including different pressure head measurement ranges in the objective function. Neglecting the lower pressure data did not affect the  $K(h)$  estimation process very much, leading to almost similar  $K(h)$  functions. This confirms that collecting water retention data over a wide range of pressure heads will give very useful prior information to the parameter estimation process for not only Andisols but also other soils.

Due to capillary hysteresis in inter aggregate pore, a hysteretic  $\theta(h)$  might be exist at the first subcurve which also similar in Sandy soil. To date, quite limited study was carried out to investigate hysteretic water retention of Andisols. A hysteretic model of soil hydraulic properties for dual-porosity soils is proposed in **Chapter 4**. The model is based on a bimodal VG model (Durner, 1994) and the K&P hysteresis model (Kool and Parker, 1987). Hysteresis is considered only in the first subregion,  $\theta_1(h)$ , affecting mainly higher water contents, while a nonhysteretic behaviour is assumed in the second subregion,  $\theta_2(h)$ , affecting mainly lower water contents. The main hysteretic loop is described with  $\alpha_1^d$  for the main drying curve,  $\theta_1^d(h)$ , and  $\alpha_1^w (>\alpha_1^d)$  for the main wetting curve,  $\theta_1^w(h)$ . Remaining parameter values are the same for the main drying and wetting curves. For soils with the larger  $n_1$  (e.g.,  $n_1 = 2.56$ ), hysteresis affects mainly the first part of the retention curve  $\theta(h)$  near saturation. On the other hand, for soils with the smaller  $n_1$  (e.g.,  $n_1 = 1.2$ ), some hysteresis extends from the full saturation to lower pressure heads, also affecting the second part of the retention curve  $\theta(h)$ . Scanning curves of  $\theta(h)$  can also be successfully described using the K&P model in the first subregion of  $\theta_1(h)$ . The observed main hysteretic loop and scanning curves for Andisols aggregates could be reasonably well described using this proposed hysteretic model.

The drying and wetting unsaturated hydraulic conductivity functions  $K^d(\theta)$  and  $K^w(\theta)$ , respectively, are almost identical for higher water contents. However,  $K^d(\theta)$  is greater than  $K^w(\theta)$  for lower water contents. To overcome this unrealistic phenomenon in the conductivity function, we use an additional constraint on the value of the  $\alpha_1$  parameter and use a single value  $\alpha_1^k$  for both drying and wetting functions. As a result, an almost nonhysteretic  $K(\theta)$  function is obtained for the entire range of water contents. It is necessary to experimentally investigate  $K(\theta)$  for low water contents to determine the  $\alpha_1^k$  value.

**Chapter 5** presents a numerical evaluation for the roles of aggregate structure of Andisol in water flow in the root zone. Water infiltration then followed by redistribution were compared in Kumamoto Andisols from **Chapter 3**, sandy loam and clay soils. Kumamoto Andisol exhibits large infiltration as well as drainage rate which was similar to sandy loam soil because of large  $K_s$ . Interaggregate pores in Andisols is responsible on high  $K_s$ . Kumamoto Andisol shows greater water and air storages, the potential and actual PAW than those in the two soils. For water storage and the potential and actual

PAW, Kumamoto Andisol is similar to clay soil, however, for air storage, Kumamoto Andisol has similarity to sandy loam soil. It is not suppressing because the shape of unsaturated hydraulic conductivity of Andisols which is similar to sandy loam in high pressure head and clay in low pressure head. Therefore, Kumamoto Andisol combines beneficial properties in sandy loam and clay soils for plant growth.

Intra interaggregates and interaggregates pores in Andisol have different roles for plant growth. Intraaggregate pores are responsible on water storage and the potential and actual PAW which corresponding to water supply for root water uptake. Contrary, interaggregate pores are responsible on soil aeration which corresponding to oxygen supply for root.

## 6.2 FUTURE PERSPECTIVES

### *Coupling unsaturated water flow with solute transport model in Andisols*

Water flow and solute transport processes in Andisols are of considerable interest because of their unique physical and chemical properties. Large drainage rate in Andisols (**Chapter 5**) can lead to nutrient leaching and then groundwater contaminant under agricultural field. Mostly previous study solute transport in Andisols (Vogeler et al., 2000, Magesan, et al., 2003, Nakagawa, et al., 2011) did not conducted simultaneously with unsaturated water flow analysis. Coupling unsaturated water flow and solute transport model will improve understanding on solute transport in Andisols. Combination of the Richard equation and the bimodal VG parameters (**Chapter 3**) are used for the unsaturated water flow, while the mobile-immobile transport model (MIM) (Ritter et al., 2005), and or the reactive transport model (Nakagawa, et al., 2011) can be used for the transport model because Andisols have interaggregate and intraaggregate pores and or a high cation and anion exchange capacity, respectively.

### *Coupling unsaturated water flow with root water uptake model in Andisols*

In the **Chapter 5**, water supply for root was described using the actual PAW in the root zone which does not account the potential evapotranspiration. In reality, root water uptake is strongly corresponding to the potential evapotranspiration; therefore, inclusion of root water uptake model could improve our understanding that Andisols could provide favorable condition for plant growth. Uncompensated root water uptake



proposed by Feddes et al. (1978) or compensated root water uptake proposed by Jarvis (1989), and Jarvis (2011) and compensated root water and nutrient uptake model (Šimůnek and Hopmans, 2009) can be used for root water and nutrient uptake model.

### ***Implementing hysteretic model in water flow numerical code***

Accounting the hysteretic model of hydraulic properties in numerical analysis of unsaturated water flow will improve the prediction results (Kool and Parker, 1987) especially on water balance (Beese and van der Ploeg, 1976). Therefore, it is necessary to implement hysteretic model in the water flow numerical code. Furthermore, combination of the code with the optimization procedure which resulted in the inverse method will also be useful for determining the hysteretic model parameters. Transient flow experiment can be obtained by multistep outflow-inflow experiment. This numerical code also can be used to evaluate the parameter  $\alpha_1^k$  for non-hysteretic  $K(\theta)$  (**Chapter 4**) from the dynamic water flow experiment such as the soil evaporation experiment followed by the upward infiltration (Šimůnek et al., 2001).

## **6.3 REFERENCES**

- Beese, F., and R. R. van der Ploeg. 1976. Influences of hysteresis on moisture flow in an undisturbed soil monolith. *Soil Sci. Soc. Am. J.* 40:480-484. doi:10.2136/sssaj1976.03615995004000040012x
- Dahlgren, R.A., M. Saigusa, F.C. Ugolini. 2004. The nature, properties and management of volcanic soils. *Adv. Agron.* 82:113-182. doi:10.1016/S0065-2113(03)82003-5
- Durner, W. 1994. Hydraulic conductivity estimation for soils with heterogeneous pore structure. *Water Resour. Res.* 30:211-223. doi:10.1029/93WR02676
- Feddes, R.A., P.J. Kowalik, and H. Zaradny. 1978. *Simulation of field water use and crop yield*. John Wiley & Sons. New York, NY. p. 188.
- Jarvis, N.J. 1989. A simple empirical model of root water uptake. *J. Hydrol.* 107:57–72. doi:10.1016/0022-1694(89)90050-4
- Jarvis, N.J. 2011. Simple physics-based models of compensatory plant water uptake: concepts and eco-hydrological consequences. *Hydrol. Earth Syst. Sci.* 15:3431-3446. doi:10.5194/hess-15-3431-2011

- Kool, J.B., and Parker, J.C. 1987. Development and evaluation of closed-form expressions for hysteretic properties. *Water Resour. Res.* 23:105–114. doi:10.1029/WR023i001p00105
- Magesan, G. N., I. Vogeler, B. E. Clothier, S. R. Green, and R. Lee. 2003. Solute Movement through an Allophanic Soil. *J. Environ. Qual.* 32:2325–33. doi:10.2134/jeq2003.2325
- Miyamoto, T., T. Annaka, and J. Chikusi. 2003. Soil aggregate structure effects on dielectric permittivity of an andisol measured by time domain reflectometry. *Vadose Zone J.* 2:90–97. doi:10.2136/vzj2003.9000
- Nakagawa, K., K. Momii and R. Berndtsson. 2011. Modeling Solute Transport in Volcanic Ash Soils with Cation Exchange and Anion Retardation. *Environ. Model Assess.* 16:335–342. doi:10.1007/s10666-011-9262-6
- Nanzyo, M. 2002. Unique properties of volcanic ash soils. *Glob. Environ. Res.* 6: 99–112.
- Nanzyo, M., S. Shoji, and R.A. Dahlgren. 1993. Physical characteristics of volcanic ash soils. In: Shoji, S., M. Nanzyo, and R.A. Dahlgren. *Volcanic ash soils: Genesis, properties, and utilization.* Elsevier Amsterdam, the Netherlands. p:89–207. doi:10.1016/S0166-2481(08)70268-X
- Nanzyo, M. 2002. Unique properties of volcanic ash soils. *Glob. Environ. Res.* 6: 99–112.
- Ritter, A., R. Muñoz-Carpena, C.M. Regalado, M. Javaux, and M. Vanclooster. 2005. Using TDR and Inverse Modeling to Characterize Solute Transport in a Layered Agricultural Volcanic Soil. *Vadose Zone J.* 4:300–309. doi: 10.2136/vzj2004.0094
- Shoji, S., M. Nanzyo, and R.A. Dahlgren. 1993. Volcanic ash soils: Genesis, properties, and utilization. Elsevier Amsterdam, the Netherlands. p. 1–288.
- Shoji, S., M. Nanzyo, and R.A. Dahlgren. 1993. Productivity and utilization of volcanic ash soils. In: Shoji, S., M. Nanzyo, R.A. Dahlgren. *Volcanic ash soils: Genesis, properties, and utilization.* Elsevier Amsterdam, the Netherlands. p:209–251. doi:10.1016/S0166-2481(08)70269-1
- Shoji, S., and T. Takahashi. 2002. Environmental and agricultural significance of volcanic ash soils. *Glob. Environ. Res.* 6:113–135.

- Šimůnek, J., and J. W. Hopmans. 2009. Modeling compensated root water and nutrient uptake, *Ecological Modeling*. 220:505-521. doi:10.1016/j.ecolmodel.2008.11.004
- Šimůnek, J., O. Wendroth, N. Wypler, and M. Th. van Genuchten. 2001. Nonequilibrium water flow characterized from an upward infiltration experiment. *European J. of Soil Sci.* 52:13-24. doi:10.1046/j.1365-2389.2001.00361.x
- Vogeler, I., C. Duwig, B.E. Clothier, and S.R. Green. 2000. A Simple Approach to Determine Reactive Solute Transport Using Time Domain Reflectometry. *Soil Sci. Soc. Am. J.* 64:12–18. doi:10.2136/sssaj2000.64112x

## 6 Concluding remarks and perspective

# LIST OF SYMBOLS AND ABBREVIATIONS

## Lowercase

Symbol	Description	Dimension
$h$	matric potential head	L
$h_{\Delta}$	pressure head at reversal point	L
$h_{wp}$	pressure head at wetting point	L
$h_{fc}$	pressure head at wetting point	L
$h_m$	shape parameter of Kosugi model ( $h_{m1}, h_{m2}$ )	L <sup>-1</sup>
$\ell$	pore connectivity and tortuosity factor	
$m$	van Genuchten shape parameter ( $m = 1 - 1/n$ ); ( $m_1, m_2, m_i$ ) for the bimodal VG model	
$m_y$	number of type flow parameter	
$n$	van Genuchten shape parameter; ( $n_1, n_2, n_i$ )	
$n^d$	n for main drying curve; ( $n_1^d, n_2^d, n_i^d$ )	
$n^w$	n for main wetting curve; ( $n_1^w, n_2^w, n_i^w$ )	
$n_j$	the number of measurements for a certain measurement type $j$	
$p$	vapor pressure of the air	M L <sup>-1</sup> T <sup>-2</sup>
$p_o$	saturation vapor pressure at sample temperature	M L <sup>-1</sup> T <sup>-2</sup>
$r_w$	sink term	T <sup>-1</sup>
$q_{\text{evap}}$	time-variable evaporation rate	L T <sup>-1</sup>
$q_{\text{in}}$	rainfall rate	L T <sup>-1</sup>
$t$	time	T
$v_j$	weight for normalization of type flow parameter	
$w_2$	weight factor in the bimodal vG model ( $w_1 + w_2 = 1$ )	
$w_{i,j}$	weight for individual measured data	
$y_j^*$	measured flow variable	
$y_j$	model predicted flow variable	
$z$	vertical coordinate	L

# List of symbols and abbreviations

$zr$	root zone depth	L
------	-----------------	---

## Uppercase

Symbol	Description	Dimension
$AC$	air content; ( $AC_1$ , $AC_2$ ) in interaggregate and intraaggregate pores	L
$CD_i$	cumulative drainage	L
$D_i$	drainage rate	L T <sup>-1</sup>
$H$	hydraulic head	L
$J_w$	vertical water flux	L T <sup>-1</sup>
$K(h)$ , $K(\theta)$ , $K(S)$	unsaturated hydraulic conductivity	L T <sup>-1</sup>
$K_s$	saturated hydraulic conductivity	L T <sup>-1</sup>
$M$	molecular mass of water ( $1.8 \times 10^{-5} \text{ m}^3 \text{ mol}^{-1}$ )	L N <sup>-1</sup>
$PAW$	Plant available water (potential PAW, PAW <sub>0</sub> , actual PAW, potential PAW <sub>1</sub> , actual PAW <sub>1</sub> , potential PAW <sub>2</sub> , actual PAW <sub>2</sub> )	L <sup>3</sup> L <sup>-3</sup>
$R$	the gas constant ( $8.314 \text{ J mol}^{-1} \text{ K}^{-1}$ )	M L <sup>2</sup> T <sup>-2</sup> N <sup>-1</sup> $\Theta^{-1}$
$S$	effective saturation, ( $S_1$ , and $S_2$ ) for the bimodal VG model	
$S^d$	$S$ for main drying curve ( $S_1^d$ , and $S_2^d$ ) for the bimodal VG model	
$S^w$	$S$ for main wetting curve ( $S_1^w$ , and $S_2^w$ ) for the bimodal VG model	
$T$	Kelvin temperature of the sample	$\Theta$
$WS$	water storage; ( $WS_1$ , $WS_2$ ) in interaggregate and intraaggregate pores	L

List of symbols and abbreviations

**Lower Greek**

Symbol	Description	Dimension
$\alpha$	van Genuchten shape parameter; ( $\alpha_1$ , $\alpha_2$ ) for the bimodal VG model,	$L^{-1}$
$\alpha^d$	$\alpha$ for main drying curve; ( $\alpha_1^d$ , $\alpha_2^d$ )	$L^{-1}$
$\alpha^w$	$\alpha$ for main wetting curve; ( $\alpha_1^w$ , $\alpha_2^w$ )	$L^{-1}$
$\alpha_\theta$	scaling factor for drying and or wetting scanning curves	
$\alpha_l^k$	$\alpha_l$ for non-hysteretic $K(\theta)$	$L^{-1}$
$\alpha_{rs}$	parameter for Ross and Smettem model	$L^{-1}$
$\beta$	the optimized parameter vector	
$\phi$	porosity	$L L^{-3}$
$\Phi$	objective function	
$\rho_b$	bulk density	$M L^{-3}$
$\sigma$	shape parameter of Kosugi model ( $\sigma_1$ , $\sigma_2$ )	
$\theta$	volumetric water content	$L^3 L^{-3}$
$\theta(h)$	water retention, $\theta_1(h)$ , and $\theta_2(h)$ for the first and second subregions of the bimodal VG model	$L^3 L^{-3}$
$\theta_r$	residual water content; $\theta_{r1}$ , and $\theta_{r2}$ for the first and second subregions of the bimodal VG model	$L^3 L^{-3}$
$\theta_r^d$	$\theta_r$ for main drying curve; ( $\theta_{r1}^d$ , $\theta_{r2}^d$ , $\theta_{ri}^d$ )	$L^3 L^{-3}$
$\theta_r^w$	$\theta_r$ for main wetting curve; ( $\theta_{r1}^w$ , $\theta_{r2}^w$ , $\theta_{ri}^w$ )	$L^3 L^{-3}$
$\theta_r^*$	fictitious $\theta_r$ for wetting scanning curve; ( $\theta_{r1}^*$ )	$L^3 L^{-3}$
$\theta_s$	saturated water content; $\theta_{s1}$ , and $\theta_{s2}$ for the first and second subregions of the bimodal VG model	$L^3 L^{-3}$
$\theta_s^d$	$\theta_s$ for main drying curve; ( $\theta_{s1}^d$ , $\theta_{s2}^d$ , $\theta_{si}^d$ )	$L^3 L^{-3}$
$\theta_s^w$	$\theta_s$ for main wetting curve; ( $\theta_{s1}^w$ , $\theta_{s2}^w$ , $\theta_{si}^w$ )	$L^3 L^{-3}$
$\theta_s^*$	fictitious $\theta_s$ for drying scanning curve; ( $\theta_{s1}^*$ )	$L^3 L^{-3}$
$\theta_\Delta$	water content at reversal point; ( $\theta_{\Delta 1}$ )	$L^3 L^{-3}$
$\theta_{wp}$	water content at wetting point	$L^3 L^{-3}$

## List of symbols and abbreviations

$\theta_{fc}$	water content at field capacity	$L^3 L^{-3}$
$\rho_b$	soil bulk density	$M L^{-3}$
$\psi$	soil water potential	$M L^{-1} T^{-2}$

---

## Abbreviation

Abbreviation	Description
CV	coefficients of variation
DSC	drying scanning curve
K&P	Kool and Parker
MDC	main drying curve
MWC	main wetting curve
NASA	National Aeronautics and Space Administration
PAW	plant available water
RMSE	root mean square error
SE	standard errors
VG	van Genuchten
WSC	wetting scanning curve

---